Doctorate Dissertation

学位論文

M8 class earthquake cycle in the southernmost part of the Kuril subduction zone

(千島海溝最南部沈み込み帯の M8 級の地震サイクル)

A Dissertation Submitted for Degree of Doctor of Philosophy

April 2018

平成 30 年 4 月博士（理学）申請

Department of Earth and Planetary Science, Graduate School of Science,

The University of Tokyo

東京大学大学院理学系研究科

地球惑星科学専攻

Hiroaki Kobayashi

小林 広明

Abstract

The earthquake cycle consists of three periods: interseismic, coseismic, and postseismic. It is necessary to examine these three periods to understand the earthquake cycle. However, when we focus on large (M_w ~ 8) to giant (M_w ~ 9) earthquakes in a given region, the interseismic periods are often longer than the instrumental seismic observation periods, which are on the order of 100 years.

In the southernmost part of the Kuril subduction zone, six large to giant interplate earthquakes have occurred in the last 400 years. This includes the two M_w ~ 8 Tokachi-oki earthquakes that occurred in 1952 and 2003. In Hokkaido, instrumental seismic and geodetic observations began in the late 19th to early 20th centuries. Therefore, we are able to investigate more than a single *M*8 class earthquake cycle there. In this thesis, we examine the interseismic, coseismic, and postseismic periods in the southernmost part of the Kuril subduction zone to estimate slip history and budget in the *M*8 class earthquake cycle.

First, we investigated the coseismic periods. We performed joint source inversion analyses and examined the similarities and differences between the 1952 and 2003 Tokachi-oki earthquakes. We made two datasets for the 2003 earthquake, and one is nearly the same as that of the 1952 earthquake. The results reveal that in the Tokachi-oki region, the rupture processes, slip area, and slip amounts were similar for the 1952 and 2003 earthquakes. However, there are two differences: the 1952 earthquake was initiated with an M_w 6.1 earthquake, and it extended to the Akkeshi-oki region after the main rupture in the Tokachi-oki region.

Second, we analyzed the interseismic and postseismic periods prior to and after the 2003 earthquake using recent GNSS data. We investigated the crustal deformation rate prior to the 2003 earthquake and obtained the yearly slip deficit/afterslip distribution between 25 September 2000 and 24 September 2010. We confirmed that there was no yearly scale transient phenomenon prior to the 2003 earthquake in the Tokachi-oki region. The obtained slip deficit showed that the large slip deficit regions prior to the 2003 earthquakes were consistent with the main rupture areas of the 1952 and 2003 earthquakes. Moreover, the afterslip of the 2003 earthquake did not reach the Akkeshi-oki region, where a large slip occurred during the 1952 earthquake.

Third, we investigated leveling data and repeating earthquakes during periods that were not covered by the GNSS data. We examined a survey route around Cape Erimo, which has been repeatedly measured without a route change. We also estimated the crustal deformation due to medium-sized ($M \geq 6.5$) earthquakes. We next investigated two M5.4 repeating earthquake groups around Cape Erimo using analog seismograms. Together with the groups investigated by previous studies, we estimated the aseismic slip rate around the groups. The results of these investigations reveal that afterslip of the 1952 earthquake may have continued until around 1980. Moreover, in the Tokachi-oki region, the state of the plate interface prior to the 1952 earthquake may be similar to that prior to the 2003 earthquake. We also found that the acceleration of aseismic slip rate in the west of Cape Erimo prior to the 2003 earthquake.

Finally, we summarized the results of the above analyses and examined the slip history in the southernmost part of the Kuril subduction zone. We found that the slip budget is unbalanced in the Tokachi-oki region both in the single earthquake cycle between the 1952 and 2003 earthquakes and in the multiple cycles since 1843. We

suggested four possible reasons for the unbalanced slip budget: stress transfer, temporal change of frictional properties, changes of slip deficit rate, and supercycle.

Contents

1. General introduction

In subduction zones where an oceanic plate is subducting beneath a continental plate, large (moment magnitude (M_w) ~ 8) to giant (M_w ~ 9) earthquakes usually occur on the plate interface. For example in the Japan Trench subduction zone the 2011 M_w 9.0 Tohoku earthquake occurred and caused serious damage with approximately 20,000 fatalities and missing persons in the Tohoku region. Because these earthquakes occurs as a result of release of strain accumulated due to tectonic loading, it is important for understanding physics of earthquake and seismic hazard to examine the strain accumulation and release process. In this thesis we call the process 'earthquake cycle'.

In early studies of earthquake cycle, Shimazaki and Nakata [1980] proposed the time-predictable and slip-predictable models. The former assumes that a constant critical stress and a variable final stress. The latter assumes a variable critical stress and a constant final stress. They tested these two models using coseismic uplift data at a site along the Nankai subduction zones around Japan and suggested that the time-predictable model is more consistent than the other. After the 2004 M_w 9.0 (GCMT) Sumatra earthquake, several paleoseismic and paleogeodetic studies have been done in a few subduction zones [Goldfinger et al., 2013; Sieh et al., 2008; Philibosian et al., 2014; Wesson et al., 2015] and the supercycle model was proposed [Goldfinger et al., 2013; Sieh et al., 2008]. However, in these studies the slip history and budget were not well examined.

Concerning a long-term and wide-scale slip budget, Scholz and Campos [2012] estimated the seismic coupling of the various subduction zones. They showed that the

coupling varies considerably from one subduction zone to another. Kanamori [1977] and Kanamori et al. [2006] indicated that in the Japan Trench subduction zone seismic slip rate estimated from large earthquakes in recent few centuries is only 1/4 of plate convergence rate and suggested that a few explanations for the difference. In fact, a giant earthquake with M_w 9.0 occurred in Tohoku in 2011 which was suggested in Kanamori et al. [2006].

When we focus on a region of a given subduction zone, intervals of large to giant earthquakes vary from several decades to a few hundreds of years. In the subduction zone from the Central Andes to Chile, the 2014 M_w 8.2 Iquique earthquake ruptured a part of the rupture zone of the 1877 M_w 8.8 earthquake [Hayes et al., 2014] and the 2010 M_w 8.8 Maule earthquake occurred in the region where an M_w 8.5 earthquake occurred in 1835 [Moreno et al., 2010]. In the Sumatra subduction zone, the last even similar to the 2005 M_w 8.7 Nias-Simeulue earthquake was an earthquake in 1861, and 2007 M_w 8.4 South Pagai and M_w 7.9 Pagai-Sipora earthquakes ruptured part of the rupture zone of the 1833 M_w 9.0 earthquake in 1833 [Chlieh et al, 2008]. In the Japan Trench subduction zone, the 1968 M_w 8.3 Tokachi-oki earthquake, which is called the "Tokachi-oki earthquake" even though its source region is located in northern Sanriku [Nagai et al., 2001], had a rupture area similar to an earthquake in 1856 [Hatori, 1975], and there had been no giant earthquakes for at least 400 years prior to the 2011 M_w 9.0 Tohoku earthquake. In the Nankai subduction zone, where the history of large to giant earthquakes has been well documented over the last 1400 years, the intervals of these earthquakes are 90–474 years [Furumura, 2015]. These examples indicate that the intervals of large to giant earthquakes are usually longer than the seismic and geodetic observation periods, which started in the late 19th century at the earliest, making it

difficult to understand even a single cycle of such earthquakes using the seismic and geodetic data.

In the southernmost part of the Kuril subduction zone, which includes the Tokachi-oki, Akkeshi-oki, and Nemuro-oki regions (Figure 1-1), the Pacific Plate is subducting beneath the North America or Okhotsk plates with a convergence rate of approximately 8.5 cm/year [Drewes, 2009] and five large earthquakes have occurred in recent two hundred years [Satake, 2017]. Moreover, paleoseismic studies [e.g., Sawai et al., 2009] suggested that giant earthquakes have occurred in the southernmost part of the Kuril subduction zone and the last such earthquake occurred in the 17th century (Figure 1-1b). In the Tokachi-oki region, earthquakes with Japan Metrological Agency (JMA) magnitudes (M_{JMA}) of 8.2 and 8.0 occurred in 1952 and 2003, respectively. In Hokkaido, geodetic and seismic observations began in the late 19th to early 20th century. Therefore, this is one of the few cases where more than one large earthquake occurred during the seismic and geodetic observation periods, and we can estimate slip history and budget for examining the *M*8 class earthquake cycle in the southernmost part of the Kuril subduction zone including the Tokachi-oki region.

In Chapter 2, we investigate the coseismic periods by analyzing the source rupture processes of the 1952 and 2003 Tokachi-oki earthquakes. We perform joint source inversions using strong motion, teleseismic, and geodetic data. Because the amount of data is limited for the 1952 earthquake, we make two datasets for the 2003 earthquake, one of which is almost equivalent to the 1952 dataset. We examine the similarities and differences between the two earthquakes using the results.

In Chapter 3, we investigate the interseismic and postseismic periods around the 2003 earthquake using recent GNSS data. To check whether there was a long-term

transient event prior to the 2003 earthquake, we compare the three-year crustal deformation rate from 30 March 1997 to 29 March 2000 to the rate from 25 September 2000 to 24 September 2003. In addition, we perform a yearly slip deficit/afterslip inversion from 25 September 2000 to 24 September 2010 to investigate the temporal evolution of the slip deficit/afterslip. We discuss the relationship between the slip deificit/afterslip distribution and coseismic slip of the 1952 and 2003 earthquakes.

In Chapter 4, we investigate the 100-year crustal deformation and historical repeating earthquakes using the leveling survey data and analog seismograms. We select a survey route and two groups of the repeating earthquakes around Cape Erimo. We also examine $M \geq 6.5$ earthquakes in the study area and estimated the coseismic deformations due to these earthquakes. The results are used to infer the state of the plate interface in the pre-GNSS age.

In Chapter 5, we summarize the results obtained in Chapters 2 to 4 and examine the slip history in the southernmost part of the Kuril subduction zone. We conduct a quantitative examination in the Tokachi-oki region. We indicate two features in the slip history and suggest geophysical explanations for the features.

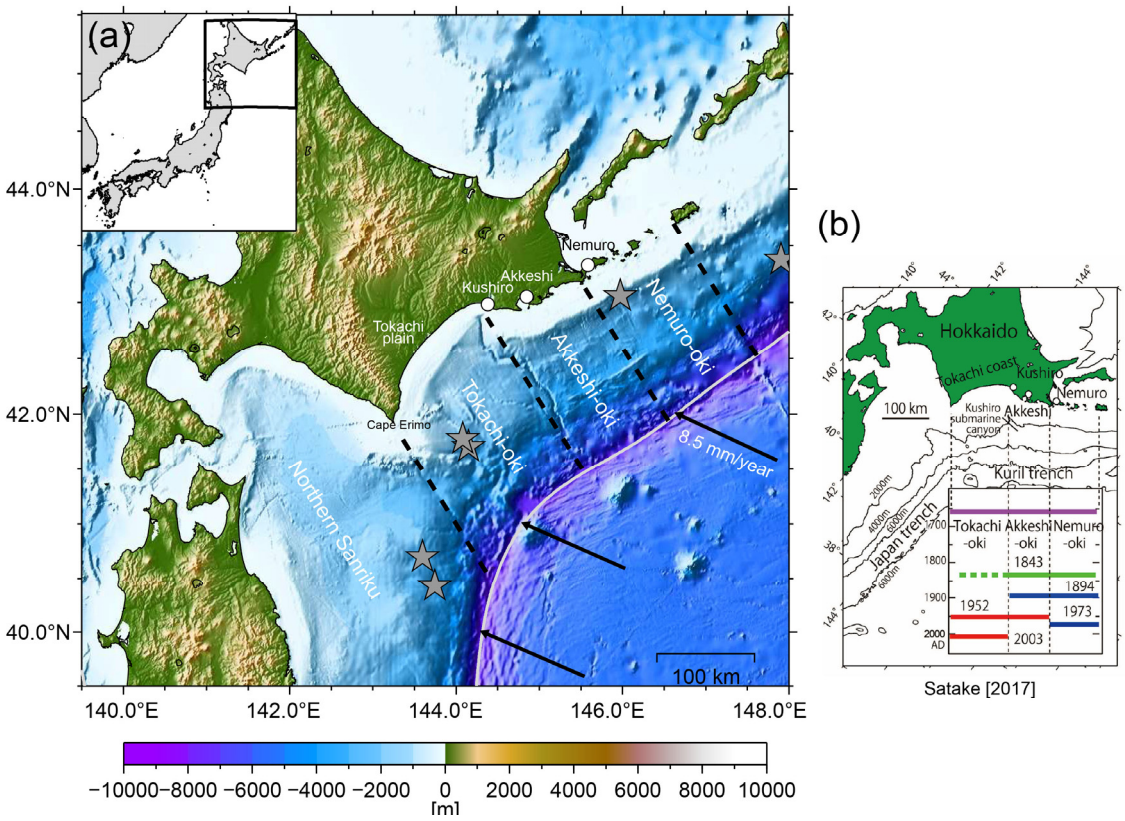

Figure 1-1. (a) Index map. Gray stars denote the epicenters of the $M_w \geq 7.7$ interplate earthquakes that have occurred since 1950. The black rectangle in the inset map represents the map area. The gray line shows the trench axis [Iwasaki et al., 2015]. Black arrows indicate the motion of Pacific Plate relative to North America Plate [Drewes, 2009]. The background colors show the topography of the General Bathymetric Chart of the Oceans (GEBCO) 2014 [Weatherall et al., 2015]. (b) Tsunami source area of the historical earthquakes [Satake, 2017].

2. Rupture processes of the 1952 and 2003 Tokachi-oki earthquakes

2.1. Introduction

The 1952 and 2003 Tokachi-oki earthquakes occurred on 4 March 1952 and 25 September 2003, respectively (universal coordinated time, UTC). Because they have similar epicenters and magnitudes (Table 2-1 and Figure 2-1), there have been several comparative studies of these earthquakes.

Hamada and Suzuki [2004] investigated their aftershocks and seismic intensity distributions. Nishimura [2006] performed source inversions using geodetic survey data. These studies concluded that the two earthquakes ruptured only the Tokachi-oki region. A source fault model of the 1952 earthquake estimated by Kasahara [1975] based on leveling survey data also were located only in the Tokachi-oki region. In addition, Yamanaka and Kikuchi [2003] performed a strong motion inversion of the 1952 earthquake and a teleseismic inversion of the 2003 earthquake. Even though the most of the strong-motion data for the 1952 earthquake that they used went off scale after the *S*-wave arrival, such that a sufficient data length was not available, they suggested that the two earthquakes have at least a common rupture area in the Tokachi-oki region.

However, tsunami analyses of the two earthquakes have suggested a different result. East of Kushiro, the observed tsunami run-up heights of the 1952 earthquake were higher than those of the 2003 earthquake [Tanioka et al., 2004b] and analyses of the tsunami waveforms have suggested that the rupture area of the 1952 earthquake extended to the Akkeshi-oki region [Hirata et al., 2003; Satake et al., 2006]. Hirata et al.

[2007] also examined the tsunami source area of the 1952 earthquake based on eyewitness testimony and concluded that the rupture area of the 1952 earthquake reached the Akkeshi-oki region. Note that Hartzell and Heaton [1985] estimated the source time functions of various large earthquakes including the 1952 earthquake using waveforms recorded in Pasadena, USA, and their result has two peaks, indicating that the 1952 Tokachi-oki earthquake had multiple shocks. The previous source studies of the 1952 earthquake are summarized in Table 2-2.

A rupture process analysis of the 1952 earthquake using seismic waves has already been performed by Yamanaka and Kikuchi [2003]. However, as noted above, we cannot analyze the entire rupture process using only strong motion data. Therefore, in Chapter 2, we perform joint source inversions of teleseismic data that were recorded with sufficient lengths and strong motion data to understand the entire rupture process of the 1952 earthquake. The 2003 earthquake was recorded by various observation networks, and there are over ten studies concerning the source of the earthquake using various datasets (Table 2–3). However, detailed parameters such as the maximum slip and seismic moment vary. This is probably due in part to the different datasets, model settings and analysis methods. Therefore, we also performed joint source inversions of the 2003 Tokachi-oki earthquake using the same method and fault model and examined the similarities and differences between the two Tokachi-oki earthquakes.

2.2. Data and Methods

The distributions of the observation stations are shown in Figure 2-1. For the waveform data of the 1952 earthquake, copies of analog seismograms were collected from the United States Geological Survey (USGS), the Japan Agency for Marine-Earth

Science and Technology (JAMSTEC), and JMA. In addition, we used the Headquarters for Earthquake Research Promotion (HERP) data retrieval system of the JMA analog seismograms and the records printed in JMA [1957]. These records were manually digitized to obtain the data. Parameters of the historical seismographs used in this study are shown in the Appendix.

Information concerning the time of day is needed to perform source inversion using strong-motion data. However, it is often difficult to obtain such information in the case of old seismograms. To address this problem, we picked *P*-wave arrival times while comparing seismograms of high-gain and strong motion (low-gain) seismographs and assumed that the picked arrival times corresponded to the arrivals reported in the Central Meteorological Observatory (CMO) [1953]. Conversely, the reference time of the teleseismic data in the inversion analysis is the *P*-wave arrival time. We picked these arrivals for both earthquakes. Even though some waveforms have unclear initial arrivals, we determined the arrival times of these waveforms while considering the theoretical arrival times and waveforms with clear initial arrivals. We also used the phase arrival signature written by the operators on those days and the reported arrival times if these were available.

First, we compared the waveforms of the two earthquakes recorded in the stations whose locations were close to each other (Figure 2-1). Because the waveforms of the two earthquakes were recorded by different seismographs, we convolved the instrument responses of the old seismographs to the 2003 waveforms. As shown in Figures 2-2 and 2-3, the waveforms of the two earthquakes have comparable amplitudes, indicating that these two earthquakes had similar magnitudes. However, there are two distinct differences in the waveforms of the two earthquakes. One is that, in some 1952

teleseismic waveforms such as the UD components of FLO and DBN, there is a large phase near T = 80 s (Figure 2-3) that cannot be seen in the 2003 waveforms, even though it is unclear in the strong motion waveforms. The other is that, in some 1952 waveforms, it is clearly seen that the waveforms begin with a small phase, which also cannot be seen in the 2003 waveforms (Figure 2-4). The Kyoshin Net (K-NET) record is a trigger type record and a sufficient data length prior to the *P*-wave arrival is not available. Therefore, we used the waveforms of the Full Range Seismograph Network of Japan (F-net) in Figure 2-4.

For the source inversion analysis of the 1952 earthquake, we used teleseismic *P*-wave waveforms of 22 components at 11 stations and strong motion waveforms of 9 components at 5 stations (Figure 2-1 and Table 2-4). For the 2003 earthquake, we obtained the teleseismic data from the Incorporated Research Institutions for Seismology Data Management Center (IRIS-DMC) and the strong motion data from K-NET. We used coseismic displacement data estimated using the Global Navigation Satellite System (GNSS) by Larson and Miyazaki [2008]. We made two datasets for the inversion analyses of the 2003 Tokachi-oki earthquake because the amount of data for the 1952 Tokachi-oki earthquake is limited. As shown in Table 2-4, the 2003-L dataset consists of teleseismic, strong motion, and geodetic data and includes a large amount of data. The 2003-S dataset has the same amount of data as the 1952-S dataset and consists of strong motion and teleseismic data. In the inversion analyses, all waveforms were integrated to the displacement, band-pass filtered at 0.02–0.2 Hz for the teleseismic waveforms and at 0.05–0.2 Hz for the strong motion waveforms, and resampled with 0.5 s. We removed the instrument response from the teleseismic waveforms.

We used the source inversion method of Yoshida et al. [1996] and Hikima and

Koketsu [2005]. This method is based on a multi-time window formulation and solves the linear problem with spatial and temporal smoothness constraints using nonnegative least squares. The determination process of the parameter that controls the relative weight of the constraints is described in Section 2.3. We calculated the strong motion, teleseismic, and geodetic Green's functions using the methods of Kohketsu [1985], Kikuchi and Kanamori [1991], and Zhu and Rivera [2002], respectively. One-dimensional (1-D) velocity structure models were extracted from the Japan Integrated Velocity Structure Model (JIVSM) [Koketsu et al., 2008, 2012] underneath each station and were used to calculate the strong motion Green's functions. In the inversion analyses using the 1952-S and 2003-S datasets, the instrumental response was convolved to the strong motion Green's functions. To calculation the teleseismic Green's functions considering the JIVSM around the hypocenters of the two earthquakes, we constructed a 1-D velocity structure model for the near-source structure (Table 2-5). We used the Jeffrey–Bullen model [Bullen, 1963] for the near-receiver structure (Table 2-6). Because geodetic Green's functions are less sensitive to the velocity structure model than waveform Green's functions, we used the same 1-D velocity structure model constructed from the JIVSM for all geodetic stations (Table 2-7). We assumed that the basis source time function for each time window was a boxcar function with a rise time of 5 s and that a rake angle varies between 110±45°. The weights for the teleseismic and strong motion waveforms were set to normalize the root mean squares of the amplitudes of each component. The weight for the geodetic data was set assuming all the geodetic data were waveforms with the root mean squares of their amplitudes being the same as a normalized waveform multiplied by $2n_h + n_v$, where n_h and n_v are the number of horizontal and vertical components, respectively.

Considering the one-week aftershock distributions of the two earthquakes, we constructed a fault model as shown in Figure 2-5a. Even though the hypocentral depths of the two earthquakes determined by JMA (Table 2-1) are a few tens of kilometers deeper than the plate-boundary depth model of Iwasaki et al. [2015], in the JMA catalog, due to the lack of stations above the hypocenters, the depths of the offshore earthquakes around the 2003 earthquake tend to be mapped deeper than the depths determined using ocean bottom seismometers [Shinohara et al., 2004; Yamada et al., 2005]. Therefore, we assumed that the hypocenters of the two earthquakes were located at the plate-boundary and fit the fault model accordingly (Figures 2-5b and 2-5c). We divided the fault into 17 × 14 subfaults whose fault sizes were 15 km × 15 km. Because the distances of the epicenters of the two earthquakes are close to the subfault size, we used the same fault model for the two earthquakes but changed the location of the subfault where the rupture was initiated.

2.3. Results

First, we performed a joint source inversion using the 2003-L dataset. We set four time windows for each subfault and determined the rupture front velocity, which controls the start times of the first time windows of each subfault, to be 3.3 km/s considering the variance versus the rupture front velocity. The weight of the constraints was determined by minimizing the Akaike Bayesian Information Criterion (ABIC) [Akaike, 1980] in this dataset. The obtained slip distribution shows that the maximum slip of 7.5 m is located in the Tokachi-oki region and that the rupture primarily propagated in the down dip direction from the rupture initiation point and then in the northeastern direction (Figures 2-6a and 2-6b). The apparent moment rate function,

which was calculated by treating the fault model as a plane, has a large peak near $T = 25$ s (Figure 2-6c). We calculated the moment rate function in a simple way because we assumed a complex non-planar fault model. If we set the main rupture area in the Tokachi-oki region as shown by the light gray rectangle in Figure 2-6a, the obtained seismic moment in the area was 1.7×10^{21} Nm, which yields an M_w of 8.1. Note that we show the largest absolute eigenvalue of the moment tensor as the seismic moment in this thesis. The overall fittings of the synthetic to the observed data are satisfactory (Figure 2-7).

Next, we performed a joint source inversion using the 2003-S dataset. We re-determined the rupture front velocity as 2.8 km/s in a similar manner as the 2003-L model and set the same number of time windows. However, in the inversions of these datasets, we did not use the ABIC to determine the weight of the constraints because unreasonable slips distributions were obtained. Instead, we determined the weight so that the seismic moment of the main rupture area in the Tokachi-oki region is nearly the same as the 2003-L model. As shown in Figures 2-8a and 2-8b, the maximum slip of 6.9 m is located in the Tokachi-oki region and the rupture primarily propagated in the down dip direction from the rupture initiation point. The apparent moment rate function has a large peak near $T = 25$ s, and the overall shape is similar to that of the 2003-L model (Figures 2-6c and 2-8c). The overall fittings of the synthetic to the observed data are also satisfactory (Figure 2-9).

Finally, we performed a joint source inversion using the 1952-S dataset. We determined the rupture front velocity to be 2.5 km/s and again set four time windows. The weight of the constraints is the same as that for the 2003-S model. The obtained slip distribution shows that there are two large slip peaks of 6.9 m and 6.0 m in the

Tokachi-oki and Akkeshi-oki regions, respectively (Figure 2-10a). The rupture primarily propagated from the rupture initiation point in the down dip direction and then in the northeastern direction, which in this case leads to another large slip in the Akkeshi-oki region (Figure 2-10b). If we set the main rupture area in the Akkeshi-oki region as shown in the gray rectangle in Figure 2-10a, the seismic moment of the region was 1.1×10^{21} Nm (M_w 8.0). Conversely, the seismic moment of the main rupture area in the Tokachi-oki region was 1.6×10^{21} Nm (M_w 8.1). The apparent moment rate function has two large peaks that correspond to the ruptures in the Tokachi-oki and Akkeshi-oki regions (Figure 2-10c). The overall fittings of the synthetic to the observed data are also satisfactory (Figure 2-11).

2.4. Discussion and conclusions

The inversions cannot satisfactorily resolve the small initial rupture in the 1952 earthquake (Figure 2-4) in the inversion analysis. For this reason, we examined this small initial rupture in detail. We estimated the first motion solution of the 1952 earthquake using the polarity of the first motions that were reported to the International Seismological Centre (ISC) and JMA. To plot the polarity data we calculated takeoff angles using the 1-D JMA2001 velocity structure model [Ueno et al., 2002] for the stations whose epicentral distances are less than 2000 km and the Preliminary Reference Earth Model [Dziewonski et al., 1981] for the teleseismic stations whose epicentral distances were between 35° and 95°. As the polarity data may include errors due to various causes such as artificial mistakes and the performance of the seismographs, we determined a plausible solution via trial and error (Figure 2-12a). We then used the first motion solution to calculate the synthetic waveforms using the same method as used in

the inversion analysis and convolved the instrumental response to the synthetic waveforms. We found that the initial part of the waveforms can be reproduced well when we assume 1.8×10^{18} Nm (M_w 6.1) and an isosceles triangle source time function with a rise time of 5.5 s (Figure 2-12b). This duration was calculated using the Eq. (1) in Ekström et al. [2012].

The results of the 2003 earthquake using the 2003-L and 2003-S datasets are generally similar to each other, indicating that the 2003-S and 1952-S datasets are sufficient to obtain rough rupture processes. However, a slip with an over 4-m peak is obtained in the 2003-S model near trench (Figure 2-8a). This slip is probably an artifact due to the error of the waveform Green's function resulted from using the 1-D velocity structure models and the limited amount of data because there is only a ~2-m slip in the 2003-L model (Figure 2-6a) and a ~3-m slip in the 1952-S model (Figure 2-10a) at the same location. Moreover, the tsunami data analyses of the 2003 earthquake [Hirata et al., 2004; Tanioka et al 2004a] do not support the existence of such a slip near the trench.

The inversion results showed that the two earthquakes have similar rupture patterns in the Tokachi-oki region (Figures 2-13a and 2-13b). The last event that ruptured the Tokachi-oki region prior to 1952 may be a large earthquake in 1843 [Satake, 2017], and if that is the case, the two most recent event intervals are 109 and 51 years. This suggests that there is no relationship between the slip amounts and the events intervals. The 1952 earthquake also had a large slip in the Akkeshi-oki region (Figure 2-13b). Previous source studies of the 1952 earthquake using the tsunami data [Hirata et al., 2003; Satake et al., 2006] suggested that the rupture area of the 1952 earthquake extended to the Akkeshi-oki region. Our result is consistent with their results, even though the locations of the peak slips are slightly different from those of previous

studies (Figures 2-13b and 2-13c).

The M_w 8.3 and M_w 7.8 Nemuro-oki earthquakes [Tanioka et al., 2007] occurred in 1894 and 1973, respectively (Figure 2–13b). Tsunami data analyses suggest that the source area of the 1894 earthquake included both the Nemuro-oki and Akkeshi-oki regions and was larger than that of the 1973 earthquake, which only included the Nemuro-oki region [Tanioka et al., 2007]. The obtained large slip area in the Akkeshi-oki region in the 1952-S model is located between the source regions of the 1952 Tokachi-oki and 1973 Nemuro-oki earthquakes and may have been ruptured in the 1894 earthquake.

In 2004, M_{JMA} 7.1 and M_{JMA} 6.9 earthquakes occurred on 28 November and 6 December, respectively, approximately one year after the 2003 earthquake, in the Akkeshi-oki region (Figure 2-13a). The epicenters of these earthquakes are located near the area where a large slip occurred during the 1952 earthquake. However, according to the Global Centroid-Moment-Tensor (GCMT) Project [Ekström et al., 2012], the M_w values of these earthquakes were 7.0 and 6.7, therefore, the sum of their seismic moments is far less than the seismic moment of the 1952 earthquake in the Akkeshi-oki region. Moreover, no other earthquakes with magnitudes larger than M_w 7.0 occurred in this region prior to 2017. Furthermore, M_{JMA} 7.2 and 6.9 earthquakes also occurred on 11 August and 15 November, respectively, in 1961, approximately nine years after the 1952 earthquake, in the Akkeshi-oki region (Figure 2-13b). Even though the details of these earthquakes were not investigated in this thesis, the similarity of the waveforms recorded at the Hiroo and Obihiro JMA stations, where there was little movement between 1961 and 2004, suggests that these two M7 class earthquake pairs ruptured in nearly the same region (Figure 2-14). Therefore, there was no large strain release in the

Akkeshi-oki region after the 2003 earthquake compared to that after the 1952 earthquake, at least by regular earthquakes.

In conclusion, the rupture pattern in the Tokachi-oki region is similar for the 1952 and 2003 earthquakes. Conversely, the initiations of these two earthquakes and the large slip in the Akkeshi-oki region in the 1952 earthquake make these earthquakes different.

Table 2-1. Hypocentral information determined by JMA.

Earthquake	Origin time (UTC)	Latitude (°N)	Longitude (°E)	Depth (km)	M_{JMA}
1952 Tokachi-oki	04/03/1952 1:22:43.58	41.7057	144.1512	52	8.2
2003 Tokachi-oki	25/09/2003 19:50:07.42	41.7785	144.0785	45	8.0

Table 2-2. Results of the previous source studies of the 1952 Tokachi-oki earthquake.

Data	Maximum slip (m)	M_0 (10^{21} Nm)	M_w	Reference
Teleseismic	-	-	8.1	Hartzell & Heaton [1985]
Geodetic	-	2.0–2.6	8.1–8.2	Kasahara [1975]
Strong motion	≥2	0.58	7.8	Yamanaka & Kikuchi [2003]
Tsunami	7.16	1.87	8.1	Hirata et al. [2003]
Geodetic	3.2	1.3	8.0	Nishimura [2006]
Tsunami	4.55–6.74	1–4	8.0–8.3	Satake et al. [2006]

Table 2-3. Results of the previous source studies of the 2003 Tokachi-oki earthquake.

Data	Maximum slip(m)	M_0 (10^{21} Nm)	M_w	Reference
Teleseismic	5.8	1.0	8.0	Yamanaka and Kikuchi [2003]
Static GNSS	≥5	2.8	8.2	Miura et al. [2004]
Teleseismic and strong motion	6.1	1.7	8.1	Yagi [2004]
Strong motion	5.9	2.9	8.2	Honda et al. [2004]
Strong motion and static GNSS	7.1	2.2	8.2	Koketsu et al. [2004]
Static GNSS	4–6	-	-	Ozawa et al. [2004]
Tsunami	3.3	1.1	8.0	Tanioka et al. [2004a]
Teleseismic	5	1.8	8.1	Horikawa [2004]
1 Hz GNSS	~9	1.8	8.1	Miyazaki et al. [2004b]
Geodetic	≥4	2.0	8.2	Nishimura [2006]
Strong motion and static GNSS	7.6	2.3	8.2	Hikima et al. [2005]
Teleseismic	4.0	1.1	8.0	
Tsunami	-	1.0	8.0	
Static GNSS	5.3	-	-	Miyazaki and Larson [2008]
Strong motion	~13	2.06	8.2	Nozu and Irikura [2008]
Strong motion	≥6	3.4	8.3	Aoi et al. [2008]
Teleseismic	12.6	2.18	8.2	Robinson and Cheung [2010]
Tsunami and static GNSS	5.8	1.6	8.1	Romano et al. [2010]

Table 2-4. Number of stations and components of data used in the inversion analyses.

Dataset	Strong motion	Teleseismic	Geodetic	
			Horizontal	Vertical
2003-L	17 stations 51 components	27 stations 27 components	52 stations 52 components （GNSS)	23 stations 23 components (GNSS)
2003-S	5 stations 9 components	12 stations 22 components	Not used	Not used
1952-S	5 stations 9 components	12 stations 22 components	Not used	Not used

Table 2-5. 1-D near-source velocity structure model for the teleseismic Green's function calculation.

Thickness (km)	Vp (km/s)	Vs (km/s)	ρ (g/cm^3)
1.0	1.5	0.0	1.02
0.5	2.0	0.6	2.00
0.75	2.4	1.0	2.15
2.5	3.0	1.5	2.25
0.75	3.5	2.0	2.35
7.5	5.8	3.4	2.70
12.0	6.4	3.8	2.8
∞	7.5	4.5	3.20

Table 2-6. 1-D near-receiver velocity structure model for the teleseismic Green's function calculation.

Thickness (km)	Vp (km/s)	Vs (km/s)	ρ (g/cm^3)
15.0	5.57	3.36	2.65
18.0	6.50	3.74	2.87
∞	8.10	4.68	3.30

Table 2-7. 1-D velocity structure model for the geodetic Green's function calculation.

Thickness (km)	Vp (km/s)	Vs (km/s)	ρ (g/cm^3)	Qp	Qs
5.5	5.57	3.36	2.65	680	400
7.5	6.50	3.74	2.87	680	400
12.0	8.10	4.68	3.30	680	400
∞	7.5	4.5	3.2	850	500

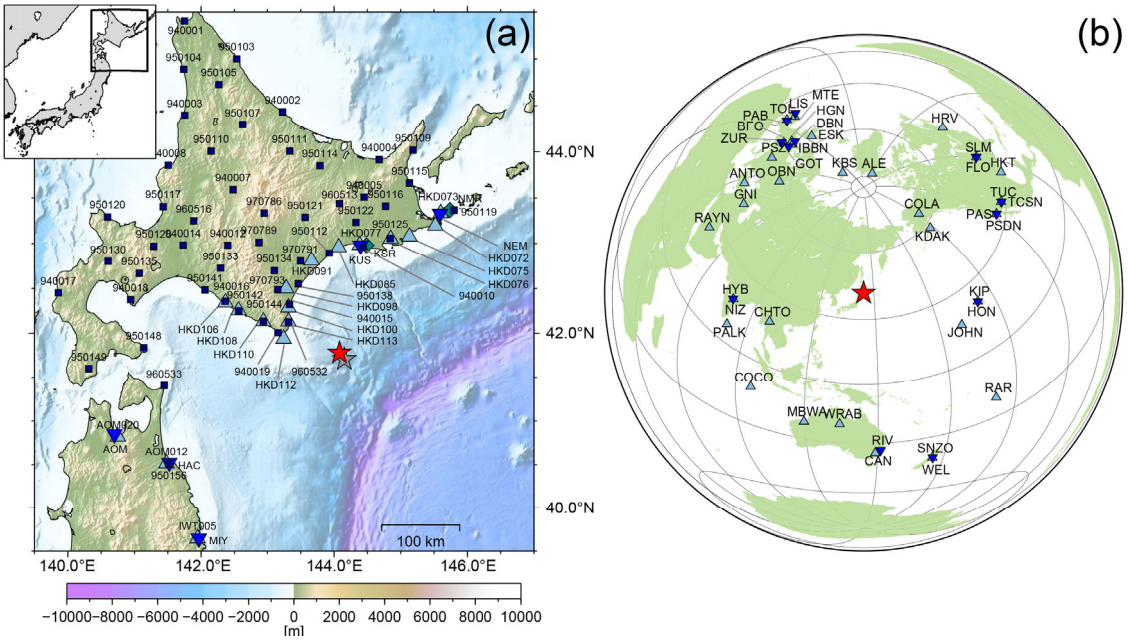

Figure 2-1. (a) Near-field and (b) teleseismic station maps. The gray and red stars denote the epicenters of the 1952 and 2003 Tokachi-oki earthquakes determined by JMA, respectively. The blue inverted triangles and sky blue triangles indicate the seismic stations in 1952 and 2003, respectively. The blue-green diamonds indicate the F-net stations. In panel (a), the black rectangle in the inset map represents the map area and the background colors show the topography of GEBCO 2014 [Weatherall et al., 2015].

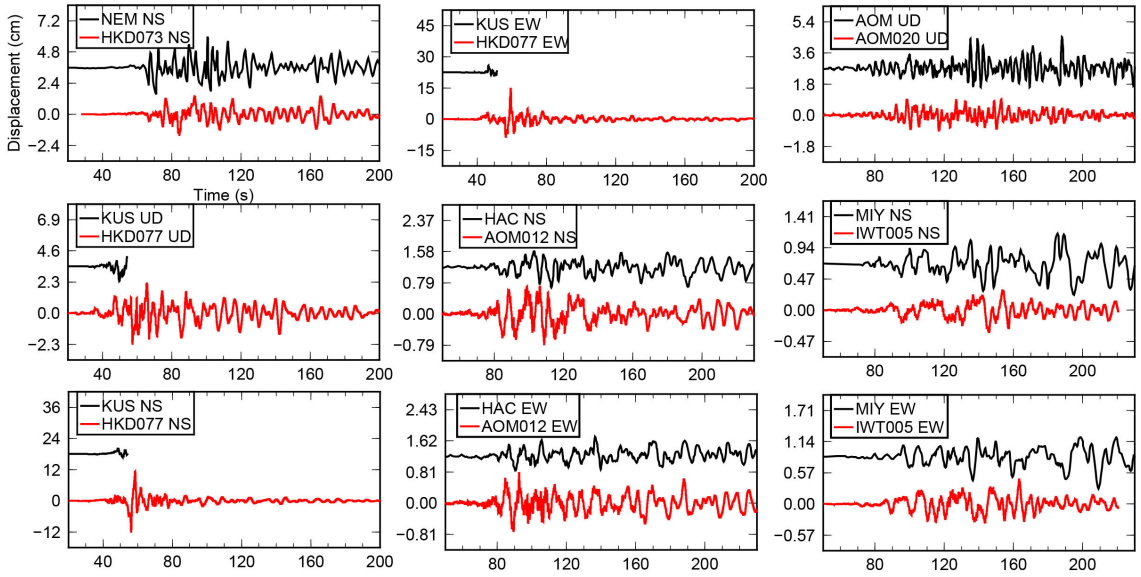

Figure 2-2. Comparisons of the strong motion waveforms. The black and red lines show the waveforms of the 1952 and 2003 earthquakes, respectively. For each waveform pair, the instrument response is equalized with the 1952 waveform. The stations names and components are shown in each legend. The 1952 and 2003 waveforms are plotted with origin times of $T = -7.5$ s and 0 s, respectively.

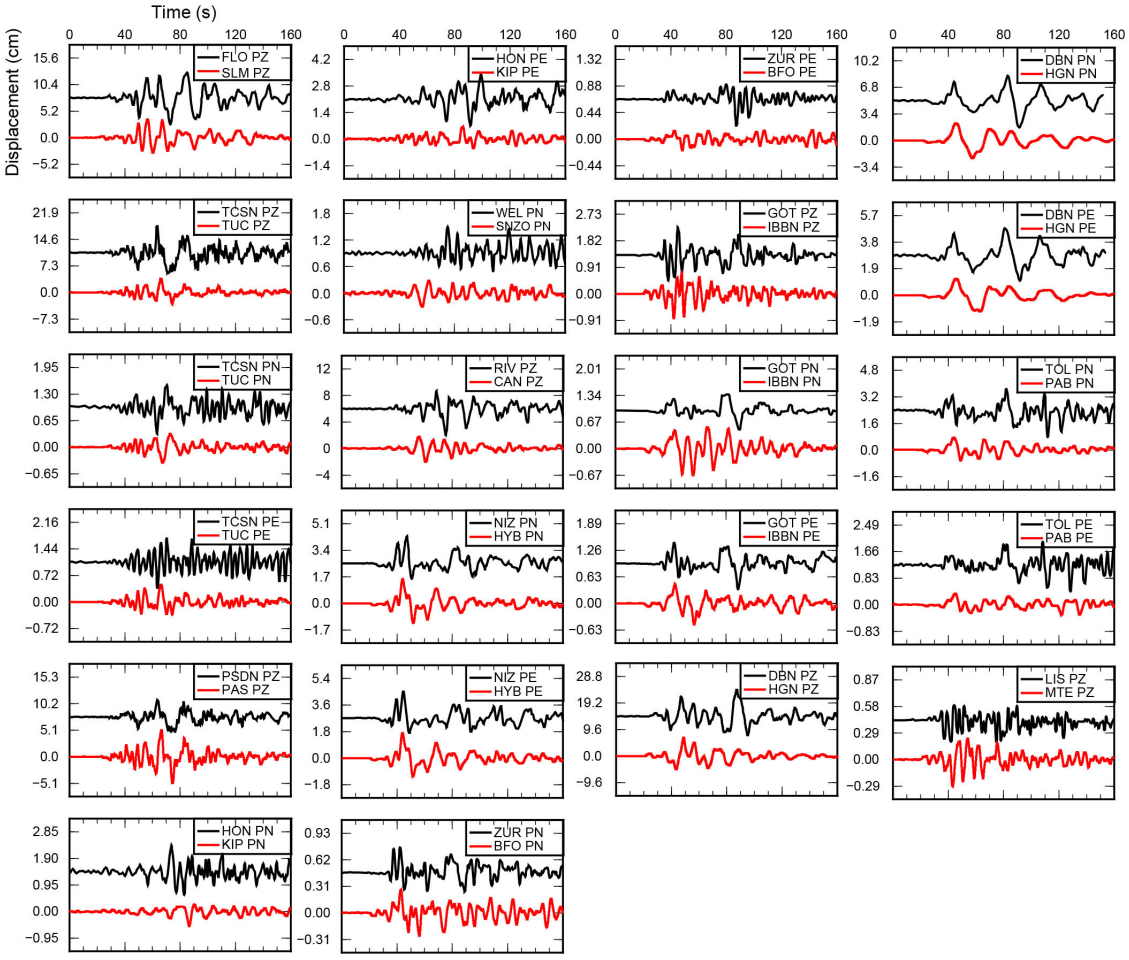

Figure 2-3. Comparisons of the teleseismic waveforms. The black and red lines show the waveforms of the 1952 and 2003 earthquakes, respectively. For each waveform pair, the instrument response is equalized with the 1952 waveform. The stations names and components are shown in each legend. The 1952 and 2003 waveforms are plotted with *P*-wave arrival times of $T = 22.5$ s and 30 s, respectively.

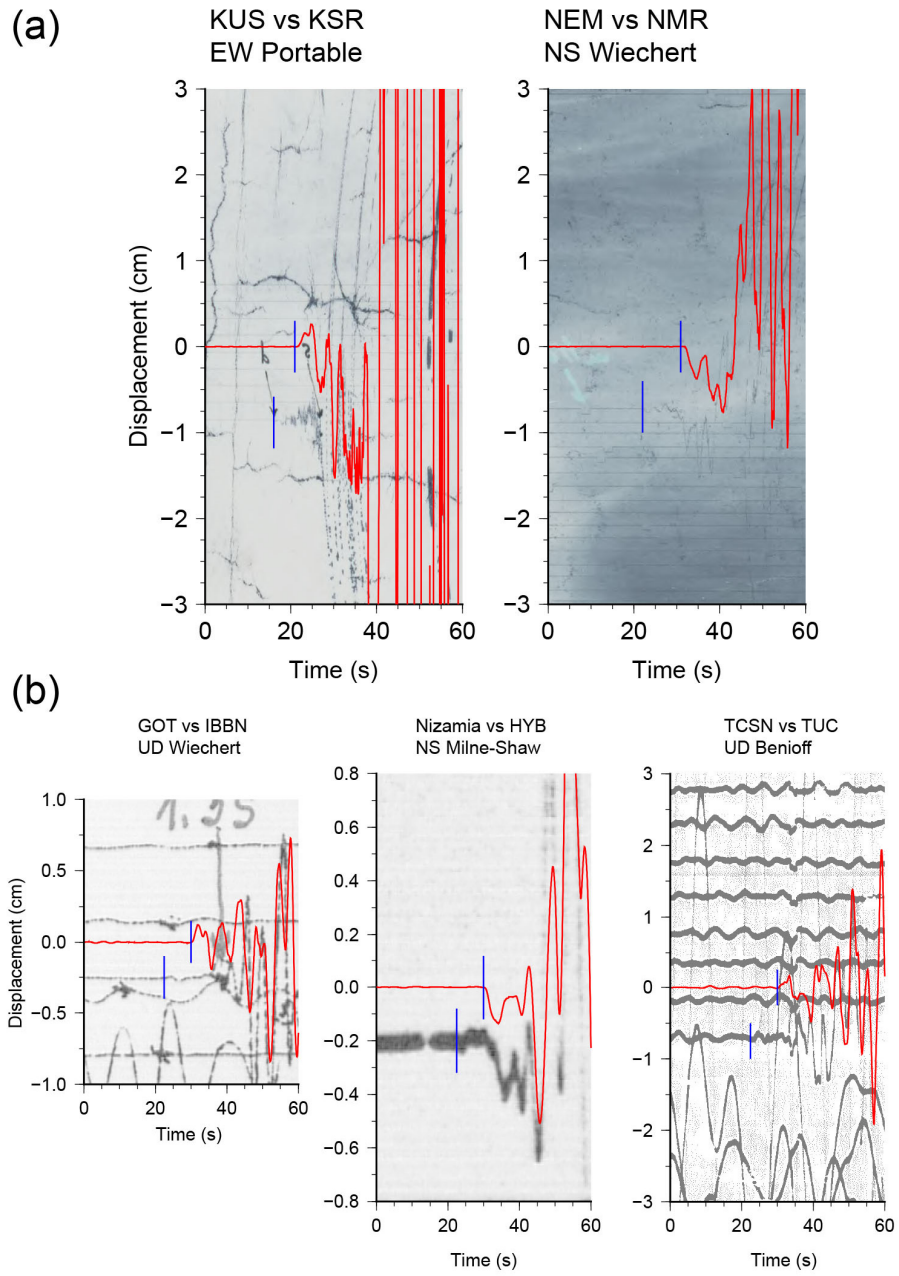

Figure 2-4. Comparisons of the initial parts of waveforms. The Red lines show the waveforms of the 2003 earthquake. The background images show the original waveforms of the 1952 earthquake. The blue lines indicate the arrival time. For each waveform pair, the instrument response is equalized with the 1952 waveform. The stations names, components, and instrument names are shown above each waveform pair. The reference times of the plots are the same as in Figures 2-2 and 2-3.

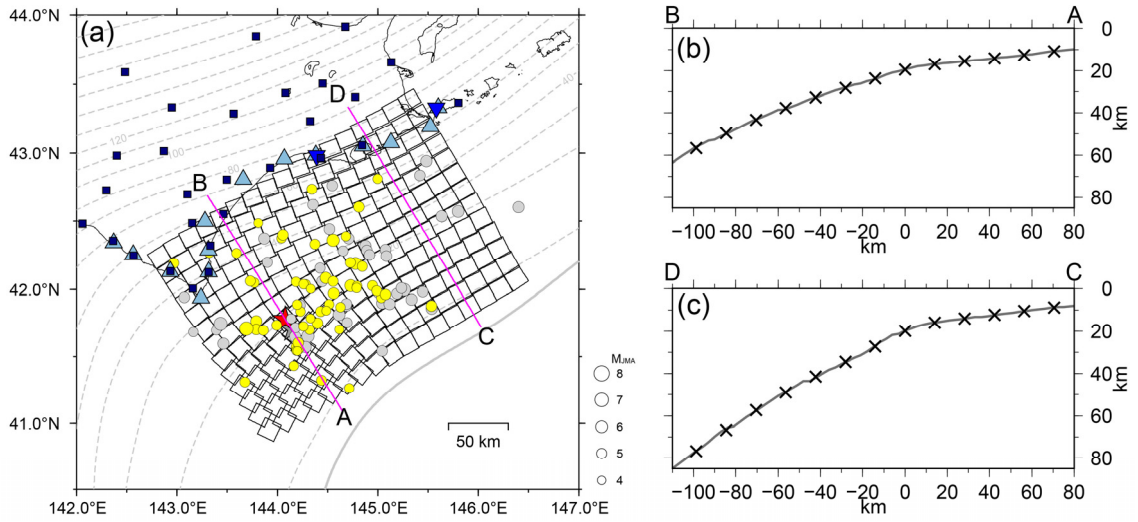

Figure 2-5. (a) Fault model of the inversion analyses. The black lines show the fault model. The light gray and yellow circles indicate the one-week aftershocks of the 1952 and 2003 earthquakes (M_{JMA} > 4.5), respectively. The plate-boundary depth and the trench axis [Iwasaki et al., 2015] are represented by the light gray broken lines with 10-km contour intervals and the light gray line, respectively. The purple lines show the locations of the cross sections described in panels (b) and (c). Other aspects are the same as in Figure 2-1a. (b) and (c) Cross sections along the lines AB and CD in panel (a). The black crosses denote the locations of the point sources (i.e., the centers of each subfault). The gray lines show the plate-boundary [Iwasaki et al., 2015].

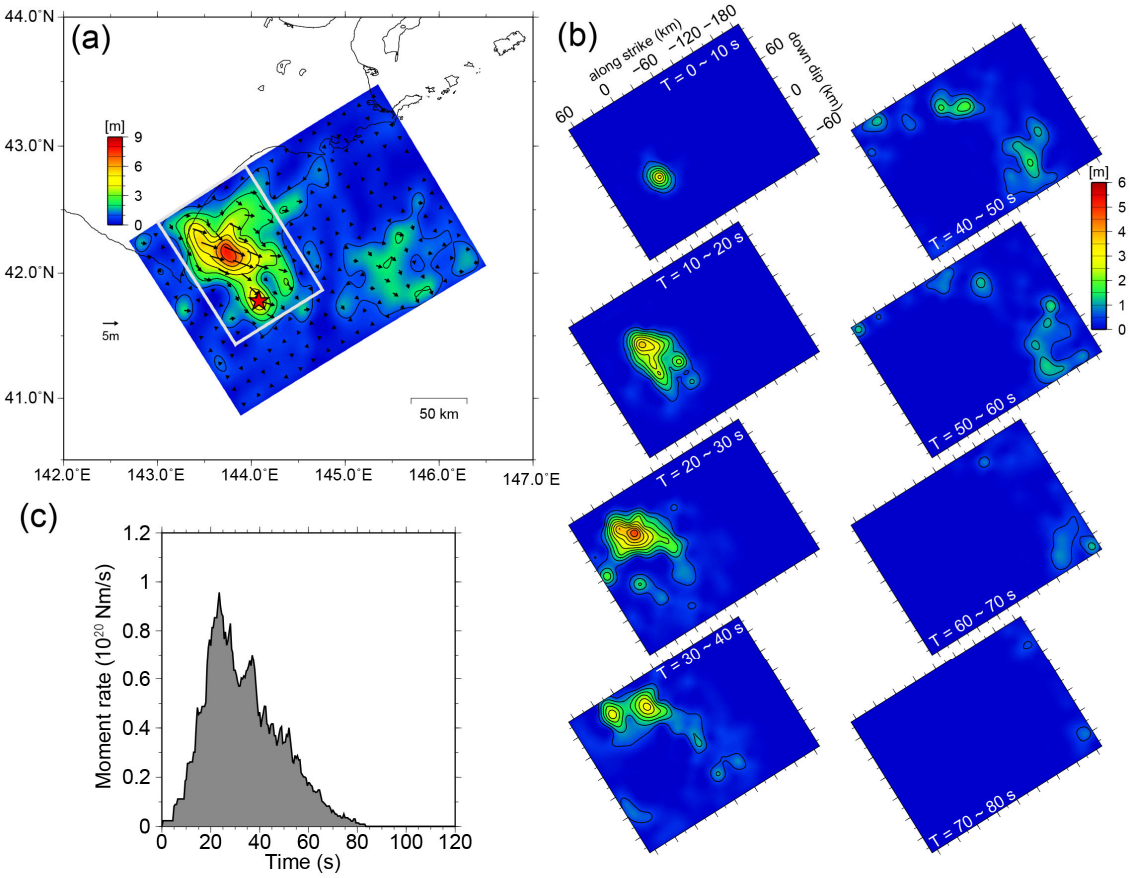

Figure 2-6. Inversion results of the 2003-L dataset. (a) The obtained slip distribution. The contour interval is 1 m. The light gray rectangle represents the main rupture area in the Tokachi-oki region. The red star denotes the epicenter of the 2003 Tokachi-oki earthquake. (b) Snapshots of the slip distribution. The contour interval is 0.5 m. (c) Apparent moment rate function.

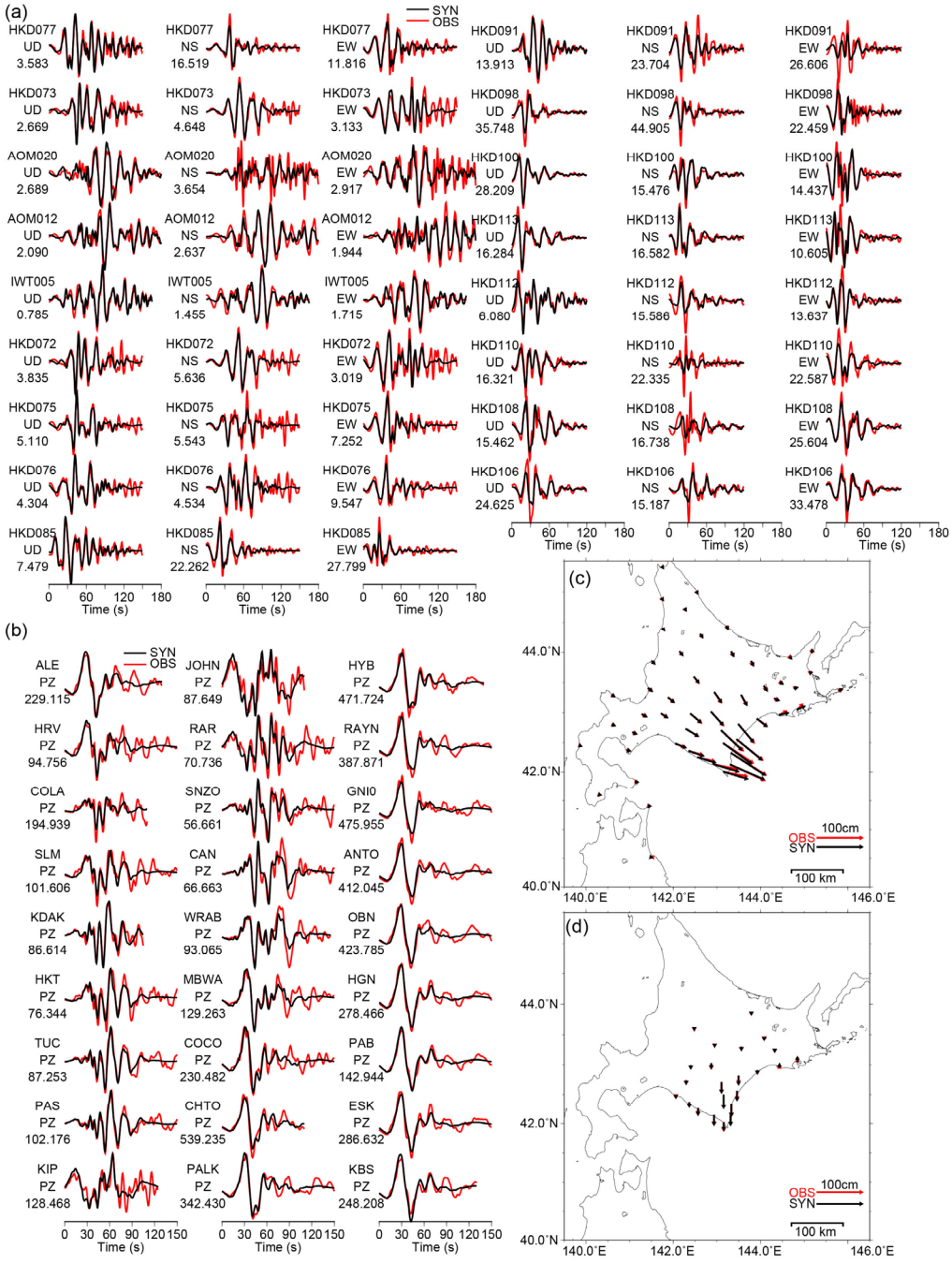

Figure 2-7. (a) Strong motion, (b) teleseismic, and (c) horizontal and (d) vertical static displacement data fittings of the 2003-L dataset. The observed and synthetic data are shown with the black and red lines/arrows, respectively. The station names, components, and maximum amplitude (cm/s for strong motion and μm for teleseismic) are shown to the left of each waveform.

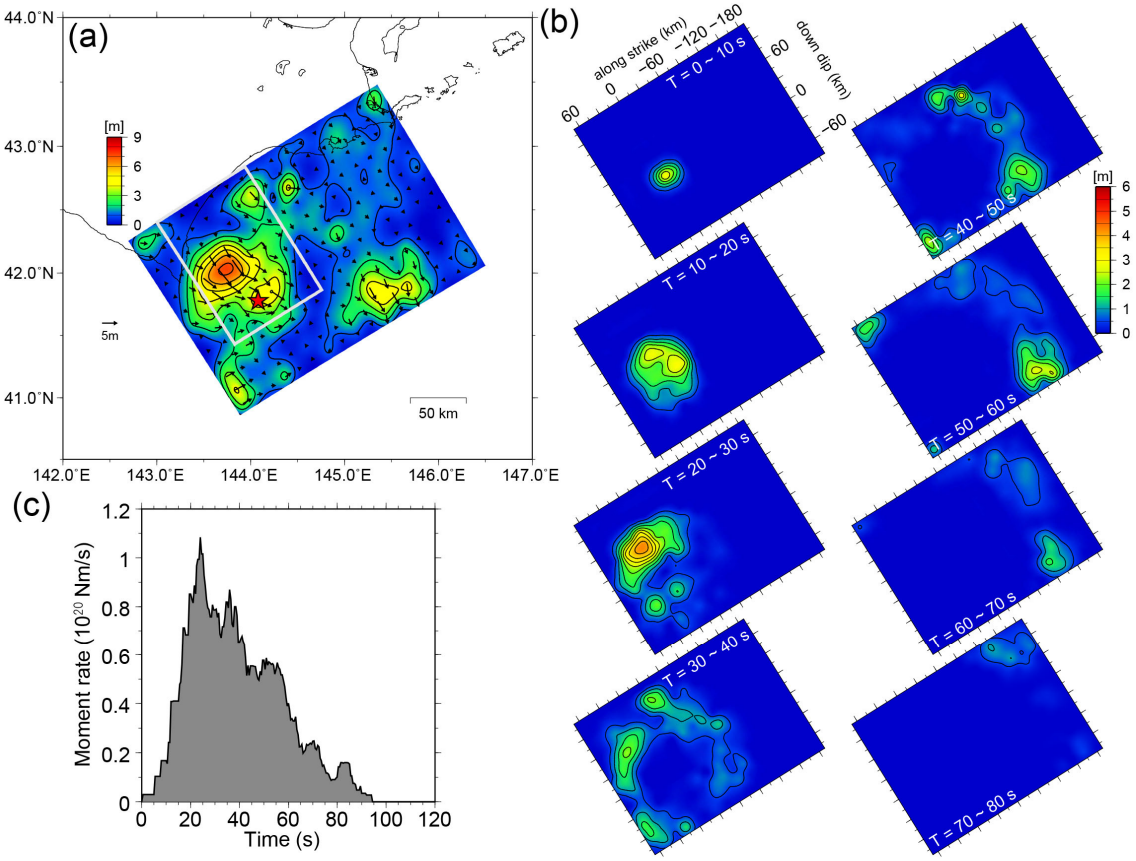

Figure 2-8. Inversion results of the 2003-S dataset. (a) The obtained slip distribution. The contour interval is 1 m. The light gray rectangle represents the main rupture area in the Tokachi-oki region. The red star denotes the epicenter of the 2003 Tokachi-oki earthquake. (b) Snapshots of the slip distribution. The contour interval is 0.5 m. (c) Apparent moment rate function.

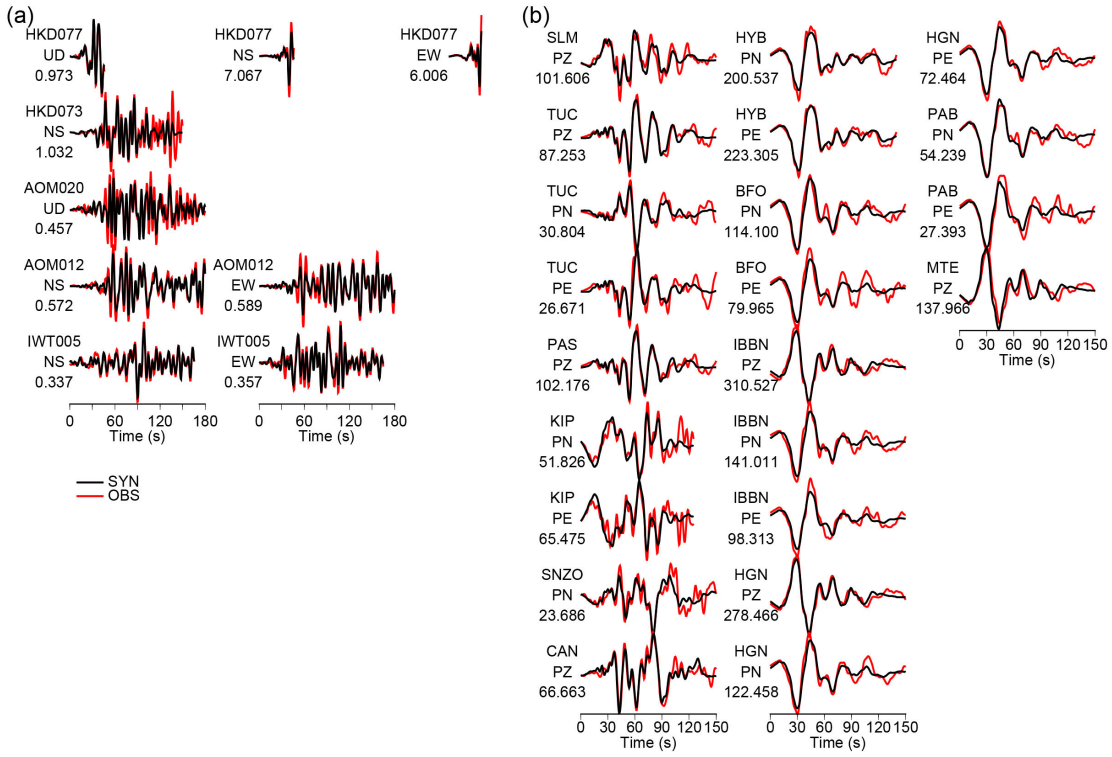

Figure 2-9. (a) Strong motion, and (b) teleseismic data fittings of the 2003-S dataset. The observed and synthetic data are shown by the black and red lines, respectively. The station names, components, and maximum amplitude (cm/s for strong motion and μm for teleseismic) are shown to the left of each waveform.

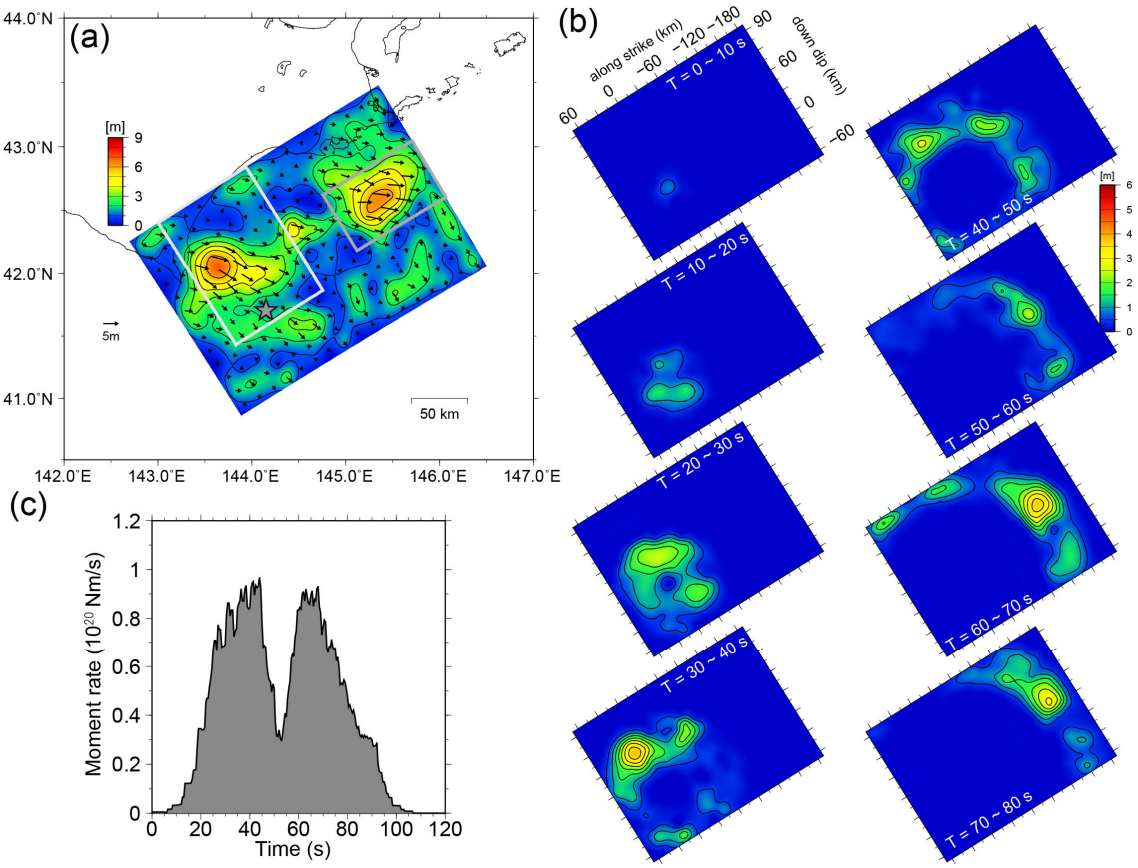

Figure 2-10. Inversion results of the 1952-S dataset. (a) The obtained slip distribution. The contour interval is 1 m. The light gray and gray rectangles represent the main rupture area in the Tokachi-oki and Akkeshi-oki regions, respectively. The gray star denotes the epicenter of the 2003 Tokachi-oki earthquake. (b) Snapshots of the slip distribution. The contour interval is 0.5 m. (c) Apparent moment rate function.

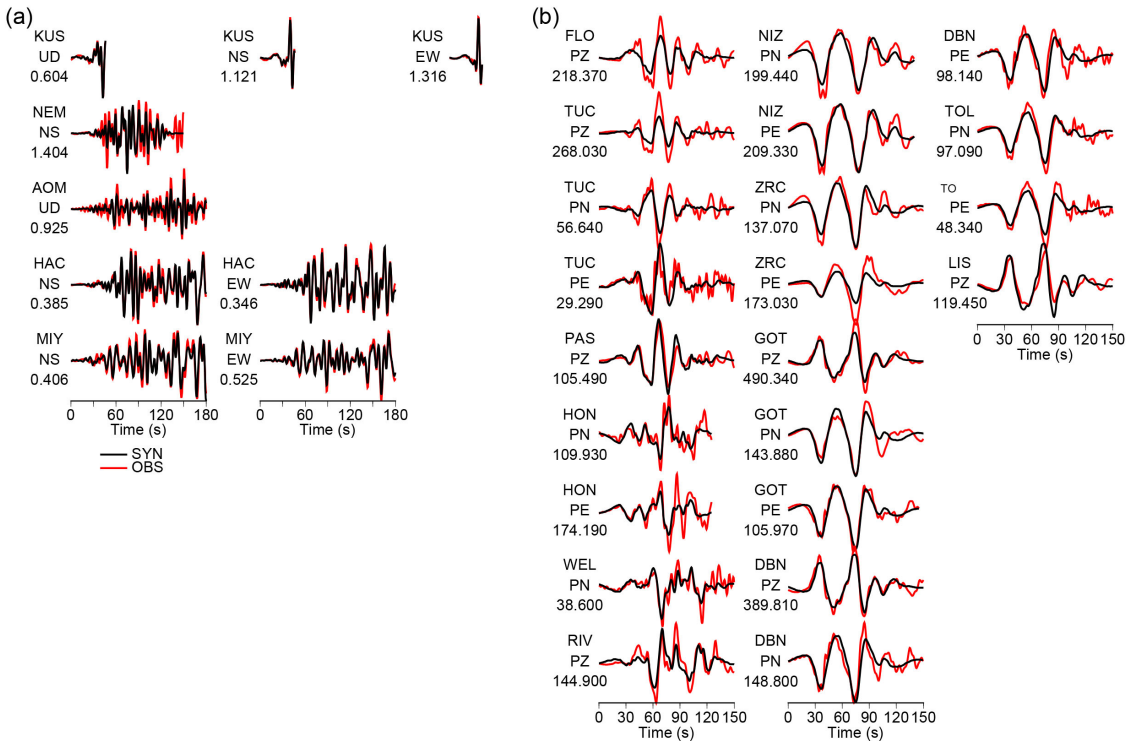

Figure 2-11. (a) Strong motion, and (b) teleseismic data fittings of the 1952-S dataset. The observed and synthetic data are shown by the black and red lines, respectively. The station names, components, and maximum amplitude (cm/s for strong motion and μm for teleseismic) are shown to the left of each waveform.

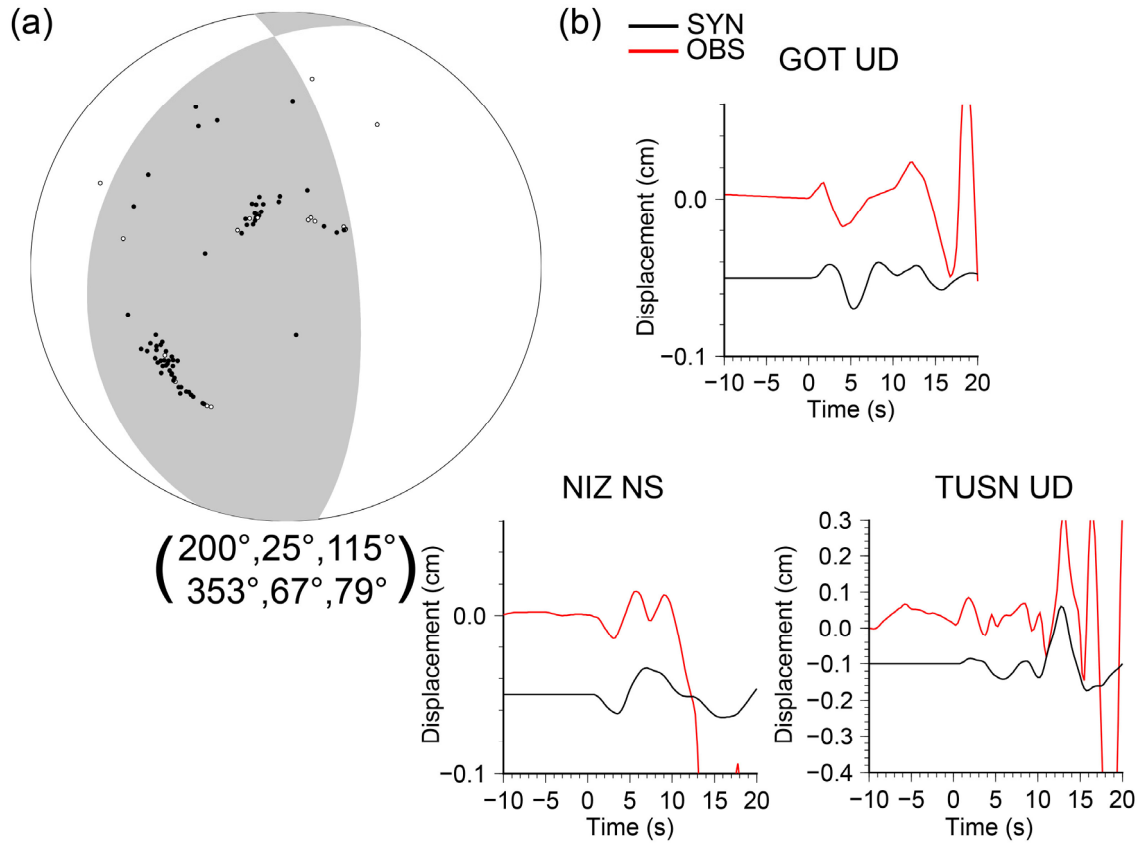

Figure 2-12. (a) Estimated *P*-wave first motion solution for the 1952 earthquake. The black and white circles indicate the reported compressional and dilatational first motions, respectively. The fault plane solutions (strike, dip, rake) are shown below the focal mechanism. (b) The observed and synthetic waveforms (0.25-s sampled and band-passed between 0.001 Hz and 1.0 Hz). The waveforms are plotted for an initial arrival of $T = 0$ s. The station names and components are drawn above each plot.

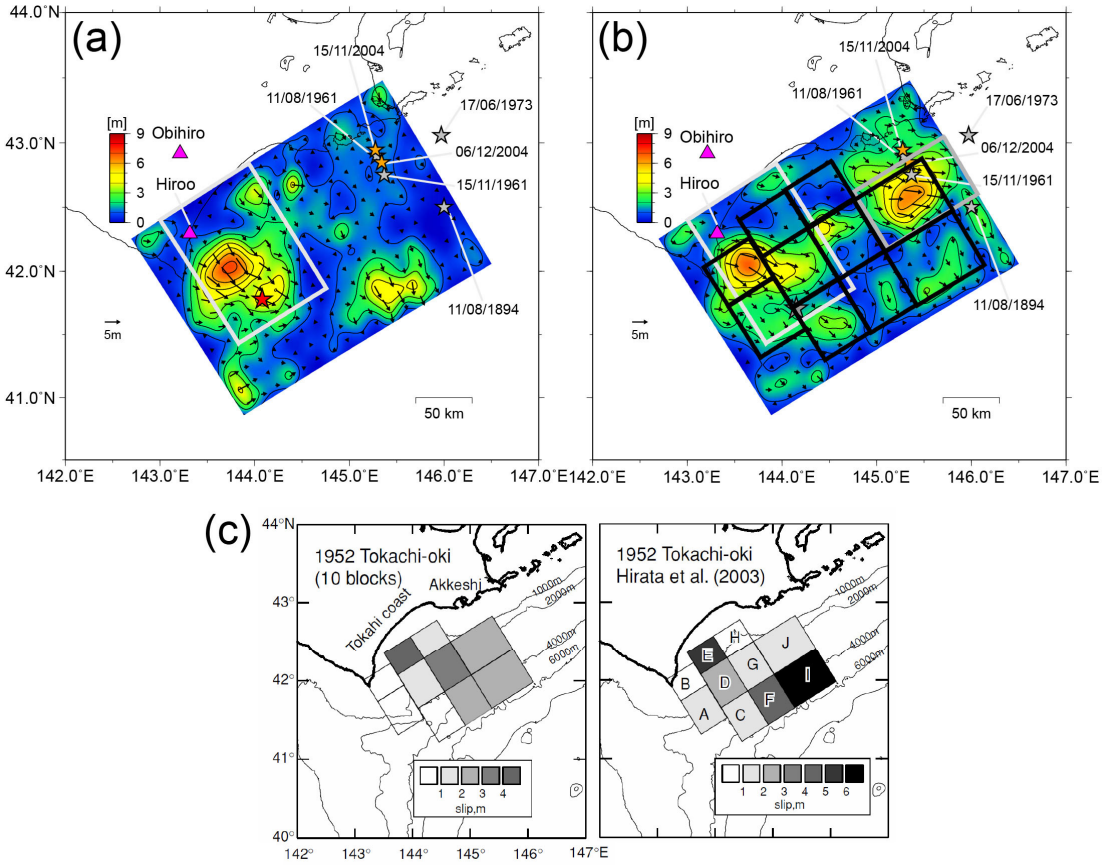

Figure 2-13. Slip distributions of the (a) 2003-S and (b) 1952-S models. The thick black lines represent the fault model of Hirata et al. [2003] and Satake et al. [2006]. The stars indicate the epicenters of significant earthquakes. The epicenter location of the 1894 Nemuro-oki earthquake is from Utsu [1982], and other locations are from the JMA catalog. The purple triangles indicate the seismic stations where the observed waveforms of the 1961 and 2004 earthquakes are shown in Figure 2-14. Other symbols are the same as those in Figures 2-8a and 2-10a. (c) Slip distributions of the 1952 earthquake estimated by Satake et al. [2006] (left) and Hirata et al. [2003] (right).

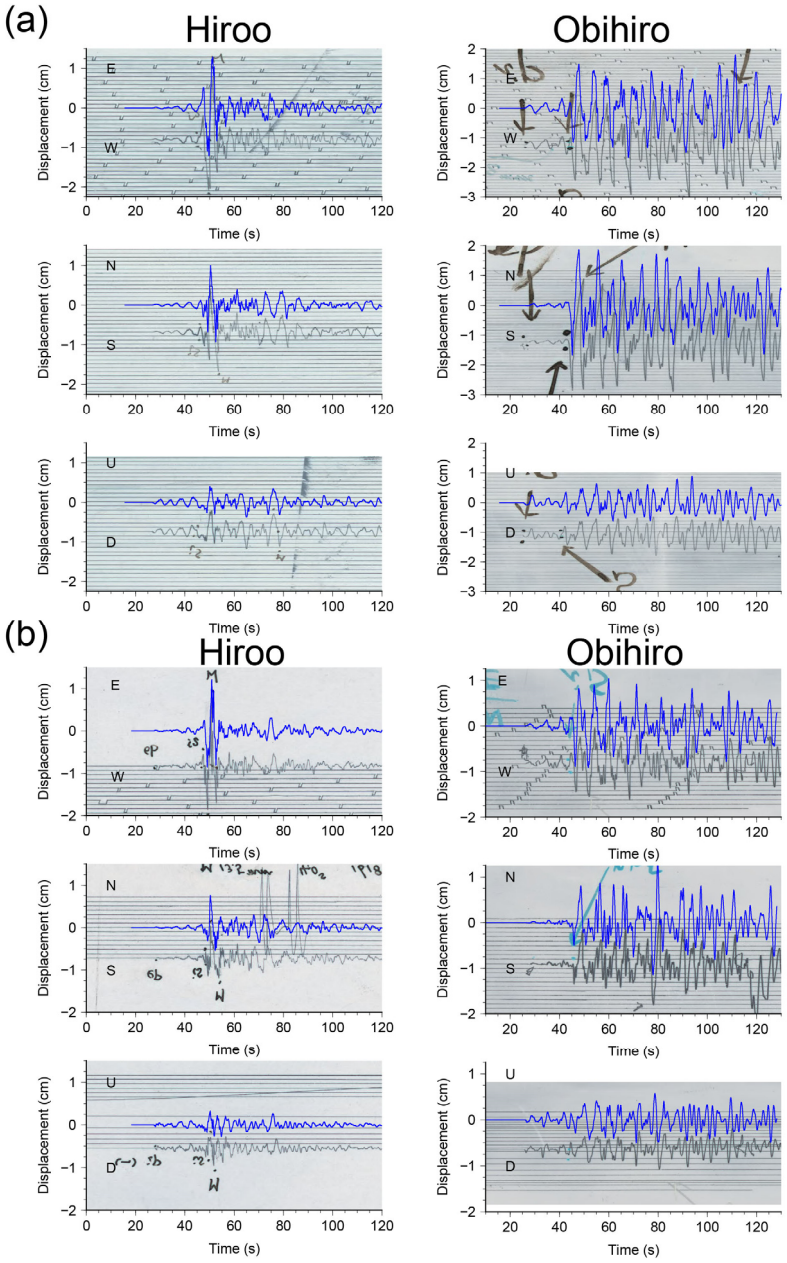

Figure 2-14. Comparisons of the observed waveforms at the Hiroo and Obihiro stations (a) between the 28/11/2004 M_{JMA} 7.1 and 11/08/1961 M_{JMA} 7.2 earthquakes and (b) between the 06/12/2004 M_{JMA} 6.9 and 15/11/1961 M_{JMA} 6.9 earthquakes. The blue lines show the observed waveforms of the 2004 earthquakes and the background images show the observed waveforms of the 1961 earthquakes. The locations of the stations are shown in Figure 2–13.

3. Slip deficit and afterslip prior to and after the 2003 Tokachi-oki earthquake

3.1. Introduction

Observed crustal deformations near subduction zones during interseismic periods can largely be attributed to the locking of the plate interface and to transient phenomena on the interface. The slip deficit model introduced by Savage [1983] that assumes the crustal deformation can be expressed by a combination of stable slips, which are negligible, and normal faulting (back slip) on the plate interface has been widely adopted for various subduction zones such as the Chile [Moreno et al., 2010; Métois et al., 2012], central Andes [Chlieh et al., 2011], Mexican [Yoshioka et al., 2004], Cascadia [Wang et al., 2003], Alaska [Suito and Freymuller, 2009], Kamchatka [Bürgmann et al., 2005], Hikurangi [Wallace et al., 2004], Sumatra [Chlieh et al., 2008], and Nankai [Yokota et al., 2016]. These studies have demonstrated the various patterns of the slip deficit distribution and that regions with large slip deficits generally correspond to the source regions of the previous large to giant earthquakes. This slip deficit model is also used to estimate the potential earthquakes in these regions.

In the Japan Trench and Kuril subduction zone, slip deficits were obtained by Hashimoto et al. [2009; 2012], Loveless and Meade [2010], and Suwa et al. [2006]. These studies used the data between 1996 and 2002 when few earthquakes with M_{JMA} > 7 occurred and obtained the average slip deficit during the data period. Recently, Yokota [2013] and Yokota and Koketsu [2015] analyzed the yearly slip deficit in the Japan Trench and Kuril subduction zone between 1996 and 2010 using the horizontal

component to examine the temporal change in the slip deficit. They reported a long-term aseismic event in Tohoku preceding the 2011 Tohoku earthquake and interpreted it as a very-long-term slow slip event. This preceding phenomenon was also pointed out by Ozawa et al. [2012] and Mavrommatis et al. [2014]. The afterslip of the 2003 Tokachi-oki earthquake up to one year after the earthquake has been examined in previous studies [Miura et al., 2004: Miyazaki et al., 2004a; Miyazaki and Larson, 2008; Ozawa et al., 2004; Baba et al., 2006; Ito and Nishimura; 2016, Sato et al., 2010]. These studies showed that the afterslip occurred around the coseismic rupture zone.

In this chapter, we investigate the crustal deformation prior to the 2003 Tokachi-oki earthquake to examine whether a long-term transient phenomenon existed prior to the earthquake. We also perform slip deficit/afterslip inversions for every year between 25 September 2000 and 24 September 2010 using both horizontal and vertical GNSS data to investigate the inter- and post- seismic periods in the southernmost part of the Kuril subduction zone. We discuss the correspondence between the slip deficit/afterslip distribution and the coseismic rupture area obtained in Chapter 2.

3.2. Crustal deformation prior to the 2003 earthquake

We used the daily coordinate of the F3 solution obtained by the Geospatial Information Authority of Japan (GSI) [Nakagawa et al., 2009]. In this section, we selected stations located in northern Tohoku and Hokkaido (Figure 3-1a). We removed the offsets caused by maintenance such as antenna changes using the values estimated by the GSI (http://www.gsi.go.jp/kanshi/faq2_2.html, in Japanese) and the plate motion using the APKIM2005-DGFI model [Drewes, 2009] assuming that northern Tohoku and Hokkaido are located on the North America plate. A common mode error was estimated

using spatial filtering [Wdowinski et al., 1997] and removed. We selected eight stations (Figure 3-1b) and assumed that the deformations of these stations were linear. Then, we detrended the time series of these stations and simply averaged the detrended data, which we treated as a common mode error. In addition, we estimated the coseismic offsets due to earthquake Nos. 1, 6, 7, 8 and 9 (Table 3-1), which did not cause significant postseismic deformation, and removed them. The coseismic offsets were calculated from the ten-day mean prior to and after the earthquake. To avoid the effect of the crustal deformation due to the eruption of the Mount Usu on 31 March 2000 and its subsequent volcanic activity, we compared the three-year linear trend of the horizontal components between 30 March 1997 to 29 March 2000 and 25 September 2000 to 24 September 2003.

As shown in Figures 3-2 and 3-3, large changes in the trends between the two periods can be seen, especially in northern Tohoku, western Hokkaido, and northeastern Hokkaido. However, no notable changes were obtained around the main rupture area of the 2003 earthquake (Figure 3-2). Around Hokkaido, five earthquakes with $M_{\mathrm{w}} \geq 7.5$ occurred during 1993–1995: the M_w 7.6 1993 Kushiro-oki, M_w 7.7 1993 Hokkaido-Naisei-oki, M_w 8.3 1994 Hokkaido-Toho-oki, M_w 7.7 1994 Sanriku-Haruka-oki, and M_w 7.9 1995 Etorofu earthquakes (Figure 3-2). Because the regions where relatively large trend changes were obtained correspond to the locations of these earthquakes, the trend changes were likely due to the postseismic deformations of these earthquakes.

3.3. Slip deficit and afterslip prior to and after the 2003 earthquake

In this section, we investigate the yearly slip deficit/afterslip distribution of the

southernmost part of the Kuril subduction zone. We used the GEONET stations shown in Figure 3-4 and the F3 solution data from 25 September 2000 to 24 September 2010 because the crustal deformation in the 1990s in Hokkaido was likely affected by the five $M_w \geq 7.5$ earthquakes as shown in Section 3.2, the 2011 Tohoku-oki earthquake and its postseismic phenomena after 2011, and, in western Hokkaido, the plate-boundary between North-America/Okhotsk and Amur/Eurasia in the Sea of Japan. After the same data processing as in Section 3.2, we fit the daily coordinate of the *i*-th component of the *j*-th station via the least-square method using Eq. (3-1) to obtain the yearly crustal deformation of the stations. In Eq. (3-1), a_{ij}–g_{ij} are unknown parameters. The first term expresses the yearly linear trend, the second and third terms express the annual deformation, the fourth term expresses the afterslip of the earthquakes, the fifth term expresses the viscoelastic relaxation, and the sixth term expresses the coseismic offset. $H_0(t)$ is the Heaviside function. We assumed that Eq. (3-1) is continuous except for the coseismic offsets. The unit of t is a day and t_n indicates 25 September of year n. We determined $T^A = 2$ and $T^V = 120$ via trial and error. We considered the afterslip term of earthquakes Nos. 3 and 4, the viscoelastic term of earthquake No. 6, and the coseismic offset term of earthquake Nos. 2, 3, 4, and 5 (Table 3-1). We subjectively determined whether to introduce these terms for each fitting. We considered a viscoelastic

$$\begin{aligned} x_{ij}(t) = \sum_n [\{H_0(t-t_n) - H_0(t-t_{n+1})\}\{a_{ij}^n + b_{ij}^n(t-t_n)] \\ + c_{ij}\sin(2\pi t/365.25) + d_{ij}\sin(2\pi t/365.25) \\ + \sum_k \left[e_{ij}H_0\left(t-t_k^{EQ}\right)\log\{1+(t-t_k)/T^A\}\right] \\ + \sum_l \left[f_{ij}H_0\left(t-t_l^{EQ}\right)(1-\exp\{-(t-t_l)/T^L\})\right] \\ + \sum_m \left[g_{ij}H_0\left(t-t_m^{EQ}\right)\right] \end{aligned} \quad (3\text{–}1)$$

relaxation term only for the EW component and only for the 2006 Kuril earthquake (No. 6, Table 3-1) because postseismic deformation of this earthquake can be seen only in the EW component and Kogan et al. [2011, 2013] suggested that the postseismic deformation after the 2006 Kuril earthquake was primarily caused by viscoelastic relaxation. We extracted the first and fifth terms of Eq. (3-1) and treated them as observation data in the inversion analysis.

We used the same inversion and Green's function calculation methods as in Chapter 2 except that we used a usual, not nonnegative, least-squares method. We assumed 15 × 10 subfaults, as shown in Figure 3-3, and each subfault had a size of 30 km × 30 km. The relative weight of the spatial smoothness constraint of each year was determined by the ABIC.

To check the resolution of our model, we performed a few tests. We calculated the crustal deformation using the three assumed slip distributions (Figures 3-5a to 3-5c). Then, we added a Gaussian error with standard deviations of 0.1 cm for the horizontal component and 0.3 cm for the vertical component according to Nishimura et al. [2004]. We performed inversion analyses treating these synthetic data as observation data. Figures 3-5d–3-5f show the inverted results for each case. These results show that the resolution of the inland and onshore subfaults is generally good at both the 90-km (Figure 3-5d) and 150-km (Figure 3-5f) scales except for the northern subfaults whose depths are greater than 100 km. The resolution of the offshore regions is poor. In particular, there is nearly no resolution ~90 km from the trench (Figure 3-5f).

Figure 3-6 shows the results of the yearly slip deficit/afterslip inversion prior to the 2003 earthquakes. The slip deficit distributions are similar to that of Hashimoto et al. [2009, 2012] in that there are large slip deficits in Tokachi-oki–Nemuro-oki region

(Figures 3-6a–3-6c). These generally correspond to the source regions of the 1952 and 2003 Tokachi-oki earthquakes. Figure 3-7 shows the results for 25/09/2003–24/09/2004, one year after the 2003 earthquake. The afterslip was obtained in and around the source region of the 2003 earthquake with the 70 cm peak and does not reach the Akkeshi-oki–Nemuro-oki region (Figure 3-7a). Figure 3-8 shows the results for 25/09/2004–24/09/2010, two to seven years after the 2003 earthquake. In 25/09/2004–24/09/2005, afterslip is obtained in the Akkeshi-oki region in addition to the Tokachi-oki region (Figure 3-8a). This is due to the M_{w} 7.0 and M_w 6.7 earthquakes that occurred in the Akkeshi-oki region during this period (Figure 3-4). The afterslip of these two M7 class earthquakes does not continue to the next year (Figure 3-8b). The slip deficit/afterslip distribution of the following years show that the afterslip of the 2003 earthquake decayed gradually but still continued up to seven years after the 2003 earthquake (Figures 3-8c and 3-8j to 3-8l). In all the analysis periods, the data fitting was satisfactory.

3.4. Discussion and conclusions

Figure 3-9a shows the three-year averaged slip deficit rate prior to the 2003 earthquake. It is not appropriate to compare the slip deficit distributions obtained in Chapter 3 in detail to the coseismic distribution obtained in Chapter 2 because the slip deficit distributions were estimated using only the geodetic data. Therefore, we performed a coseismic inversion of the 2003 earthquake using only the geodetic data and the same fault model as the slip deficit inversion. The result showed that the 2003 earthquake had a maximum slip of 5.1 m (Figure 3-9b). Then we calculated the sum of accumulated slip deficit during the interval (approximately 51.5 years), the coseismic

slip of the 2003 earthquake, and one-year afterslip of the 2003 earthquake, assuming that the slip deficit rate between the 1952 and 2003 earthquakes was constant (Figure 3-9c). It shows that the sum of the coseismic slip and one year afterslip in the Tokachi-oki region were comparable to or in part exceeding the accumulated slip deficit during the interval (Figure 3-9c).

In the Akkeshi-oki–Nemuro-oki region, the slip deficit rate was nearly constant during the analyses period, expect for the period of 25/09/2004–24/09/2005 when two M7 class earthquakes occurred whose afterslip is included in the slip deficit/afterslip distribution (Figures 3-6, 3-7, and 3-8). Even though the afterslip of the two M7 class earthquakes reached the main rupture of the 1952 earthquake in the Akkeshi-oki region, the slip amount was only comparable to the one-year slip deficit. Therefore, in the Akkeshi-oki region there was no significant strain release after the 2003 earthquake, and large slip deficit probably have been accumulated (Figure 3-9c). Note that the Nemuro-oki earthquake with ~3m slip occurred in 1973 [Tanioka et al., 2007].

The slip deficit distributions prior to the 2003 earthquake (Figure 3-9a) show that, in the Tokachi-oki region, the peak value was located on the border of the main rupture area of the 2003 earthquake, even though the coseismic slip of the 2003 earthquake had a peak value in the center of the main rupture area (Figure 3-9b). The largest afterslip occurred in the northeast region adjacent to the main rupture area of the 2003 earthquake (Figure 3-7a). Miyazaki et al. [2004a] suggested that the region surrounding the main rupture area of the 2003 earthquake had a slip-strengthening frictional property. In the slip deficit distribution, we likely see the entire region including both slip-weakening and slip-strengthening regions, which cannot be distinguished in the slip deficit inversion. If we again assume that the slip deficit between the 1952 and 2003

earthquakes was constant, in the region surrounding the main rupture area, only a part of the accumulated slip during the interval was released by the afterslip of the 2003 earthquake because the amount of afterslip was ~1 m.

Ignoring the viscoelastic relaxation could represent a major error in our model, in particular, after the 2003 earthquake. Sun and Wang [2015] suggested that ignoring the viscoelastic relaxation in case of large earthquakes results in overestimation of afterslip in deeper parts than coseismic rupture area and underestimation of afterslip in shallower parts. Ito and Nishimura [2016] studied the effect of viscoelastic relaxation due to the 2003 earthquake assuming that the afterslip pattern did not change from that of the first three months after the earthquake and that only the slip amount of the afterslip was decaying. They showed that the horizontal crustal deformation due to the afterslip was dominant until four years after the earthquake. Therefore, our results of afterslip distribution five to seven years after the earthquake may be biased.

In conclusions, from 25 September 2000 to 24 September 2003 the slip deficit was stable and there was no yearly scale transient event in the Tokachi-oki region prior to the 2003 earthquake. After the 2003 earthquake, afterslip occurred in and around the source region of the 2003 earthquake. However, it did not extend to the Akkeshi-oki region where the 1952 earthquake ruptured. In the Akkeshi-oki–Nemuro-oki region, the slip deficit was stable in all the analysis periods from 25 September 2000 to 24 September 2010.

Table 3-1. List of earthquakes whose coseismic offsets were detected by GEONET.

No.	Origin time (UTC)	Latitude	Longitude	M_{JMA}	M_w
1	28/01/2000 14:21:08.76	43.0082	146.7443	7.0	6.8
2	25/092003 19:50:07.42	41.7785	144.0785	8.0	8.3
3	08/10/2003 09:06:56.79	42.5653	144.6698	6.4	6.6
4	28/11/2004 18:32:14.53	42.9460	145.2755	7.1	7.0
5	06/12/2004 14:15:11.81	42.8477	145.3428	6.9	6.7
6	15/11/2006 11:14:09.60	46.7027	154.0475	7.9	8.3
7	17/02/2007 00:02:56.63	41.7318	143.7227	6.2	6.0
8	11/09/2008 00:20:51.35	41.7755	144,1515	7.1	6.8
9	05/06/2009 03:30:33.80	41.8123	143.6203	6.4	6.3

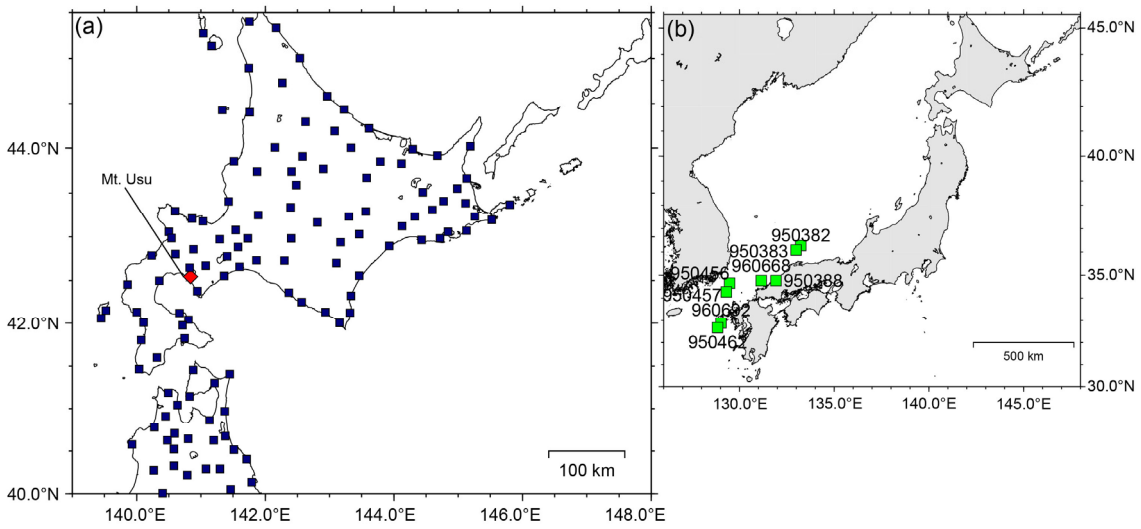

Figure 3-1. Station distribution. (a) The Dark blue squares show the GEONET stations used to exmatine the trend. The Red diamond shows the location of Mount Usu. (b) The green squares represent the GEONET stations selected for calculating the common mode error.

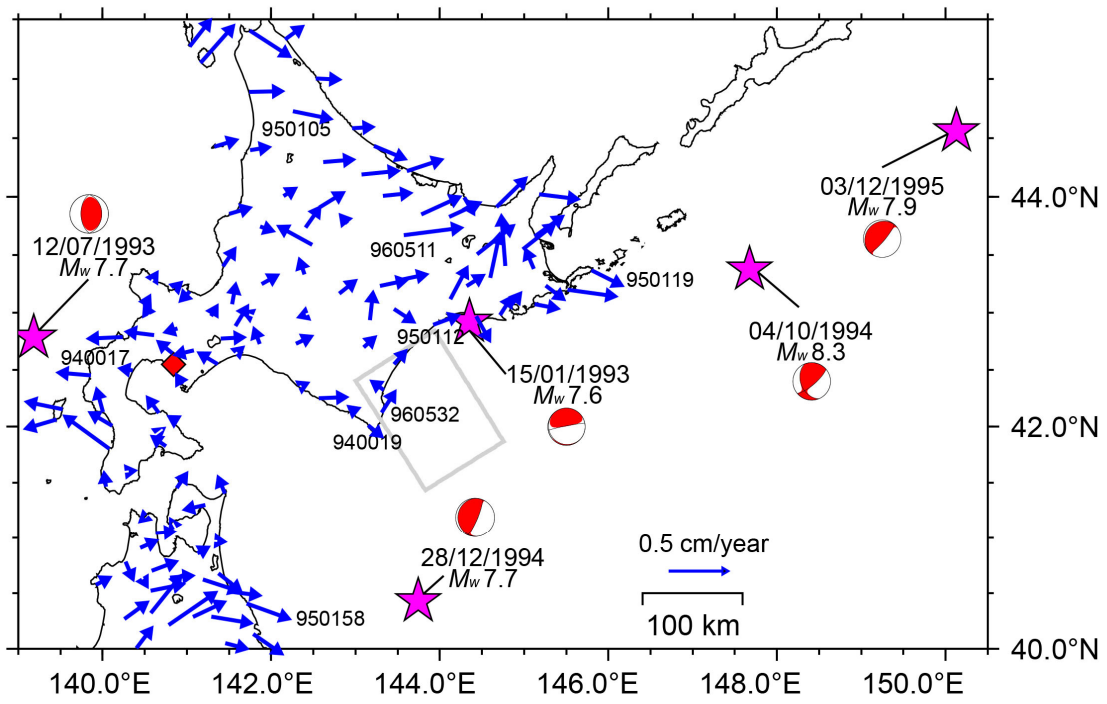

Figure 3-2. Differences in the trends of the horizontal components between 30 March 1997–29 March 2000 and 25 September 2000–24 September 2003. The blue arrows show the differences in the trends. The purple stars indicate the epicenters of the notable earthquakes that occurred during 1993–1995. The focal mechanisms of these earthquakes determined by the GCMT are also shown. The light gray rectangle represents the main rupture area of the 2003 Tokachi-oki earthquake estimated in Chapter 2. The red diamond shows the location of Mount Usu.

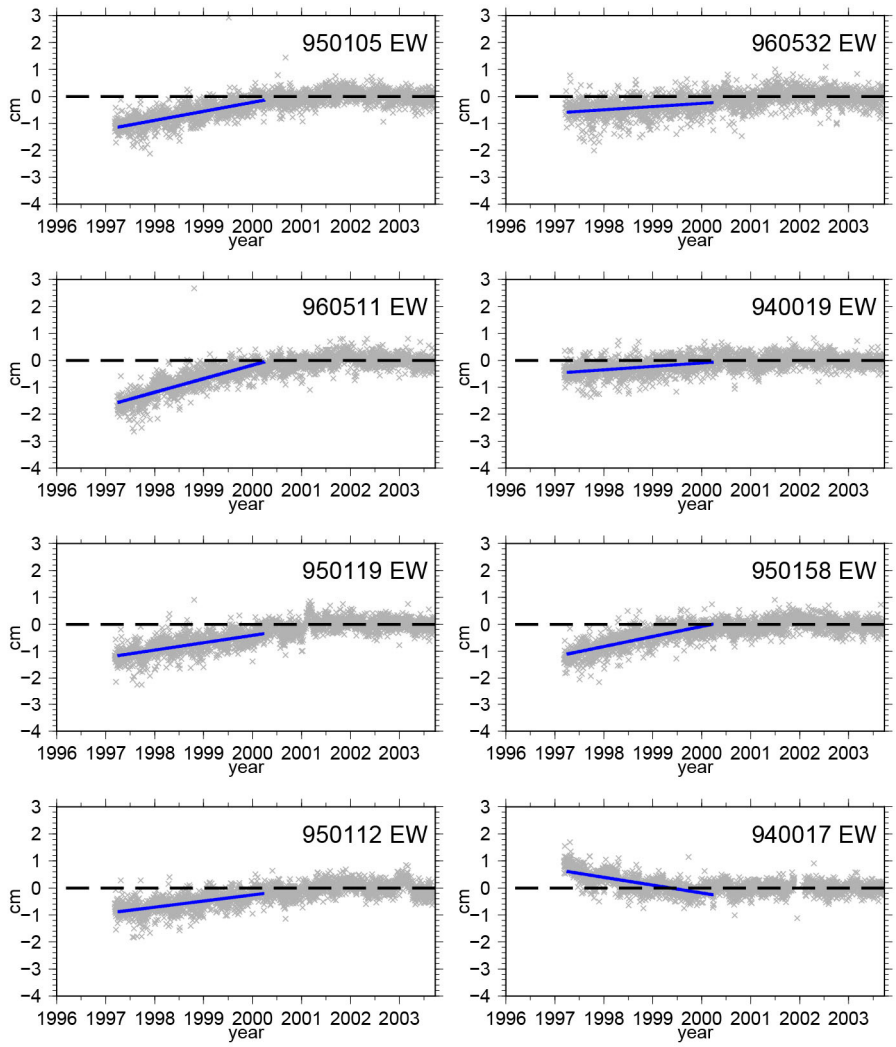

Figure 3-3. Time series of the horizontal components of selected GEONET stations. The station locations are shown in Figure 3-2. Each plot is detrended with the trend of 25 September 2000–24 September 2003. The black broken lines show the zero lines. The blue lines indicate the trend from 30 March 1997 to 29 March 2000, after the detrend.

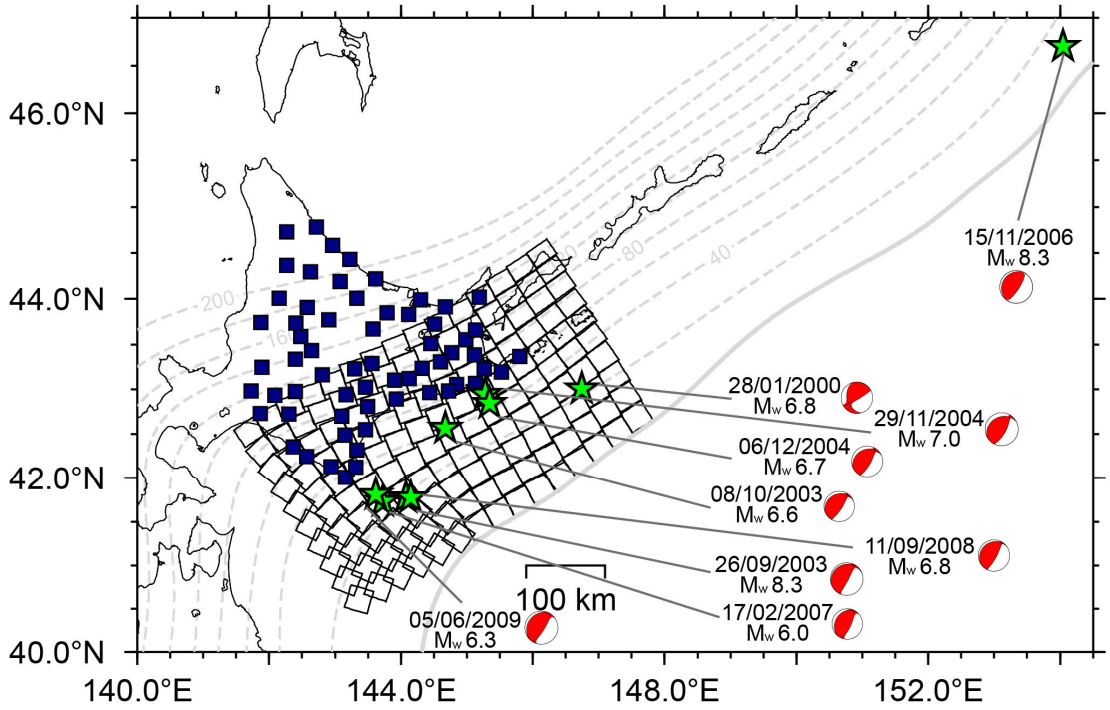

Figure 3-4. Station distribution and fault model for the inversion analyses. The green stars denote the epicenters of the earthquakes whose coseismic crustal deformations were observed by GEONET during the analysis period. The focal mechanisms of these earthquakes determined by GCMT are also shown. The plate-boundary depth up to 200 km and the trench axis [Iwasaki et al., 2015] are represented by the light gray broken lines with 20 km contour intervals and the light gray line, respectively.

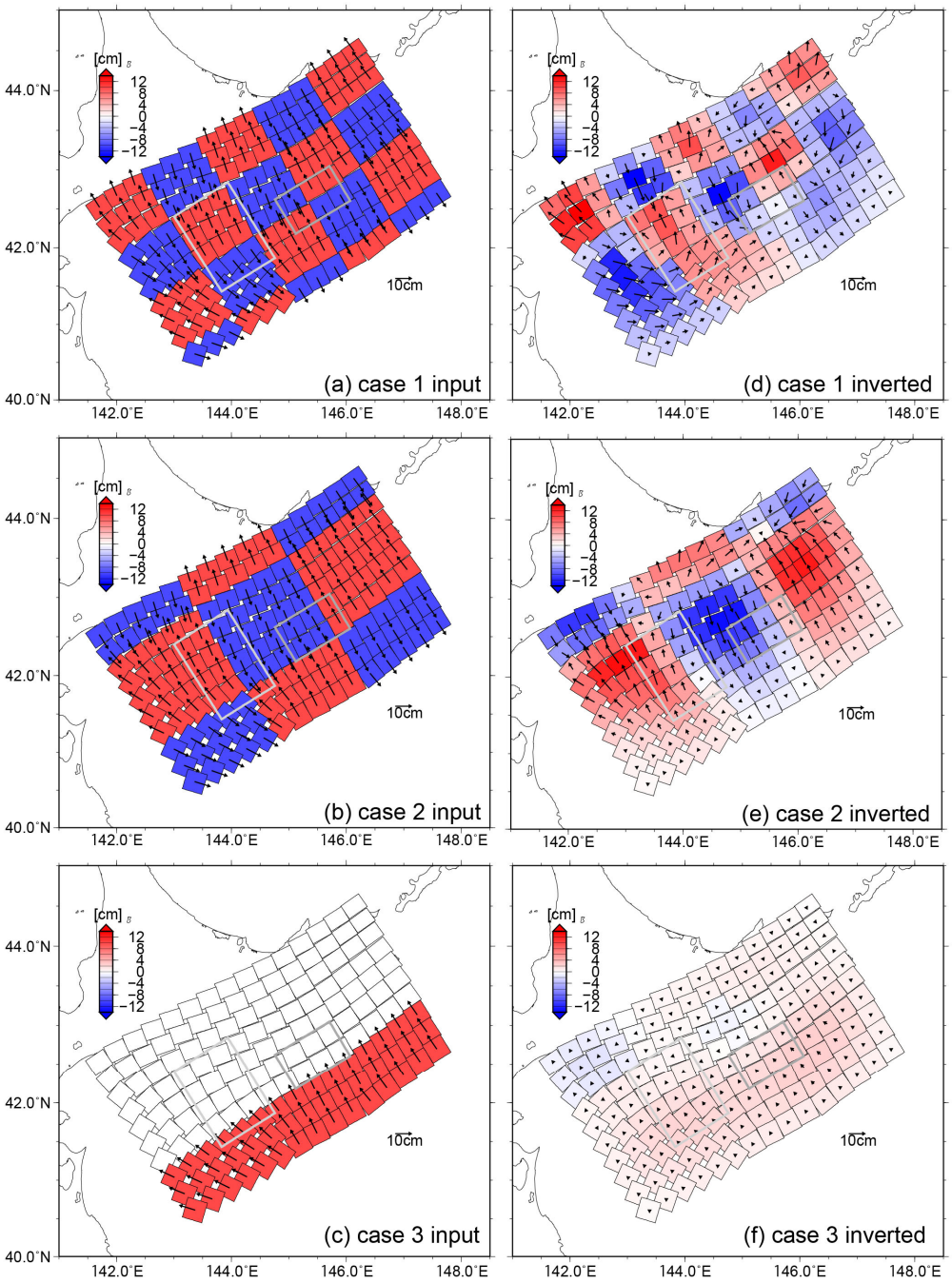

Figure 3-5. (a)–(c) The input models for the resolution test. (d)–(f) the inverted models. The light gray and gray rectangles represent the main rupture areas of the 1952 and 2003 earthquakes in the Tokachi-oki and Akkeshi-oki regions, respectively. The red color indicates normal fault motion (slip deficit) and the blue colors indicate reverse fault motion (forward slip).

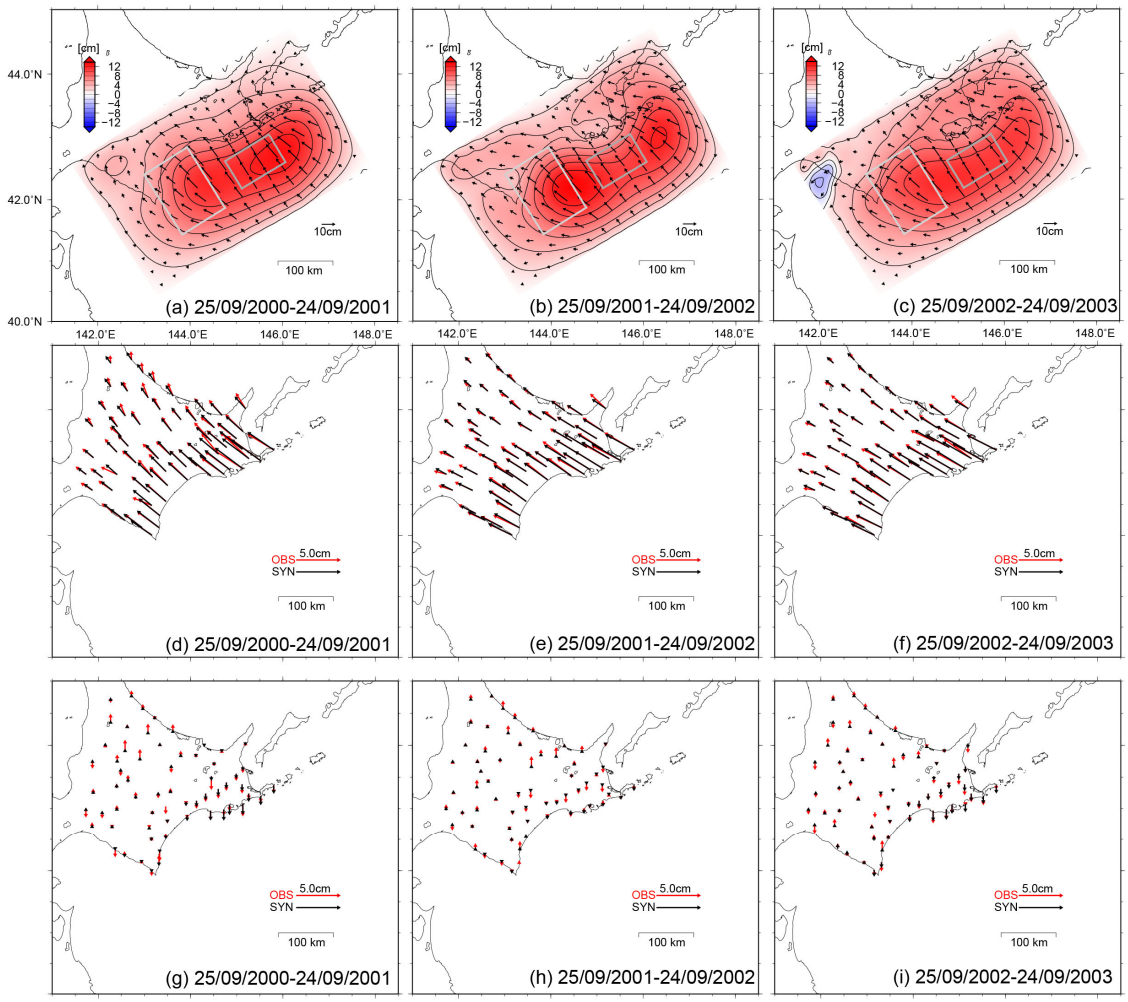

Figure 3-6. Inversion results for the yearly slip deficit/afterslip between 25 September 2000 and 24 September 2003. (a)–(c) The slip deficit distribution. The contour interval is 2 cm. The light gray and gray rectangles represent the main rupture areas of the 1952 and 2003 earthquakes in the Tokachi-oki and Akkeshi-oki regions, respectively. (d)–(f) Data fittings of the horizontal component. (g)–(i) Data fittings of the vertical component. The red and black arrows show the observed and synthetic crustal deformations, respectively.

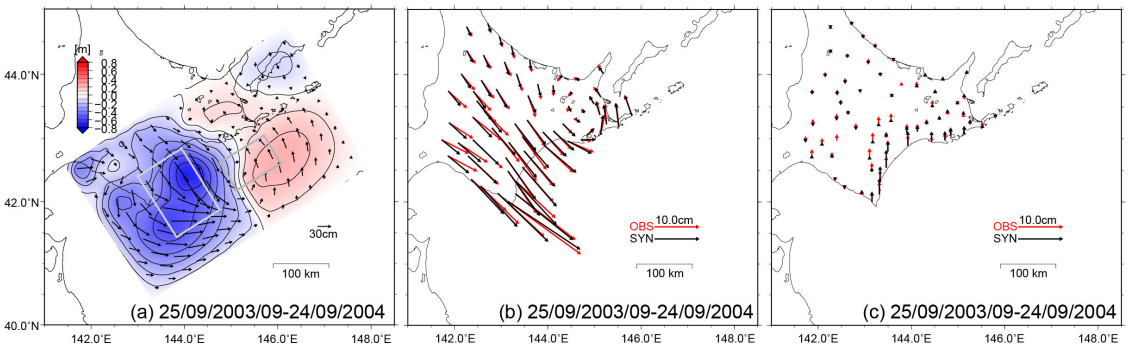

Figure 3-7. Inversion results for the yearly slip deficit/afterslip between 25 September 2003 and 24 September 2004. The contour interval is 10 cm. The other aspects are the same as in Figure 3-6.

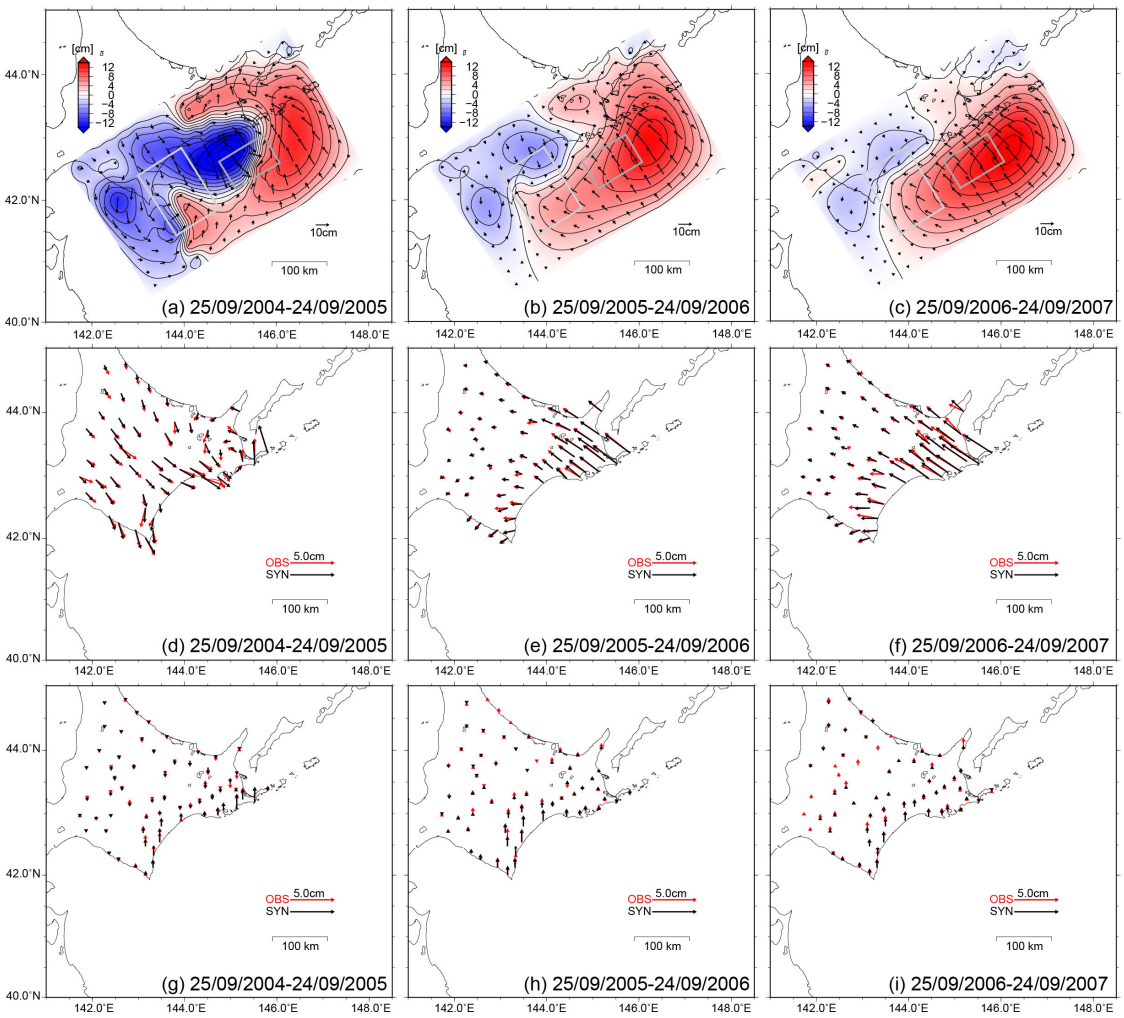

Figure 3-8. Inversion results for the yearly slip deficit/afterslip between 25 September 2004 and 24 September 2010. The contour interval is 2 cm. The other aspects are the same as in Figure 3-6.

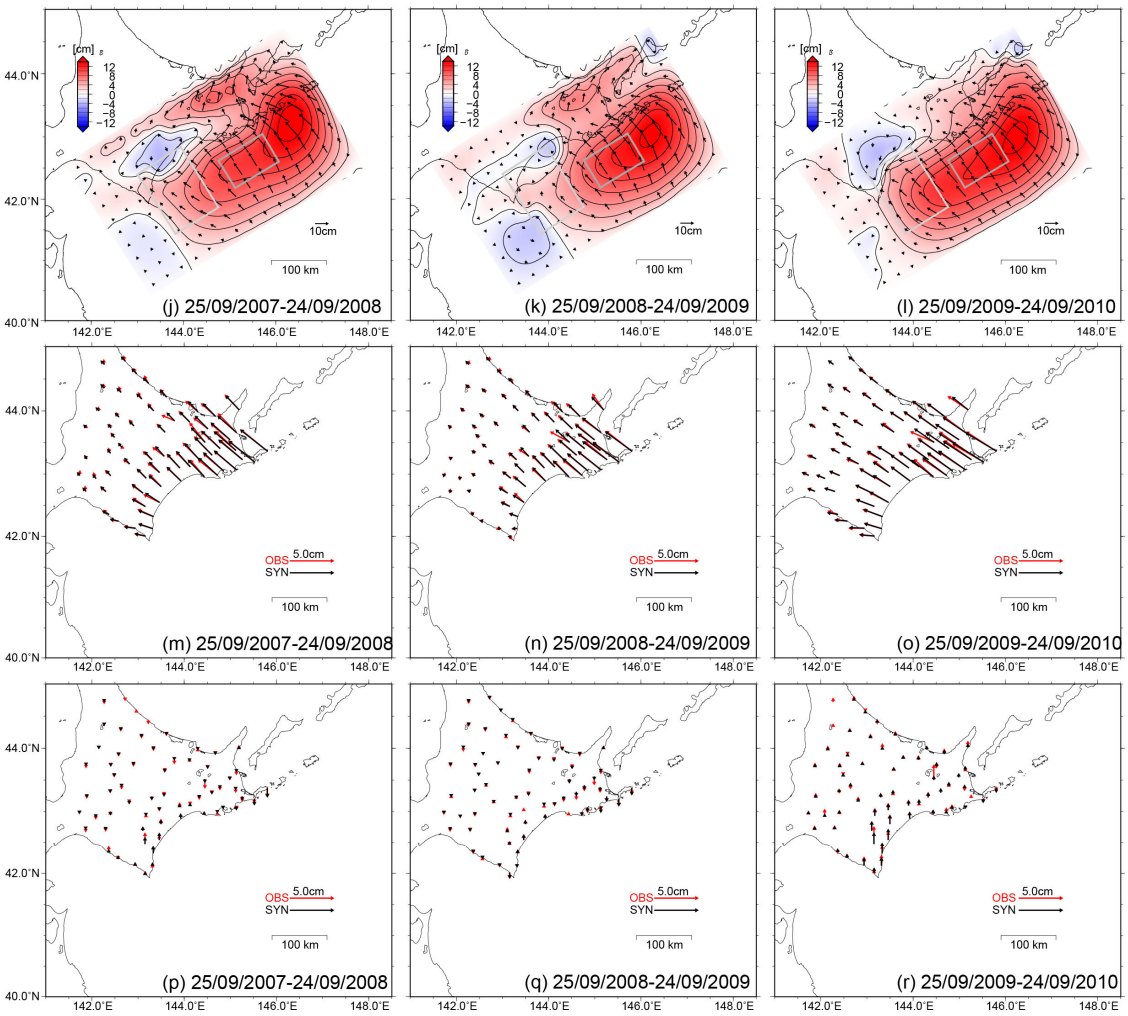

Figure 3-8. Continued.

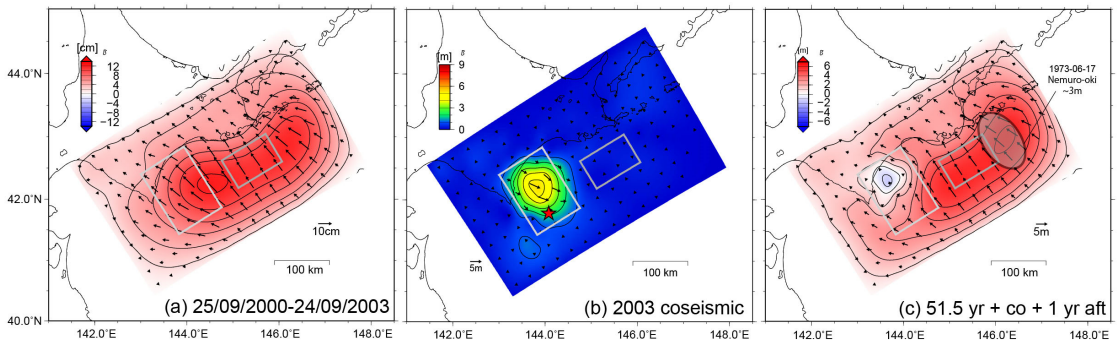

Figure 3-9. Comparisons of the slip deficit, coseismic slip, and cumulative slip deficit. (a) Three-year averaged slip deficit distribution prior to the 2003 earthquake. The contour interval is 2 cm. (b) Coseismic slip distribution of the 2003 earthquake obtained using only the geodetic data. The red star denotes the epicenter. The contour interval is 1 m. (c) The sum of 51.5 years slip deficit between the 1952 and 2003 earthquakes assuming that the slip deficit was constant, coseismic slip of the 2003 earthquake, and one year afterslip after the 2003 earthquake. The contour interval is 1 m. The source area of the 1973 Nemuro-oki earthquake is shown by the shaded ellipse. The light gray and gray rectangles represent the main rupture areas of the 1952 and 2003 earthquakes in the Tokachi-oki and Akkeshi-oki regions, respectively.

4. Vertical deformation and repeating earthquakes in southeastern Hokkaido in the last 100 years

4.1. Introduction

In Japan, seismic and geodetic observations began in the late 19th century. Leveling surveys began in 1883 and are repeated at irregular intervals. Leveling survey data are useful for investigating the crustal deformation in the pre-GNSS age and have been used, together with trilateration/trilateration data, to estimate the slip deficit of pre-GNSS age [e.g., El-Fiky and Kato, 1999; Ito and Hashimoto, 2004] and the coseismic slip of historical earthquakes [e.g., Wald and Somerville, 1995; Yabuki and Matsu'ura, 1992] around Japan. The decade to century scale vertical crustal deformation in Japan has been summarized and discussed in previous studies [e.g., Dambara, 1971; Kumini, 2001]. Murakami and Ozawa [2004] compared the vertical crustal deformation observed by GNSS with that observed by leveling surveys and confirmed that the deformation pattern of Japan in these two data periods generally agree with each other.

In Hokkaido, the first leveling survey was conducted from 1900 to 1913 and was repeated five times in the 20th century [Kumini, 2001]. The 1952 Tokachi-oki earthquake occurred between the first and second surveys. The second survey was conducted from 1952 to 1961. Due to the long intervals of the surveys, leveling survey data must include not only coseismic deformations due to earthquakes but also interseismic deformation. Previous source studies of the 1952 earthquakes were conducted under different assumptions. Kasahara [1975] constructed a fault model of the 1952 earthquake assuming that the observed deformation was primarily due to the

coseismic deformation of the 1952 earthquake. Conversely, Nishimura (2006) corrected the data using the deformation rate obtained from recent GNSS data and assumed that the rates were the same prior the 1952 earthquake to perform the source inversion. However, there is no evidence of the validity of these assumptions.

Repeating earthquakes are series of earthquakes whose observed waveforms at a station are quite similar to each other and that occur in an isolated locked area surrounded by an unlocked area. Because repeating earthquakes are thought to occur to make up for a delay in the surrounding aseismic slips, their occurrence can be used to estimate the aseismic slip rate of the surrounding area [Nadeau and McEvilly, 1999; Uchida et al., 2003]. Around Japan, many repeating earthquakes have been detected using recent digital records [Uchida and Matsuzawa, 2013]. It is expected that these repeating earthquakes also occurred when seismic waves were recorded using analog seismographs, in fact, repeating earthquakes have been detected in the age of analog seismographs [Matsuzawa et al., 2002; Sakoi et al., 2012; Seismology and Volcanology Research Department of Meteorological Research Institute et al., 2014 (hereafter referred to as SVRD et al. 2014)]. Therefore, we can infer the previous plate boundary conditions via the occurrence of such repeating earthquakes.

In this chapter, we examine the vertical deformation and repeating earthquakes in southeastern Hokkaido in the last 100 years to investigate the state of plate interface in the pre-GNSS age. We choose the leveling survey data around Cape Erimo and estimate the effect of the $M \geq 6.5$ earthquakes to the survey data. We investigate the historical repeating earthquakes using analog seismograms.

4.2. Leveling survey

4.2.1. Data

A leveling survey was conducted by the GSI and their results are published on their website (http://vldb.gsi.go.jp/sokuchi/level/KENSOKUSYUROKU/, in Japanese). We chose the survey route around Cape Erimo (Figures 1-1 and 4-1a) because the survey was conducted in 1952 and 1953 after the 1952 earthquake, the route has not changed since the first survey and is located near coast, and there is likely no subsidence due to the pumping of underground water. Figure 4-1b shows the history of the leveling survey on this route. Figure 4-2 shows the vertical deformation along the route for each period. We set the reference point as the benchmark 7966. The coseismic deformations of the 1952 and 2003 earthquakes are included in periods (i) and (vi), respectively. The notable deformation in period (iv) is primarily due to the M_w *6.9* Urakawa-oki earthquake that occurred in 1982. The leveling survey was conducted under the condition that the measurement difference between the outward and homeward surveys was less than $2.5\sqrt{S}$ mm after 1960 and less than $1.5\sqrt{2S}$ mm prior to 1960. S is the distance between the benchmarks in unit of km. We show the value of $2.5\sqrt{2S}$ for the distance–displacement plot and $2.5\sqrt{S}$ for the time–displacement plot as the observation error when we plot the figures.

4.2.2. Coseismic deformation due to the $M \geq 6.5$ earthquakes since 1908

We first examined the coseismic deformation due to $M \geq 6.5$ earthquakes because the $M \geq 6.5$ earthquakes such as the 1982 Urakawa-oki earthquake can cause significant coseismic deformation as shown in Figure 4–2.

Table 4-1 and Figure 4-3 show the $M \geq 6.5$ earthquakes that occurred around the survey route in the period of 1908–2003 according to the JMA catalog and Utsu [1982], except for the 1952 and 2003 earthquakes and their largest aftershocks. We used the method of Okada [1992] to estimate the coseismic deformation of these earthquakes. We assumed a half-space with a Poisson's ratio of 0.25 and a rectangle fault with a uniform slip. We placed the hypocenter on the center of the subfault and assumed that ratio of the fault length and the width was 2:1; however, we used the centroid depth if available and changed its depth if the values are too shallow. We calculated the length and width using the empirical relationships between the rupture area, average slip, and seismic moment proposed by Iwata and Asano [2011], Murotani et al. [2008], and Somerville et al. [1999] for the intraplate, interplate, and crustal earthquakes, respectively. We categorized the earthquakes into the three types according to their focal mechanisms and depths.

The focal mechanisms and seismic moment of some earthquakes have been estimated in previous studies (Table 4-1). We used these values as well. For earthquake No. 9, we performed a point source analysis using the method of Kikuchi and Kanamori [1991] and the velocity structure shown in Tables 2-5 and 2-6. We digitized the World Wide Standardized Seismograph Network seismograms to obtain the waveform data. The waveforms were resampled with 0.5 s and filtered between 0.01 Hz and 0.5 Hz. We also removed the instrumental response from the waveforms. The results are shown in Figure 4-4. Considering the obtained focal depth, we categorized earthquake No. 9 as a crustal earthquake. For the other earthquakes after 1923, we used the first motion solution and M/M_{JMA} as M_w. Even though Ichikawa [1971] determined the first motion solution of the earthquakes occurred near Japan in 1926–1968, not all earthquakes listed

in Table 4-1 were included and the JMA started revising their catalog after Ichikawa [1971]. Therefore, we estimated the plausible first motion solution of the earthquakes via trial and error (Figure 4-5) using the polarity data reported to the ISC and JMA and the revised JMA catalog. In addition, we used the data of Kitada [1931] and picked the polarity of several seismograms.

Prior to 1923, the polarity data were not reported. However, the waveform of earthquake No. 3 observed by the Omori seismograph in Nagano is available in the HERP data retrieval system; therefore we digitized and examined this waveform. We then compared it to several waveforms of recent earthquakes observed around Nagano (Figure 4-6a). We found that the amplitude of the earthquake No. 3 is comparable to that of the 2013 intraplate earthquake and much smaller than those of the 2008 and 2016 interplate earthquakes (Figure 4-6b). Considering that earthquake No. 3 has a magnitude of 7.0, it is highly likely that earthquake No. 3 is an intraplate earthquake. Therefore, we assumed that this earthquake had the same mechanism and depth as earthquake No. 14 which is also an intraplate earthquake. Because there is no useful data for earthquake Nos. 1, 2, 4, and 5, we simply assumed that these earthquakes were typical interplate earthquakes.

Figure 4-7 shows the calculated vertical crustal deformation of the earthquakes listed in Table 4-1. For the intraplate earthquakes we only show the results of the nearly horizontal fault planes because all of the recent earthquakes (earthquake Nos. 18, 20, and 21) have such fault planes [Sasatani, 1985; Sapporo District Meteorological Observatory, 1987; Takeo et al., 1993]. For the crustal earthquakes, except earthquake Nos. 17 and 19 whose fault planes ware estimated in previous studies [Moriya, 1972; Moriya et al., 1983; Tada, 1987], we show the results of both fault planes because it is

not clear which is the true fault plane. These results indicate that there are two earthquakes that could have caused more than 10 cm of vertical deformation around the survey route. One is earthquake No. 19, which is the 1982 Urakawa-oki earthquake, and its deformation can be clearly seen in the leveling survey data (Figure 4–2). The other is earthquake No. 8. This earthquake occurred in 1931; therefore, the deformation due to this earthquake is likely included in data period (i).

4.2.3. Crustal deformation prior to and after the 1952 earthquake

Figure 4-8a shows comparisons of the vertical deformation along the survey route between periods (i) and (vi), which include the coseismic deformation of the 1952 and 2003 earthquakes, respectively. We set the reference point to benchmark 7966. In spite of a survey interval difference of approximately 30 years, these two periods have similar deformation patterns and amounts. We also show the coseismic deformation estimated using the source model of the 2003 earthquake obtained in Chapter 3. The estimated deformation generally agrees with the deformation in period (vi), even though there is some difference around 140 km, which may be due to the error in the source model and the effect of the early postseismic and approximately 10 years of interseismic deformations.

If we sum up the deformation in periods (ii), (iii), (vi), and (v), excepting that of period (iv), which has only a one-year survey interval and includes the deformation due to the 1982 Urawaka-oki earthquake, and compare it to the deformation of period (i), these two deformations are completely different, and the former is nearly flat (Figure 4-8b). This indicates that the coseismic deformation due to the 2003 earthquake nearly balanced the deformation in periods (ii), (iii), (vi), and (v). The difference between the

two periods shown in Figure 4-8b can be seen at 60–100 km and 180–220 km. Because we cannot explain these differences using the coseismic deformations due to the $M \geq 6.5$ earthquakes, these differences are due the difference between the interseismic deformation rate prior to and after the 1952 earthquakes.

Figure 4-9 shows the time series of the relative vertical deformation of the selected benchmarks and the GEONET stations along the survey route (Figure 4-1a). In this figure, we again ignore data period (iv). We set the reference points to 7966 for the benchmarks and 940016 for the GEONET stations. Even though the GEONET stations are not located in exactly the same place as the benchmarks, the GEONET data may reflect the deformation at the benchmarks prior to and after the 2003 earthquake. The observed leveling survey data and GEONET data show that the deformation rates between 1952 and 2003 earthquakes appear not to be constant. Moreover, the linear trends of the GEONET stations prior to the 2003 earthquake do not fit the data between 1952 and 2003 earthquakes. It is probably because the afterslip and viscoelastic relaxation of the 1952 and 1968 Tokachi-oki earthquakes have affected the deformation rate after these earthquakes. The feature is unchanged even if we correct the data using the estimated coseismic deformation of the $M \geq 6.5$ earthquakes and the 1952 and 2003 earthquakes. We assumed that the deformation is the same for the 1952 and 2003 earthquakes because in our coseismic analyses in Chapter 2 they have similar rupture area and amount in the Tokachi-oki region. Note that the corrected data point after the 2003 earthquake includes deformation due to early (1–2 months) afterslip. Even though there is only one data point before the 1952 earthquake, considering the corrected data point just after the 1952 earthquake, the deformation rate prior to the 1952 earthquake appears to be similar to that prior to the 2003 earthquake (Figures 4-9d–4-9f). Note that

the deformation rate was clearly affected by the 2011 Tohoku earthquake (Figure 4-9f).

4.3. Repeating earthquakes

To investigate the historical occurrences of repeating earthquakes, we chose two groups around Hokkaido whose average M_{JMA} is 5.4 from the catalogs of Uchida and Matsuzawa [2013] and SVRD et al. [2014] (Figure 4-10). Using the JMA catalog, we selected earthquakes occurring prior to 1993 whose epicentral distance from the known repeating earthquakes was less than 20 km and whose M_{JMA} was between 5.1 and 5.7 (Tables 4-2 and 4-3). Because we did not consider the hypocentral depth and the focal mechanism, the selected earthquakes may include not only interplate earthquakes but also intraplate and crustal earthquakes. In addition, we checked a few earthquakes whose epicentral distances were less than 30 km. We used the HERP data retrieval system to obtain copies of the analog seismograms. Even though the instrumental response of the analog seismograms might vary slightly even in the same seismograph, we visually determined the repeating earthquakes (Figures 4-11 and 4-12). Even though the waveforms of earthquakes Nos. A9, A12, and A14 were a little different from other repeating earthquakes at short period (Figures 4-11) we categorized these earthquakes as the repeating earthquakes of the group A

Figure 4-13 shows the magnitude–time diagrams for the repeating earthquake groups in this study and SVRD et al. [2014] (Figure 4-10). Moreover, assuming that M_{JMA} is equal to M_w and using the relationships between the seismic moment M_0 in dyne·cm and the slip amount d in cm (Eq. 4-1) [Nadeau and Johnson, 1998] and between the seismic moment and moment magnitude (Eq. 4-2) [Hanks and Kanamori, 1979], we estimated the aseismic slip rate around the repeating earthquake

$$\log(\mathrm{d}) = -2.36 + 0.17\log(M_0) \quad (4\text{–}1)$$

$$\log(\mathrm{M_0}) = 1.5M_w + 16.1 \quad (4\text{–}2)$$

groups (Figure 4-13).

In groups A and B the aseismic slip rates after the 2003 earthquake were clearly faster than those prior to the 2003 earthquake. This indicates that afterslip occurred around the groups, which is supported by the slip deficit/afterslip analyses in Chapter 3 (Figures 3-7 and 3-8). A little acceleration of the aseismic slip rate after the 2003 earthquake also can be seen in groups P3 and P4. Moreover, in group A, the aseismic slip rate after the 1952 earthquake was also faster than that prior to the 1952 earthquake. This indicates that afterslip also occurred after the 1952 earthquake around group A and the 1.3–1.4-year afterslip was similar for the 1952 and 2003 earthquakes. The aseismic slip rate around group A was still faster than 10 cm/year even 6 years after the 2003 earthquakes. This is likely due to a small afterslip of M_w 6.8 earthquakes occurred around group A in 2008 (Figures 3-4 and 3-8k). In group A, the repeating earthquakes occurred approximately two weeks after the 1952 and 2003 earthquakes. Miura et al. [2004] estimated the 12-day afterslip of the 2003 earthquake. According to their results the slip amount of the 12-day afterslip around group A was approximately 20 cm. The aseismic slip rate shown by the red lines in Figure 4-13 were calculated by simply dividing the slip amounts of the repeating earthquakes by the intervals. If we assume that the slip amounts of two-week afterslip is 20 cm the red broken lines were more plausible than the red lines as the aseismic slip rate prior to the 1952 and 2003 earthquakes. If this is the case, the aseismic rate around group A was decelerated around 1980. The aseismic slip rates prior to the 1952 and 2003 earthquakes were similar around group A.

The aseismic slip rate around group B after the 1952 earthquake was not as fast as that after the 2003 earthquake. This suggests that afterslip did not occur around group B after the 1952 earthquake. The temporal acceleration of the aseismic slip rate around 1945 was possibly due to two M7 earthquakes that occurred at offshore Hachinohe in 1943 and 1945, or the earthquake in 1944 (No. 11 in Table 4-1). The aseismic slip rate in group B was accelerated around 1980. This timing corresponded to the deceleration of group A. Note that the acceleration of the aseismic slip rate after the 1968 Tokachi-oki earthquake can be seen in group P1 and the aseismic slip rate of group P2 were stable. The temporal acceleration of seismic slip rate in P5 is possibly due to $M <$ 6.5 earthquakes because it does not correspond to the $M \geq 6.5$ earthquakes.

4.4. Discussion and conclusions

The deceleration of the aseismic slip rate of group A around 1980 may indicates that the afterslip ended up at that time. In the leveling survey data the relative uplift rates were accelerated after the 2003 earthquake likely by the afterslip (Figure 4-9). Therefore, the end of the afterslip is expected to decelerate the uplift rate. In fact, the deceleration can be seen around 1980 (Figures 4-9d to d-9f). The acceleration of the aseismic slip rate around group B is expected to accelerate uplift rate around it. However, it is not so clear in the leveling survey data (Figure 4-9). In the southernmost part of the Kuril subduction zone the direction of the plate convergence is oblique to the trench axis (Figure 1-1). Therefore, the fast aseismic rate slip around group B causes strain accumulation in the Tokachi-oki region and may contribute to the short recurrence intervals between the 1952 and 2003 earthquakes.

In conclusion, in the Tokachi-oki region 1.3–1.4-year afterslip of the 1952

earthquake was probably similar to that of the 2003 earthquake and it may have continued until around 1980. The state of the plate interface in the Tokachi-oki region prior to the 1952 earthquake may be similar to that prior to the 2003 earthquake. The fast aseismic slip rate around B prior to the 2003 earthquake is a possible cause for the short intervals of the 1952 and 2003 earthquakes in the Tokachi-oki region.

Table 4-1. List of earthquakes plotted in Figure 4-3.

No.	Date (UTC)	Latitude (degree)	Longitude (degree)	Depth (km)	M/M_{JMA}	type	Remarks
1	16/09/1909	42.0	142.0	<100	6.8	inter	
2	20/02/1913	41.8	142.3	<100	6.9	inter	
3	17/03/1915	42.1	143.6	<100	7.0	intra	
4	18/03/1916	41.5	144.5	<100	6.6	inter	
5	16/09/1920	41.6	142.1	<100	6.5	inter	
6	04/09/1926	42.4458	143.7057	66.0	6.7	intra	
7	13/12/1930	42.6530	142.5907	62.0	6.5	crustal	
8	16/02/1931	41.1223	143.1040	32.88	6.8	crustal	
9	26/11/1932	42.3562	142.4662	66.0	6.9	crustal	
10	02/03/1936	41.7952	143.9337	14.0	6.7	inter	
11	01/02/1944	41.9778	142.4528	0.0	6.8	crustal	
12	19/09/1945	42.1353	144.1640	49.0	6.6	intra	
13	19/05/1952	41.7437	144.5253	28.0	6.5	inter	
14	23/04/1962	42.4617	143.7667	69.0	7.1	intra	
15	16/05/1968	41.5047	142.6267	8.00	7.5	crustal	
16	21/09/1968	41.9848	142.7615	54.0	6.8	inter	centroid depth 52 km, M_w 6.6 [Miyamura and Sasatani, 1986]
17	20/01/1970	42.4195	143.1498	55.0	6.7	crustal	centroid depth 34 km, M_w 6.5 [Miyamura and Sasatani, 1986]
18	23/01/1981	42.4167	142.2000	130.0	6.9	intra	centroid depth120.9 km, M_w 6.8 (GCMT)
19	21/03/1982	42.0667	142.6000	40.0	7.1	crustal	centroid depth 36.7 km, M_w 6.9 (GCMT)
20	14/01/1987	42.5367	142.9283	119.01	6.6	intra	centroid depth 89.4 km, M_w 6.8 (GCMT)
21	15/01/1993	42.9200	144.3533	100.06	7.5	intra	centroid depth 100 km, M_w 7.6 (GCMT)
22	29/09/2003	42.3597	144.5530	42.50	6.5	inter	centroid depth 35 km, M_w 6.4 (GCMT)

Table 4-2. List of earthquakes examined for group A.

No.	Date (UTC)	Latitude (degree)	Longitude (degree)	Depth (km)	M_{JMA}	Obihiro Type 59B	Sapporo Type 59C/59	Sapporo Wiechert	Nemuro Wiechert
A1	02/03/1936 04:33:27.54	41.7865	144.045	14	5.3				n
A2	13/12/1941 04:39:37.78	41.7173	143.782	73	5.2			n	
A3	26/05/1942 13:21:43.62	41.6682	143.635	69	5.4			s	s
A4	22/06/1943 01:46:03.43	41.6788	143.9002	67	5.4			n	
A5	20/06/1944 12:16:30.90	41.7168	143.6777	117	5.7				n
A6	04/03/1952 02:39:43.00	41.6518	144.1747	7	5.7			n	
A7	04/03/1952 05:23:07.03	41.7168	144.1795	0	5.1			n	
A8	16/03/1952 22:09:25.18	41.6043	143.7807	40	5.5			s	
A9	22/07/1953 12:52:12.24	41.5985	143.9462	40	5.5			s	s
A10	10/03/1957 02:55:06.27	41.5127	143.9048	27	5.6			n	
A11	01/04/1962 05:01:54.8	41.6183	143.9917	40	5.3		s		s
A12	15/03/1971 05:35:42.27	41.7193	144.0018	21	5.5		s		
A13	14/05/1976 20:40:13.35	41.6552	143.9673	19	5.1	n			
A14	30/04/1980 23:56:06.6	41.5833	144.0000	40	5.2	s			
A15	30/03/1989 14:12:14.1	41.7450	143.7800	40.01	5.6	n			
A16	26/01/1994 10:03:51.0	41.6800	143.9450	68.07	5.4	s	s		
A17	11/10/2003 18:26:19.70	41.7600	143.8212	47.98	5.5				
A18	31/01/2005 09:39:48.38	41.7640	143.8182	47.51	5.4				
A19	07/03/2009 14:33:04.71	41.7953	143.8225	39.07	5.4				

Earthquakes with bold numbers are repeating earthquakes confirmed in previous studies.
Light green shaded entries indicate that the waveforms are shown in Figure 4-10.
“s” and “n” indicate “similar” and “non-similar,” respectively.

Table 4-3. List of earthquakes examined for group B.

No.	Date (UTC)	Latitude (degree)	Longitude (degree)	Depth (km)	M_{JMA}	Obihiro Type 59B	Hiroo Type 54B	Sapporo Type 59C/59	Suttsu CMO simple	Sapporo* Wiechert	Nemuro Wiechert
B1	20/07/1930 05:50:24.56	41.7642	142.5602	53	5.2					n	
B2	02/10/1930 10:01:17.88	41.9397	142.5245	64	5.7					s	s
B3	05/04/1943 01:33:20.33	41.9155	142.4763	36	5.4					s	
B4	31/12/1946 10:28:28.38	41.9955	142.652	44	5.2				n		
B5	03/02/1950 18:27:46.04	41.7227	142.9578	52	5.6				s	s	s
B6	24/01/1951 06:06:55.98	41.8477	142.575	71	5.1					n	
B7	06/09/1960 15:24:39.24	41.9418	142.7185	65.89	5.5				n		
B8	21/05/1962 12:21:12.7	41.8633	142.6400	65	5.5			s	s		
B9	12/11/1964 19:57:36.87	41.9878	142.6883	65.37	5.1			n			
B10	15/06/1968 19:53:12.04	41.8025	142.806	49	5.3			n			
B11	26/06/1968 10:23:50.42	41.9582	142.7653	49	5.7			n			
B12	22/02/1972 19:59:56.98	41.7590	142.8828	49	5.2		n				
B13	15/07/1978 17:44:55.6	41.8500	142.6500	60	5.5	s	s	s			
B14	26/03/1982 01:55:02.0	41.9500	142.5667	20	5.4	n					
B15	26/03/1982 18:43:10.0	41.9500	142.5833	20	5.3	n					
B16	28/07/1983 15:06:44.7	41.9550	142.7300	63	5.3	n					
B17	23/10/1983 04:44:44.0	41.8150	142.6200	77	5.7	n					
B18	21/02/1986 03:08:17.5	41.8467	142.6400	62.04	5.3	s					
B19	11/01/1995 07:48:23.71	41.8427	142.5972	56.36	5.4	s					
B20	30/08/2003 10:06:41.45	41.8157	142.6710	55.27	5.4						
B21	25/06/2008 23:37:11.17	41.8257	142.6727	54.96	5.4						

Earthquakes with bold numbers are repeating earthquakes confirmed in previous studies.
Light green shaded entries indicate that the waveforms are shown in Figure 4-12.
"s" and "n" indicate "similar" and "non-similar," respectively.
*Station Sapporo was moved in 1939.

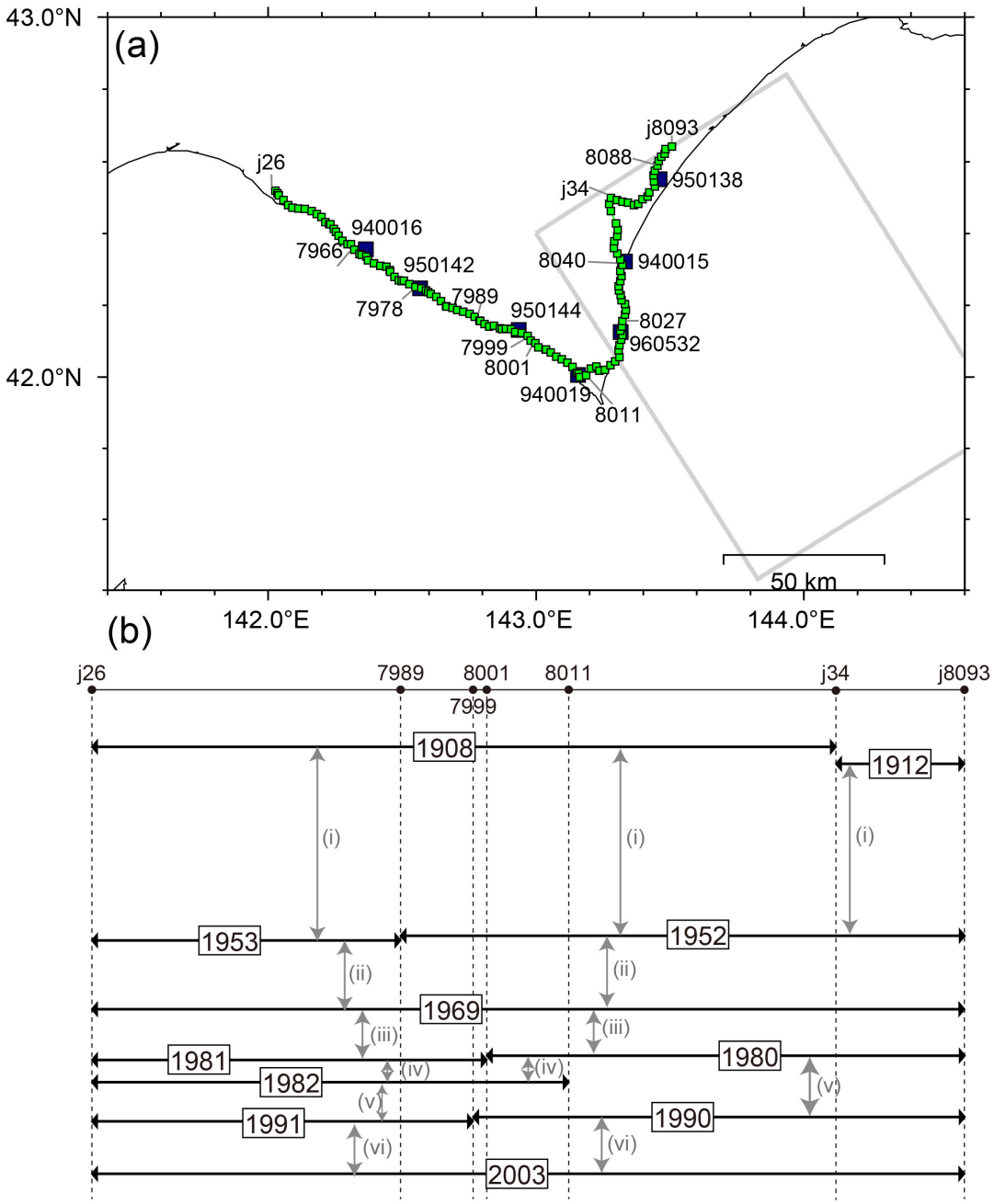

Figure 4-1. (a) Leveling survey route around Erimo-misaki. The green and dark blue squares show the benchmarks and GEONET stations, respectively. The gray rectangle indicates the main rupture area of the 2003 Tokachi-oki earthquake. (b) Survey data along the route. (i)–(vi) correspond to the data periods shown in Figure 4-2a.

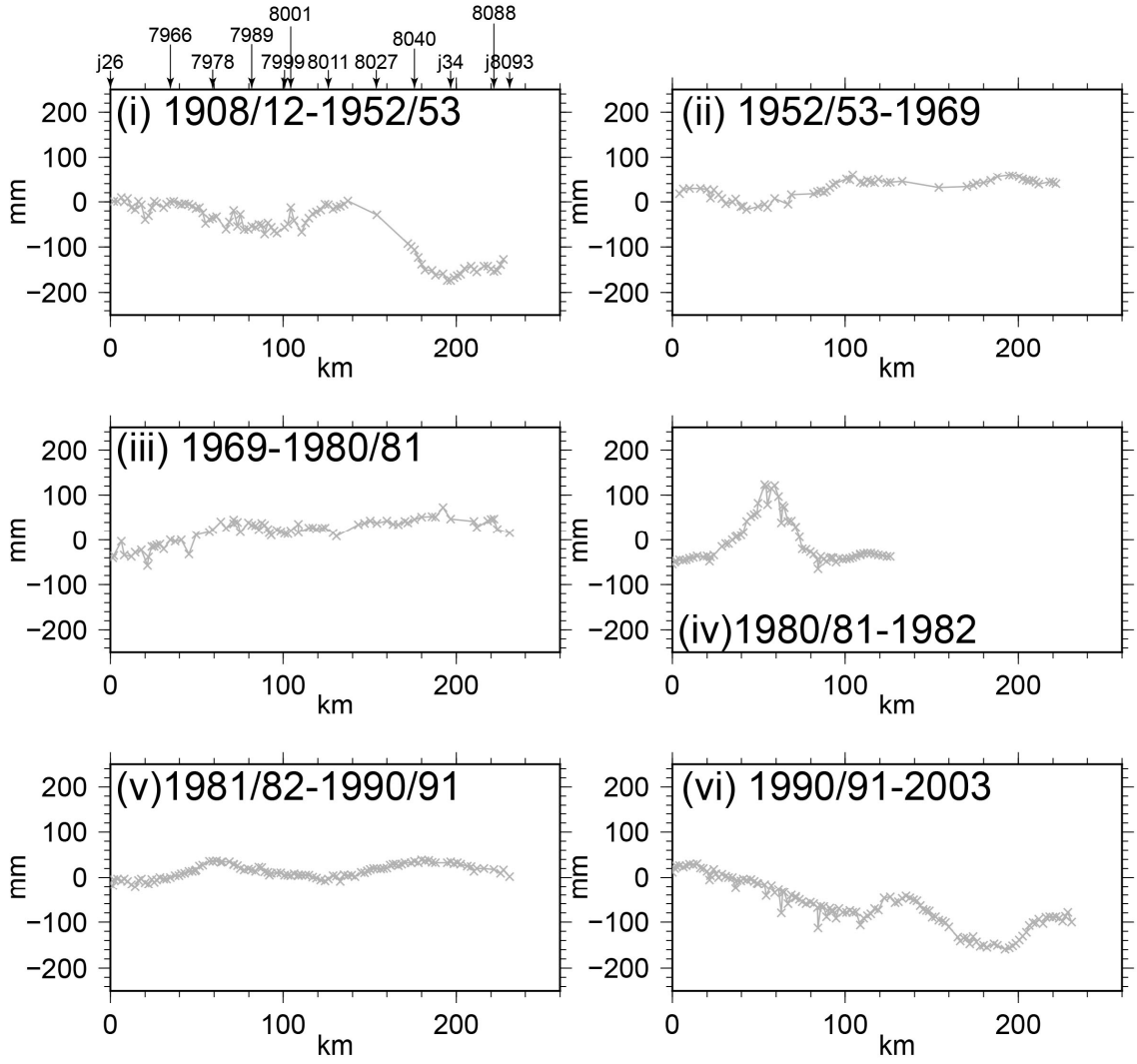

Figure 4-2. Observed vertical displacement along the survey route for each period. The reference point is benchmark 7966.

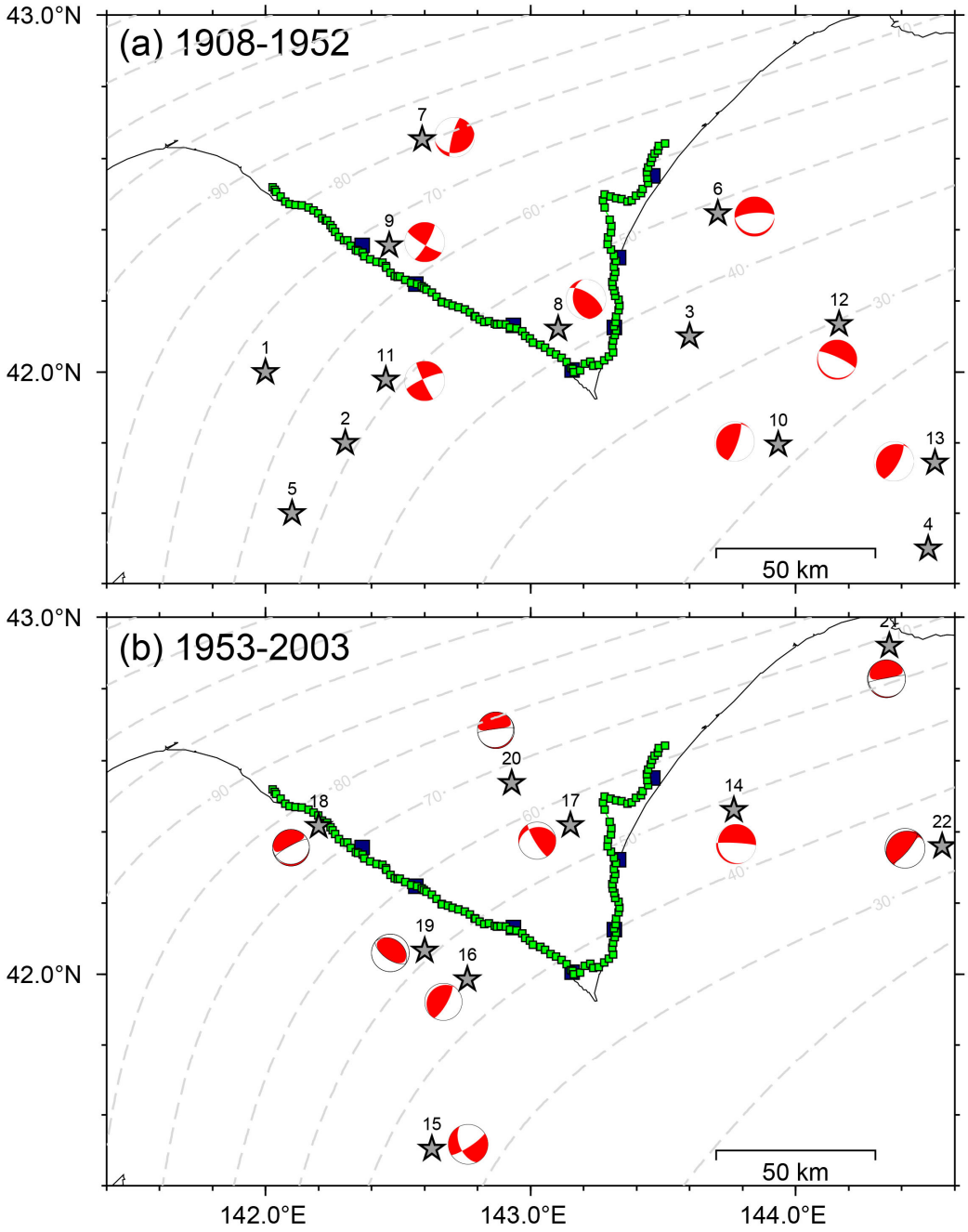

Figure 4-3. M ≥ 6.5 earthquakes that occurred around the survey route in the periods of (a) 1908–1952 and (b) 1953–2003. The stars show the epicenters of the earthquakes listed in Table 4-1. The focal mechanisms are shown by beach balls. The green and dark blue squares show the benchmarks and GEONET stations, respectively. The light gray broken lines with 10 km contour intervals represent the plate-boundary depth [Iwasaki et al., 2015].

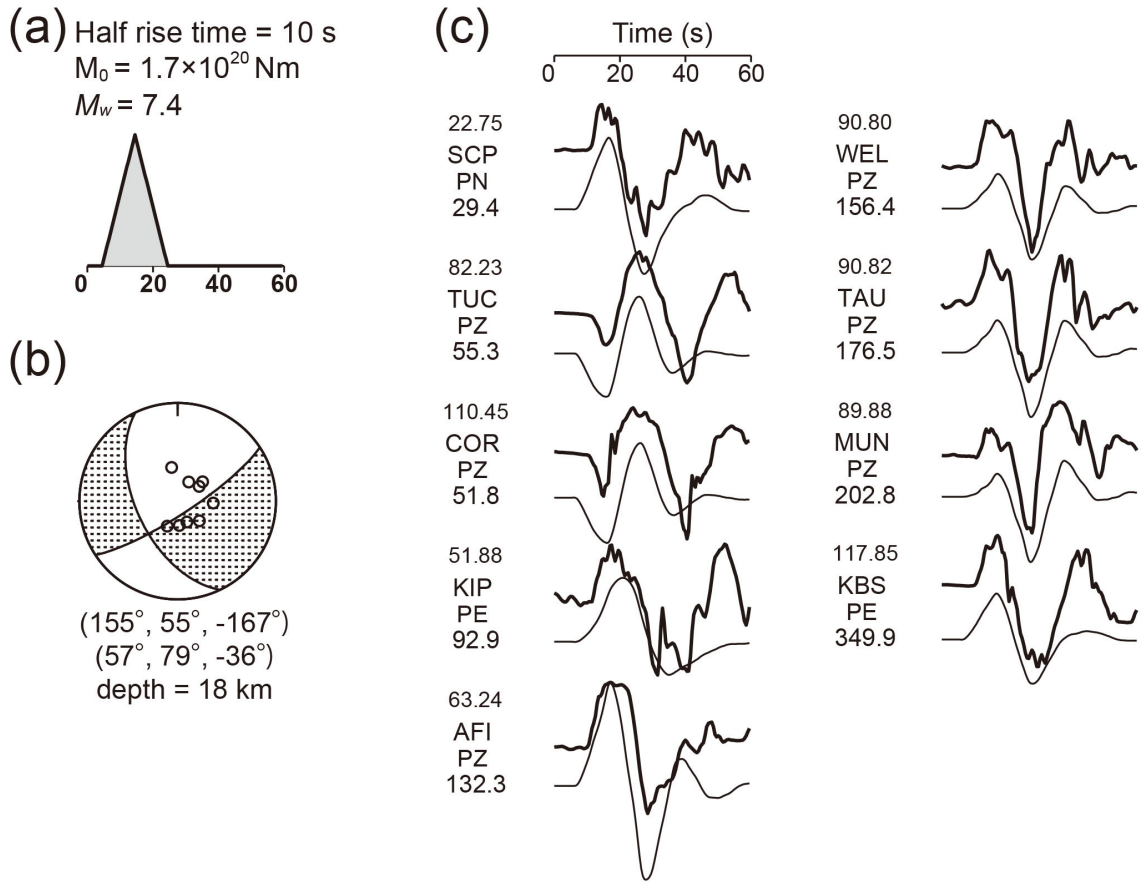

Figure 4-4. The results of the point source analysis of earthquake No. 16: (a) assumed source time function; (b) obtained focal mechanism; and (c) waveform fitting. The observed and synthetic waveforms are shown by the thick and thin lines, respectively. The observed full amplitude (μm), station name, component, and station azimuth are given to the left of each waveform.

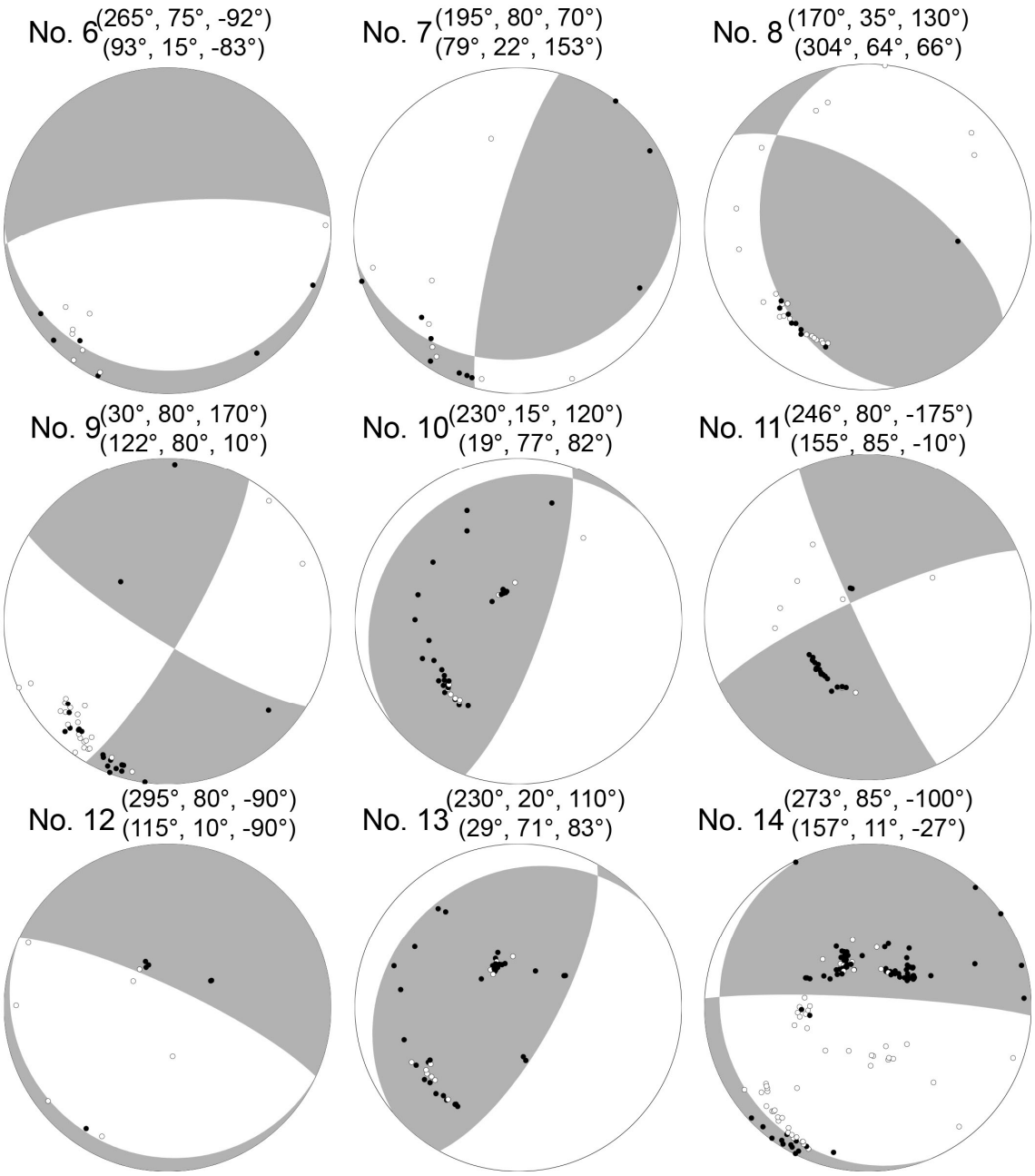

Figure 4-5. First motion solutions estimated in this study. The black and white circles indicate the reported compressional and dilatational first motions, respectively. The earthquake number and the fault plane solutions (strike, dip, rake) are shown above the focal mechanisms.

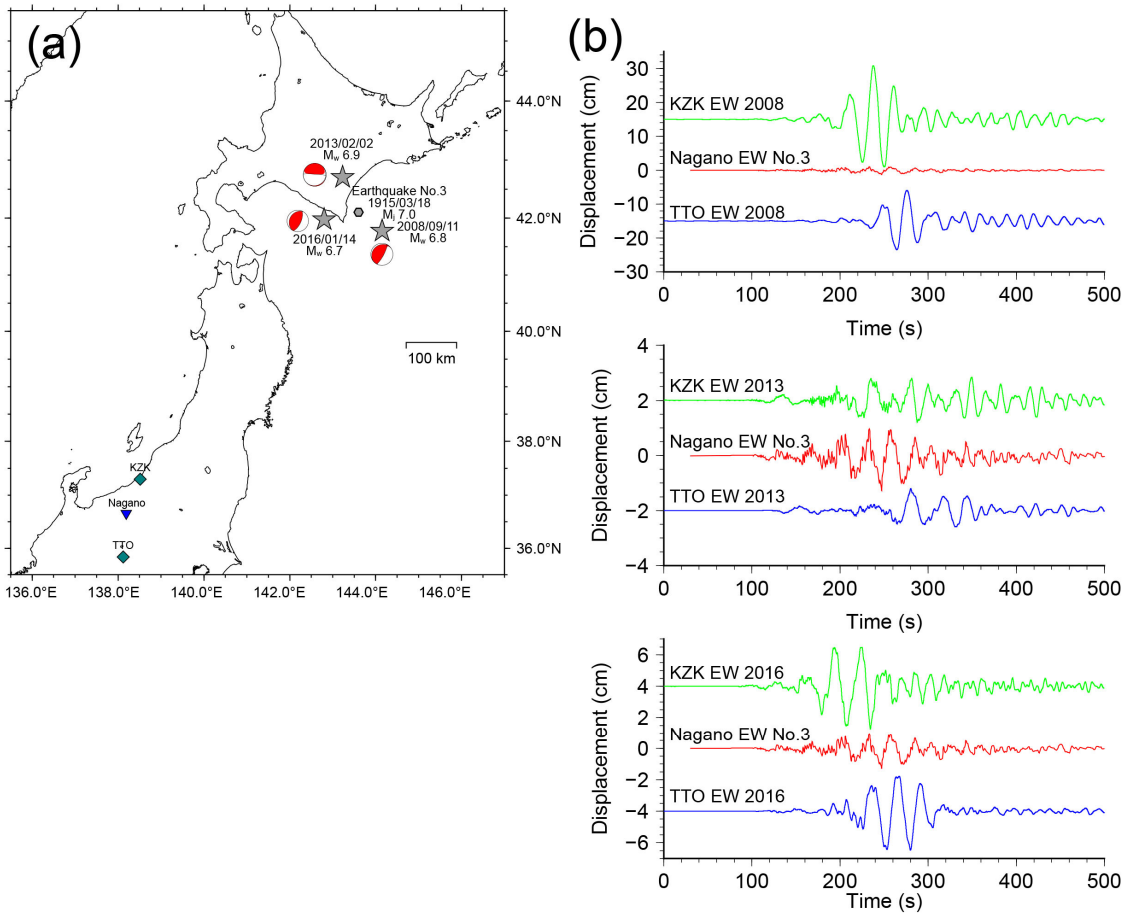

Figure 4-6. (a) Station map. The stars show the epicenters of recent earthquakes. The focal mechanisms determined by GCMT are also shown. The diamonds indicate the F-net stations. The hexagon and reverse triangle show the location of the epicenter of earthquake No. 3 and the Nagano station, respectively. (b) Comparisons of waveforms. The instrumental response of all the waveforms are equalized to that of the Omori seismograph in Nagano in 1915 (V = 20, T = 30, and ε = 1.9).

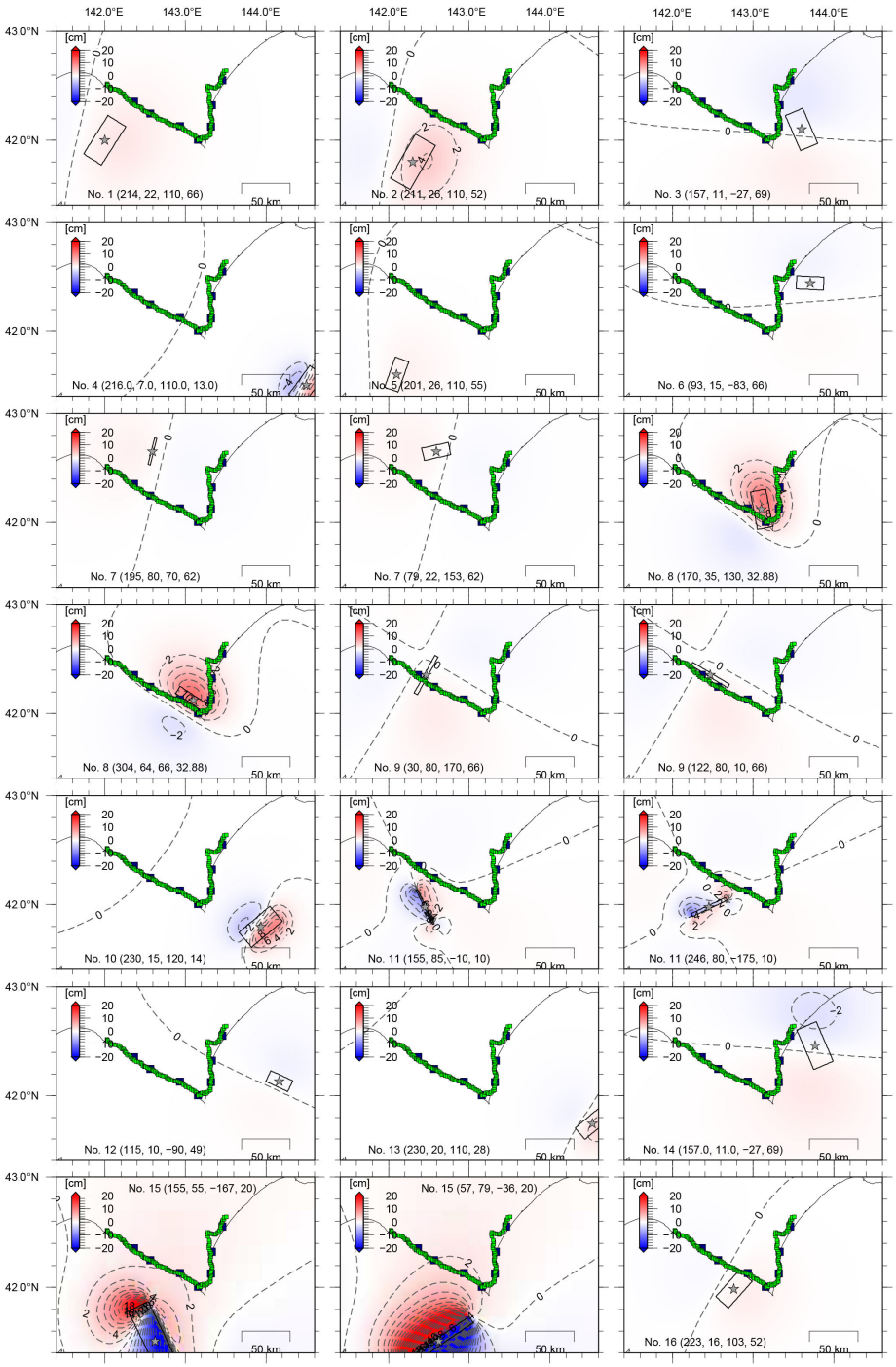

Figure 4-7. Estimated vertical crustal deformation of the earthquakes listed in Table 4-1. The contour interval is 2 cm. The stars show the locations of the epicenters. The black lines around the epicenters indicate the fault planes. The green squares indicate the benchmarks. The earthquake number, strike, dip, rake (degrees), and depth of the center of the fault (km) are shown in each figure.

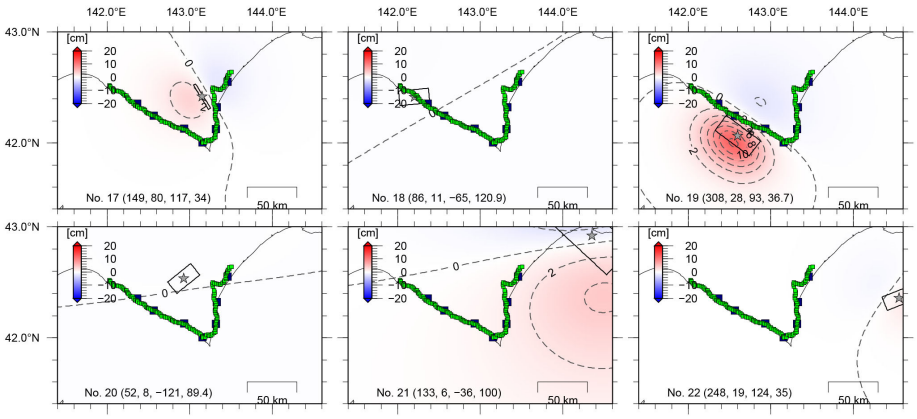

Figure 4–7. Continued.

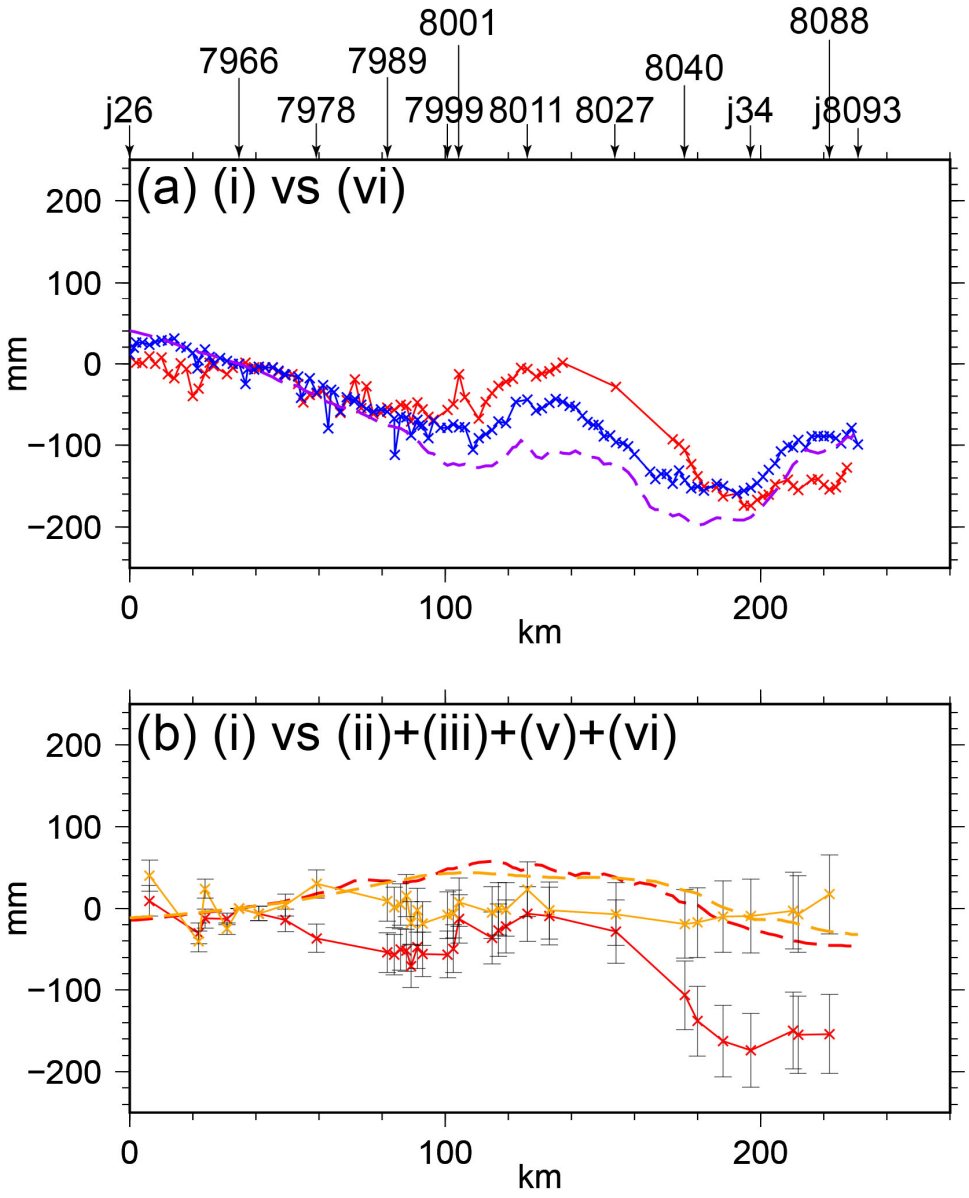

Figure 4-8. Comparisons of the vertical deformation along the survey route (a) between period (i) (red) and period (vi) (blue) and (b) between period (i) and period (ii)+(iii)+(v)+(vi) (orange). The observation error is also shown in panel (b). The purple broken line shows the calculated coseismic deformation of the 2003 earthquake using the source model in Chapter 3. The red and orange broken lines indicate the estimated coseismic deformations due to the $M \geq 6.5$ earthquakes in each period. The reference point is benchmark 7966.

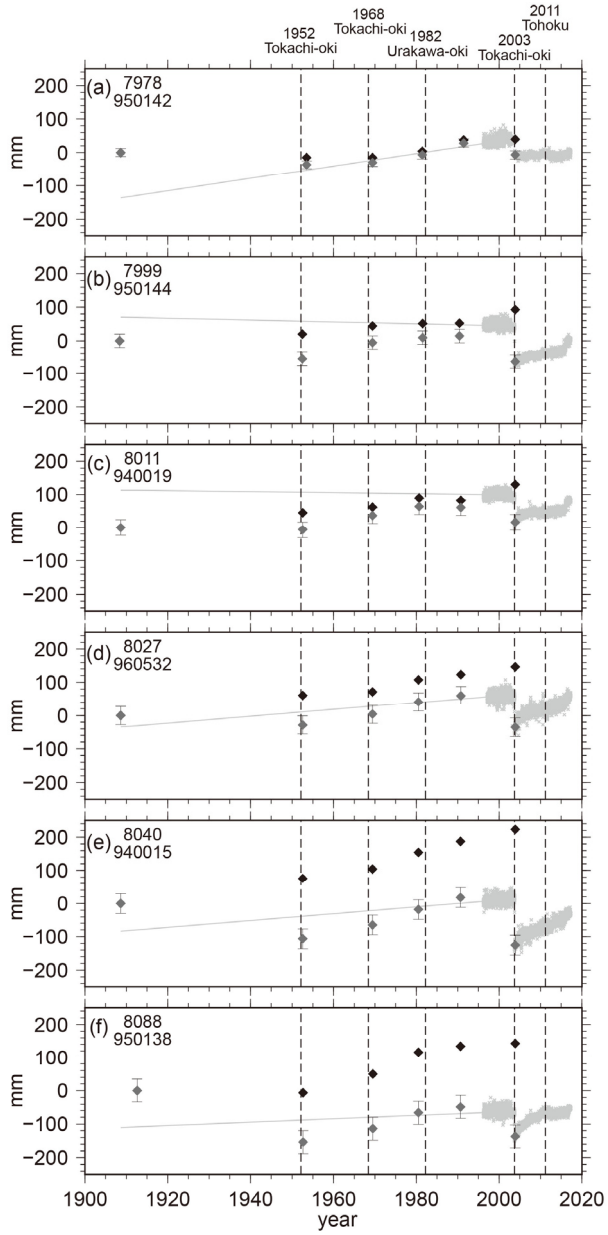

Figure 4-9. Time series of each benchmark and GEONET station. The reference points of the leveling and GNSS data are 7966 and 940016, respectively (Figure 4–1a). The gray and black diamonds denote the observed leveling data with their observation errors and the corrected leveling data, respectively. The light gray crosses represent the GNSS data. The GNSS data are vertically shifted for comparison. The light gray lines are the linear trends of the GEONET stations prior to the 2003 earthquake. The vertical broken lines indicate the notable earthquakes.

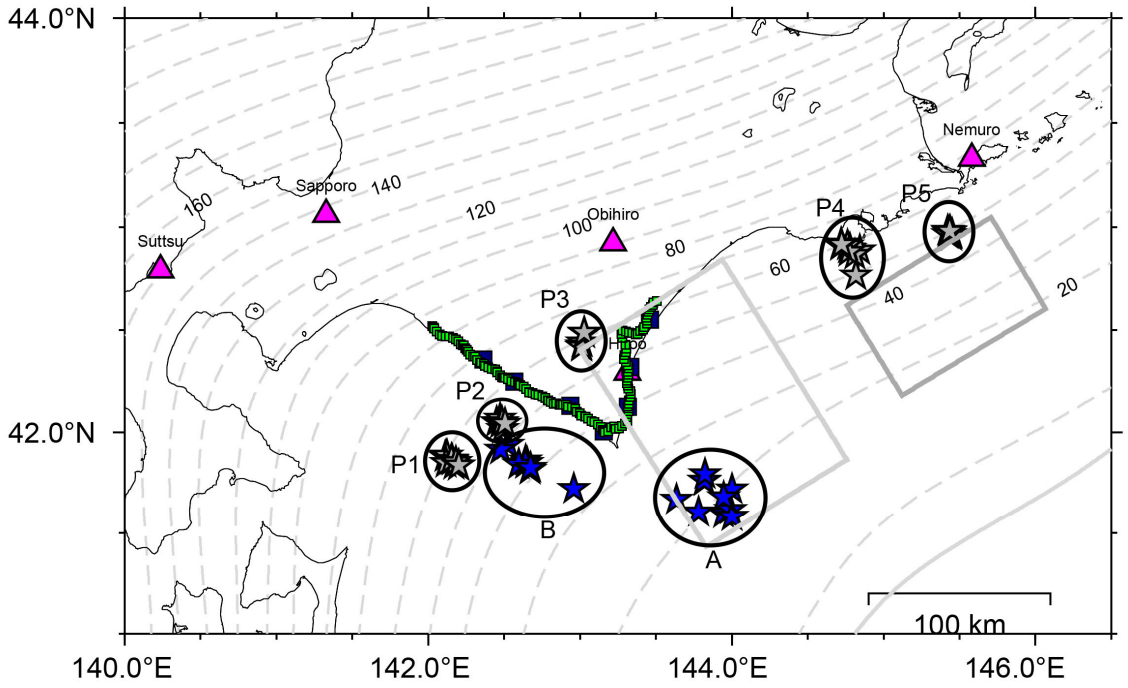

Figure 4-10. Map of the repeating earthquakes. The blue and gray stars indicate the groups studied in this study and in previous studies, respectively. The purple triangles represent the seismic stations. The light gray and gray rectangles show the main rupture areas of the 1952 and 2003 Tokachi-oki earthquakes in the Tokachi-oki and Akkeshi-oki regions, respectively. Other aspects are the same as in Figure 4-1.

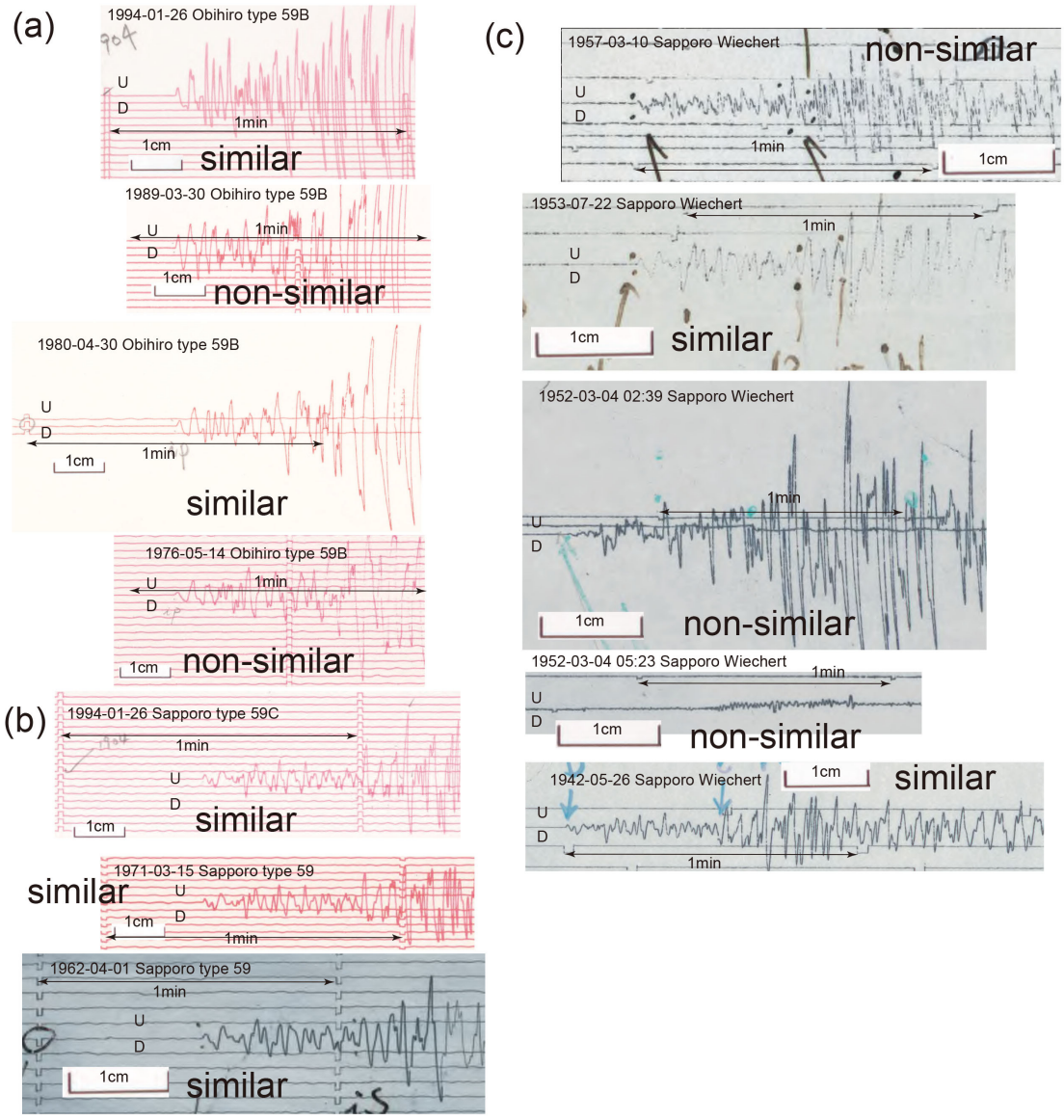

Figure 4-11. Comparisons of waveforms for group A.

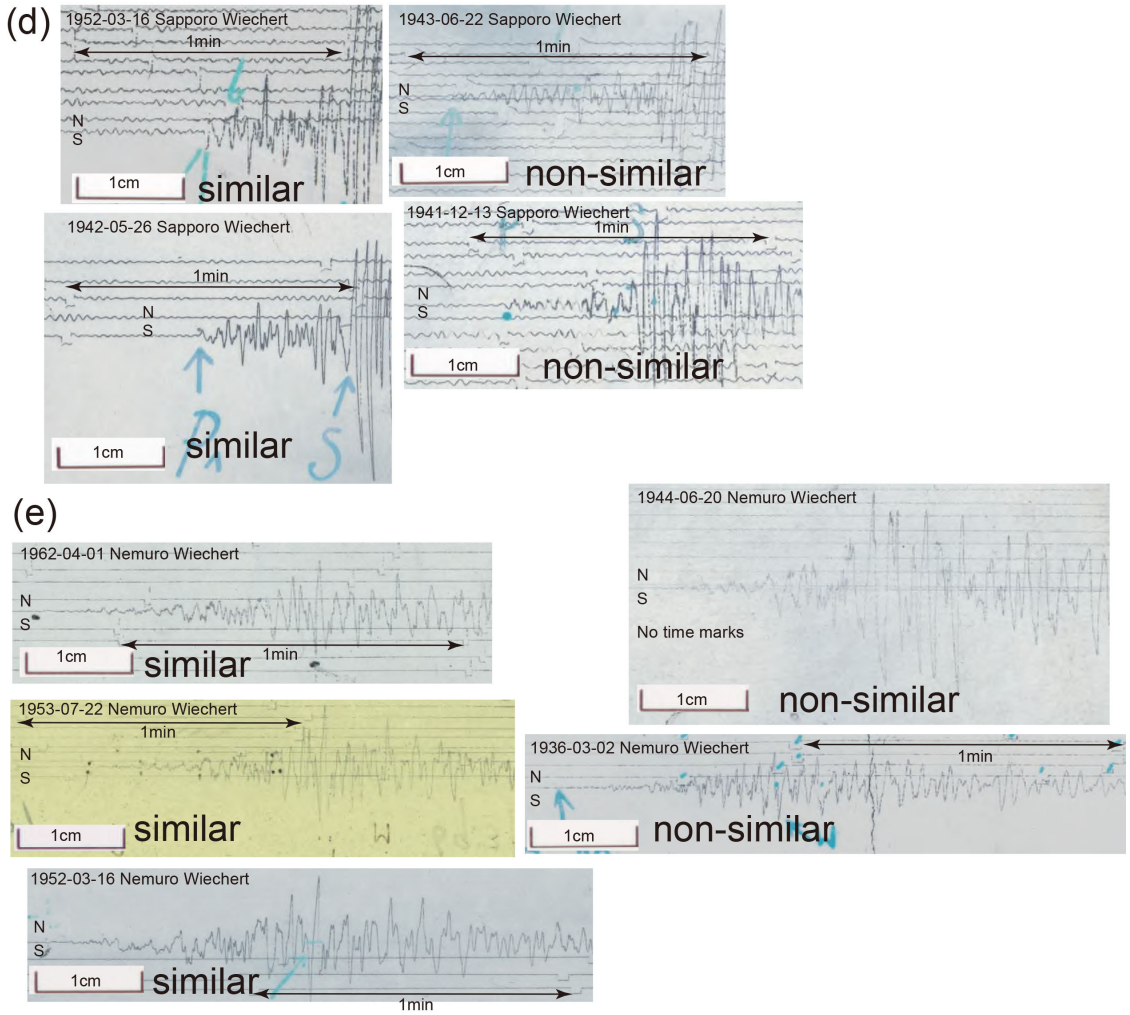

Figure 4–11. Continued.

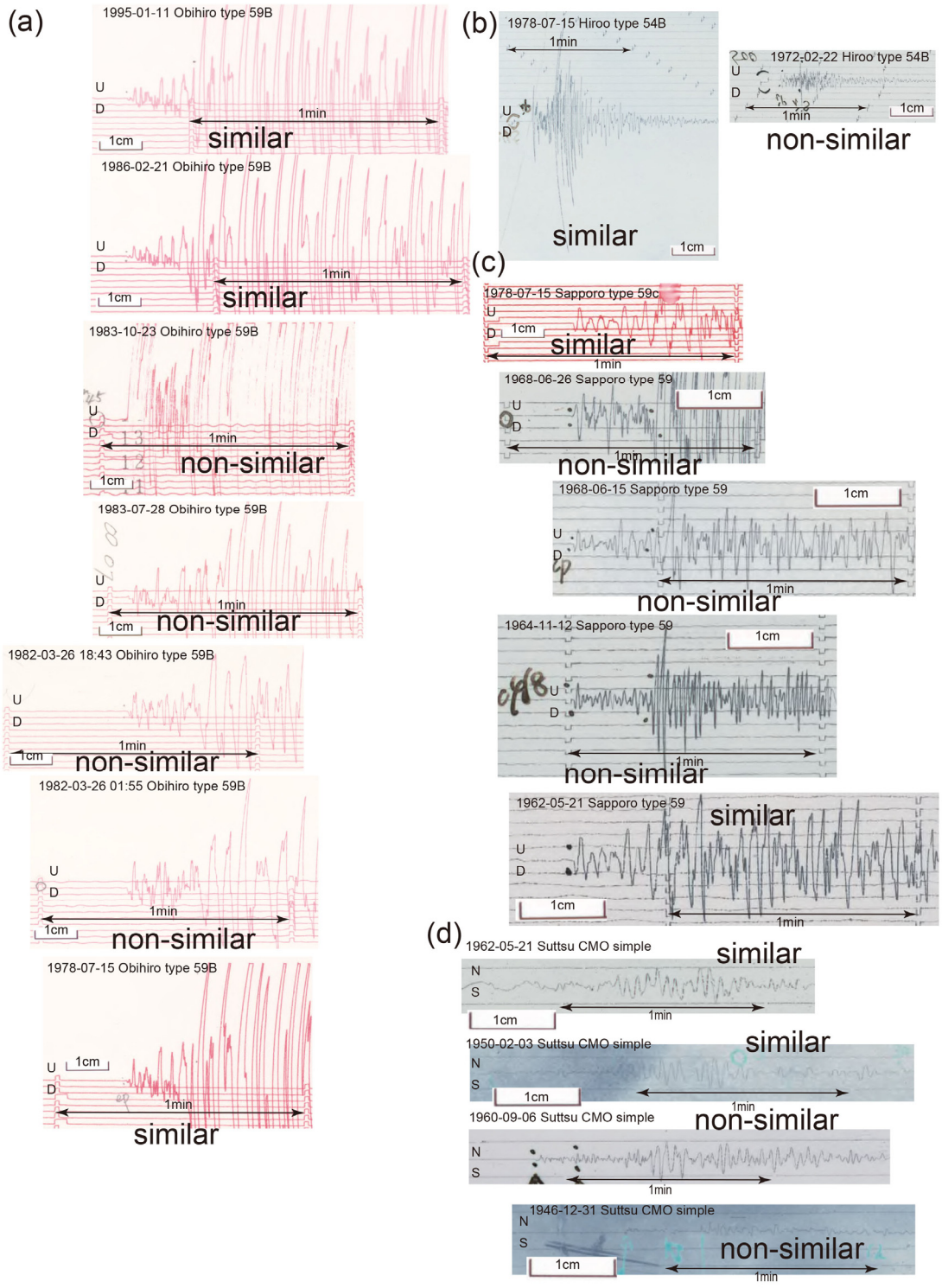

Figure 4-12. Comparisons of waveforms for group B.

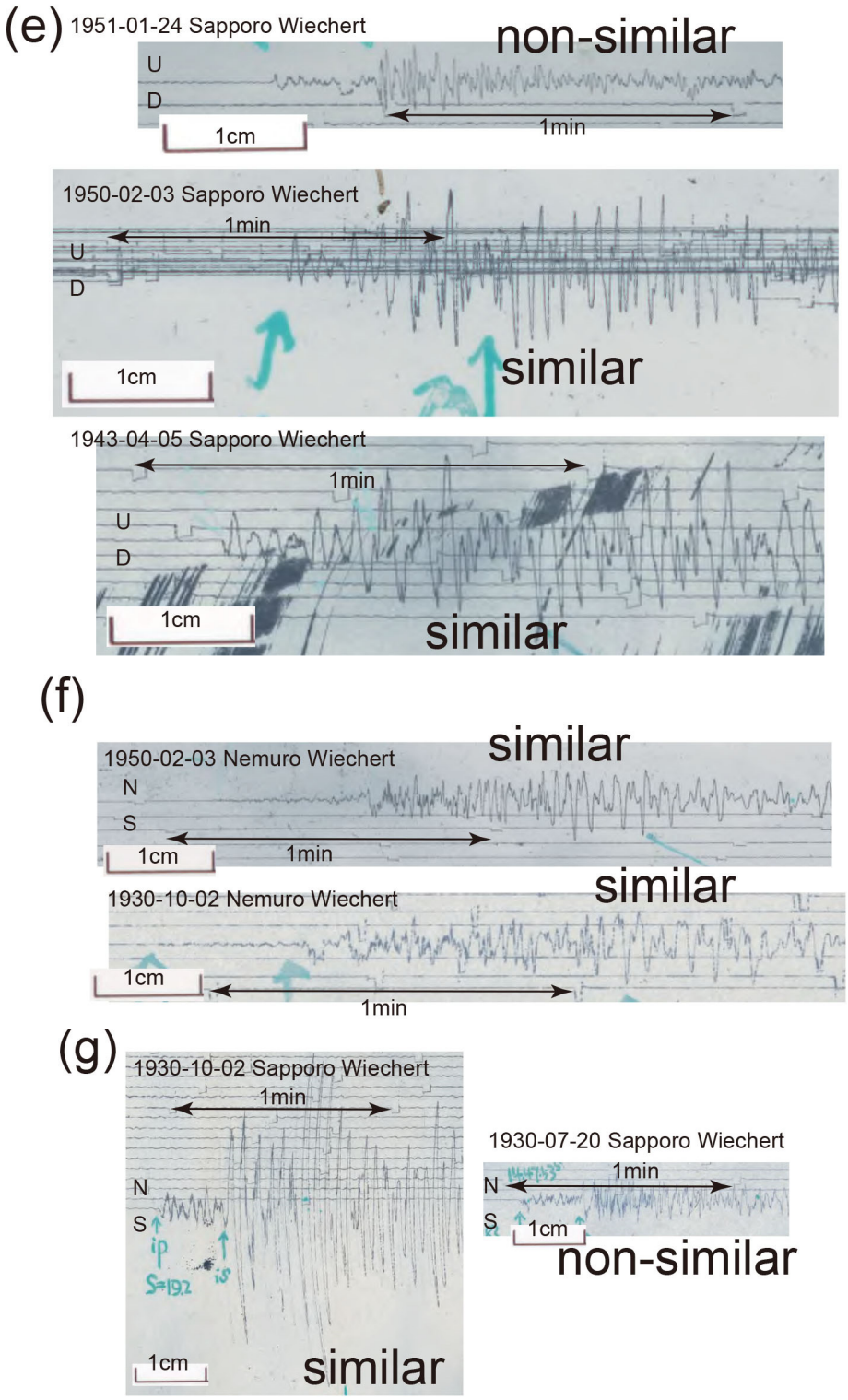

Figure 4–12. Continued.

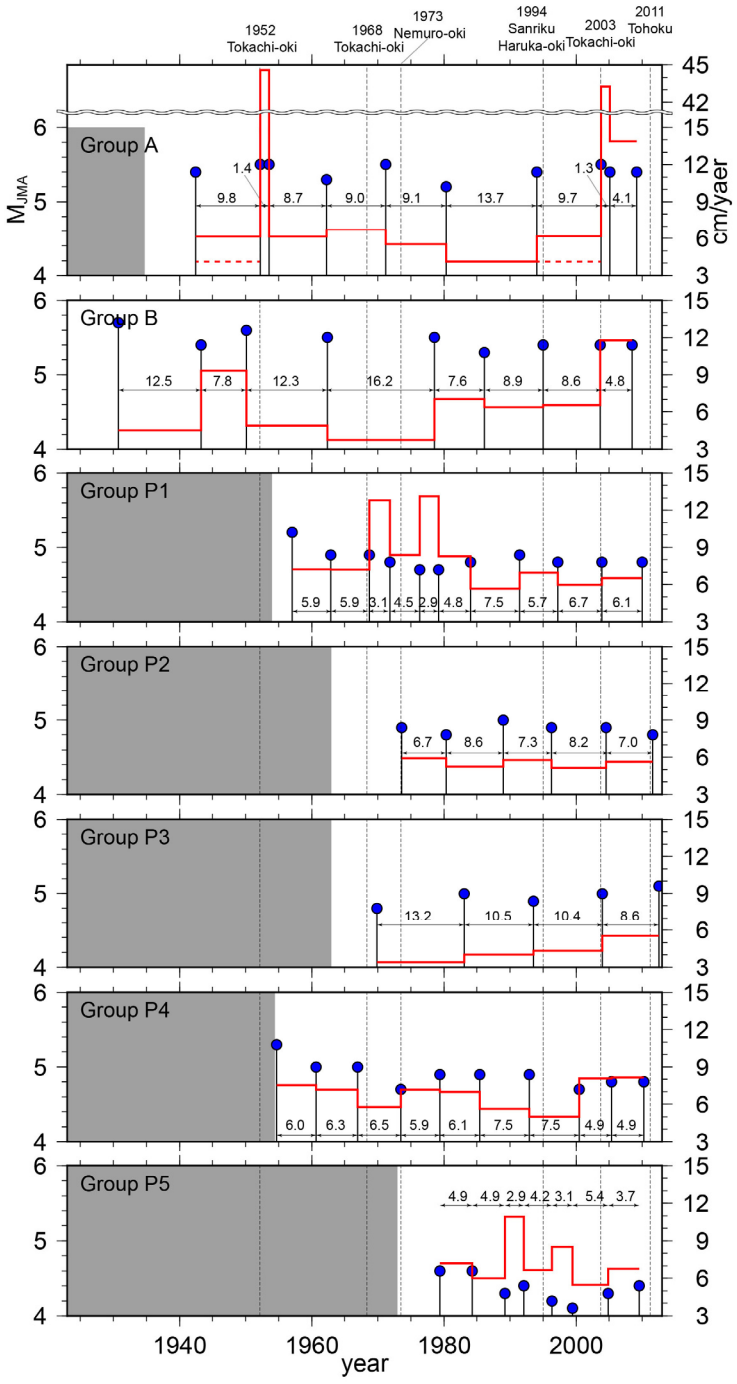

Figure 4-13. Magnitude–time diagrams for the repeating earthquake groups shown in Figure 4-10. The blue circles indicate the repeating earthquakes. The red lines show the aseismic slip rate calculated from the intervals and M_{JMA}. The broken red lines show the corrected aseismic slip rate. The shaded area indicates that the period is not addressed by the studies. The vertical broken lines indicate the large earthquakes.

5. Discussion

In this chapter we summarize the results obtained in Chapters 2 to 4 and discuss the slip history in the southernmost part of the Kuril subduction zone. In Chapter 2, we showed that the slip distributions of the 1952 and 2003 earthquakes are similar in the Tokachi-oki region. In Chapter 3, we confirmed that there is no yearly scale transient event prior to the 2003 earthquake in the Tokachi-oki region. Moreover, we obtained the distributions of slip deficit and afterslip prior to and after the 2003 earthquake. In Chapter 4, the following features were suggested in the Tokachi-oki region: the slip deficit prior to the 1952 earthquake may be similar to that prior to the 2003 earthquake; the afterslip of the 1952 earthquake continued until around 1980.

Considering the above, we draw the relative slip history of the selected subfault in the Tokachi-oki region for quantitative discussion (Figure 5-1). Even though the estimated rake angles in the coseismic model (Figure 3-9b) are not exactly opposite to that of the slip deficit/afterslip models (Figures 3-7, 3-8 and 3-9a), we ignored it and only slip amount were considered for simplicity. We draw the Figure 5-1b assuming that coseismic slip and two-year afterslip of the 1952 earthquake were the same as the 2003 earthquakes as suggested in Chapter 2 and Figure 4-13, and not considering afterslip three or more years after the 1952 earthquake.

There are two features in Figure 5-1b. The first one is that coseismic slip and afterslip of the 2003 earthquake exceeded the accumulated slip since the 1952 earthquake at the selected subfault. This is based on the slip budget for a single earthquake cycle from the 1952 earthquake to the 2003 earthquake. We used the coseismic slip of 5.1 m for the 2003 earthquake, afterslip of around 0.5 m for the 2003

earthquake. If 8.7 cm/year of slip deficit continues for 51.5 years, 4.5 m of the slip accumulation is indicated. Considering the afterslip of the 1952 earthquake, the slip accumulation is estimated smaller than 4.5 m. This indicates that the exceeding slip is more than 1 m (Figure 3-9c). Such exceeding was also indicated for other *M*8 class earthquakes [e.g., Nocquet et al., 2017]. The other feature is that the accumulated slip since the 1843 earthquake was not fully released even after the 1952 and 2003 earthquakes and their afterslip sequences. This is based on the assumption of constant yearly slip deficit even in 19th century (Figure 5-1b), indicating the accumulation of slip reached 13 - 14 m slip since the 1843 earthquake. On the other hand, when we assumed coseismic slip of 5.1 m and afterslip of 0.5 m for both the 1952 and 2003 earthquakes, 11.2 m in total is still smaller than 13-14 m mentioned above. The second feature suggests long-term earthquake cycles have fluctuations. These two features indicate the unbalanced slip budget.

There are several potential geophysical reasons for the unbalanced slip budget: stress transfer, temporal change of frictional properties, and changes of slip deficit rate, or the mixture of these reasons. Stress transfer received from other places may hasten the earthquake occurrence. The stress state would change in the Tokachi-oki region due to the 1968 Tokachi-oki earthquake and other earthquakes in neighboring region (Figure 5-2). Acceleration of repeating earthquake in the Urakawa-oki region where the backward of the plate convergence with respect to the Tokachi-oki region may trigger the 2003 earthquake and shorten the interval of earthquake cycle there. Because in Figure 5-1b we show not the stress but the slip history, these effects are not included in the figure. The temporal change of frictional properties leads to changing the slip behavior and could cause the unbalanced slip budget. The change of slip deficit rate can

be also considered as a possible reason and has been observed in other zones such as the Japan Trench subduction zone [Mavrommatis et al., 2014; Yokota and Koketsu, 2015]. This reason would apply to the second feature, but not to the first feature, since the slip deficit rate is constrained between 1952 and 2003 by the geodetic analysis.

The second feature indicates that the slip deficit is not completely released by the *M*8 class earthquake and continues to accumulate in the *M*8 class earthquake cycles. The existence of earthquake supercycle is proposed by Sieh et al. [2008] and Goldfinger et al. [2013] for *M*9 class earthquakes. Paleoseismic studies [e.g., Sawai et al. 2009; Satake, 2017] suggested that giant earthquakes have occurred in the last several thousand years in southernmost part of the Kuril subduction zone and the last such earthquake occurred in 17th century (Figure 1-1). The supercycle model could be another candidate to explain the unbalanced slip budget in the Tokachi-oki region.

The Akkeshi-oki region was ruptured in the 1952 earthquake but not in the 2003 earthquake. The slip deficit of the Akkeshi-oki region prior to 2000 is not constrained in this study. However, if we assume the constant slip deficit (10-11 cm/year, Figure 5-1) during the unconstrained period, the accumulated slip deficit since the 1952 earthquake is 5.2-5.7 m. Considering that in the 2003 earthquake the maximum slip estimated using only the geodetic data (Figure 3-9b) is approximately two meter less than the one obtained using waveforms (Figures 2-8a), that value could exceed the coseismic slip of the 1952 earthquake. If the slip of a future large earthquake in the Akkeshi-oki region is similar to the 1952 earthquake, it could be another example of unbalanced slip budget. Note that the tsunami analysis [e.g., Satake, 2017] suggested that the Akkeshi-oki region was ruptured in the 1843 and 1894 *M*8 class earthquakes (Figure 5-2).

Concluding the above, the slip budget is unbalanced in the single $M8$ class earthquake cycle and also in the multiple cycles since 1843. We suggested the four possible reasons for unbalanced slip budget: stress transfer, temporal change of frictional properties, changes of slip deficit rate, and supercycle. Because in the present study we carried out the seismological and geodetic analyses using the limited available data, Figures 5-1 and 5-2 has limitations due to the data. Moreover, we did not use the data after 2011 because the 2011 M_w 9.0 Tohoku earthquake and its postseismic phenomena affected the crustal deformation in Hokkaido. For in-depth discussion of earthquake cycles prior to the 20th century and after 2011, we have to conduct for the geological analyses and careful examination of the effect due to the giant earthquake in the adjacent region.

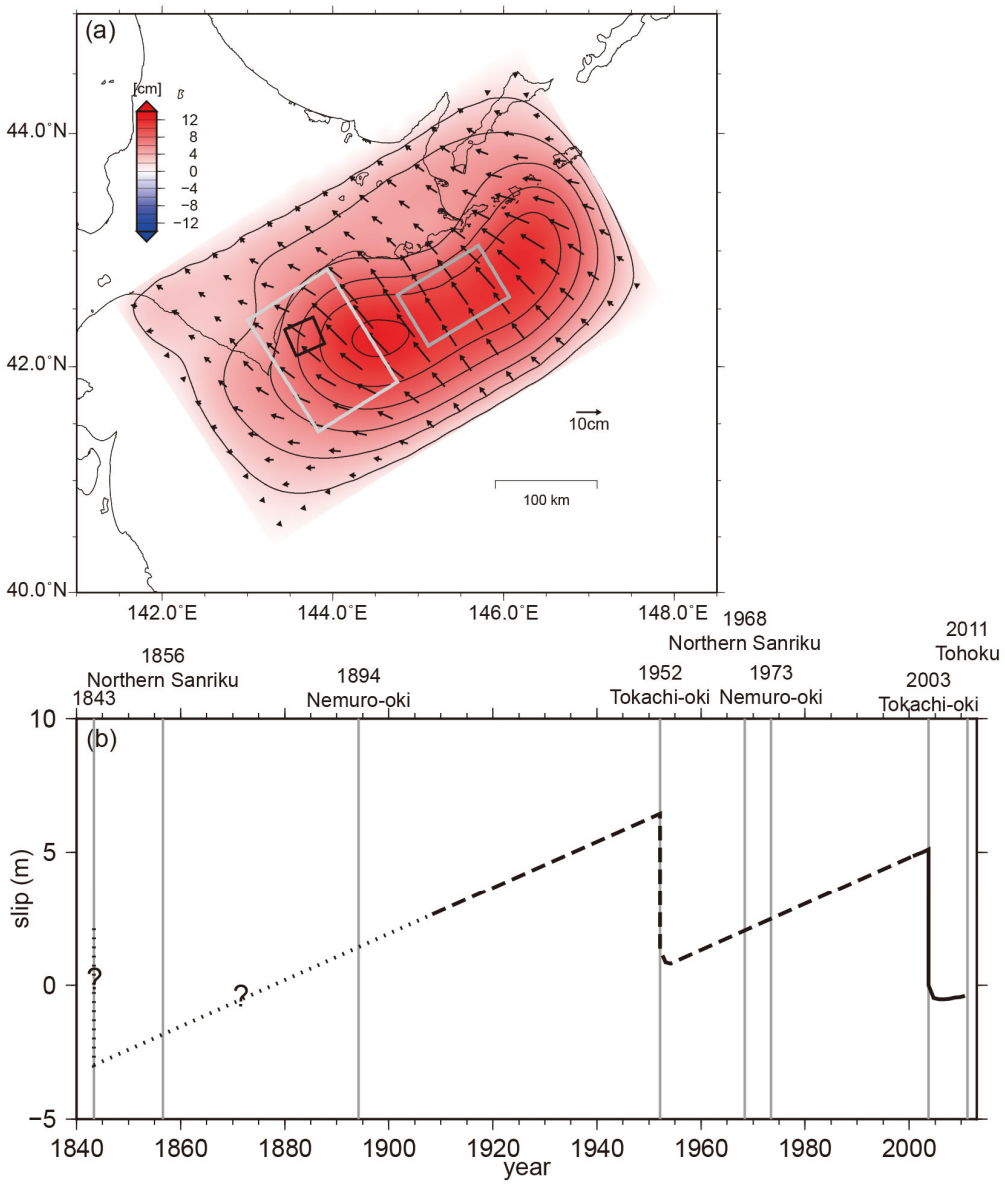

Figure 5-1. (a) Three-year averaged slip deficit distribution prior to the 2003 earthquake. The black rectangle shows the selected subfault whose slip history is shown in panel (b). The other aspects are the same as Figure 3-9a. (b) Slip history of the selected subfault shown in panel (a) which is estimated (black line) and suggested (black dashed line) in this study. The black dotted line is not constrained by this study. The vertical lines indicate the large earthquakes. The zero of the vertical axis means the state after the 2003 earthquake.

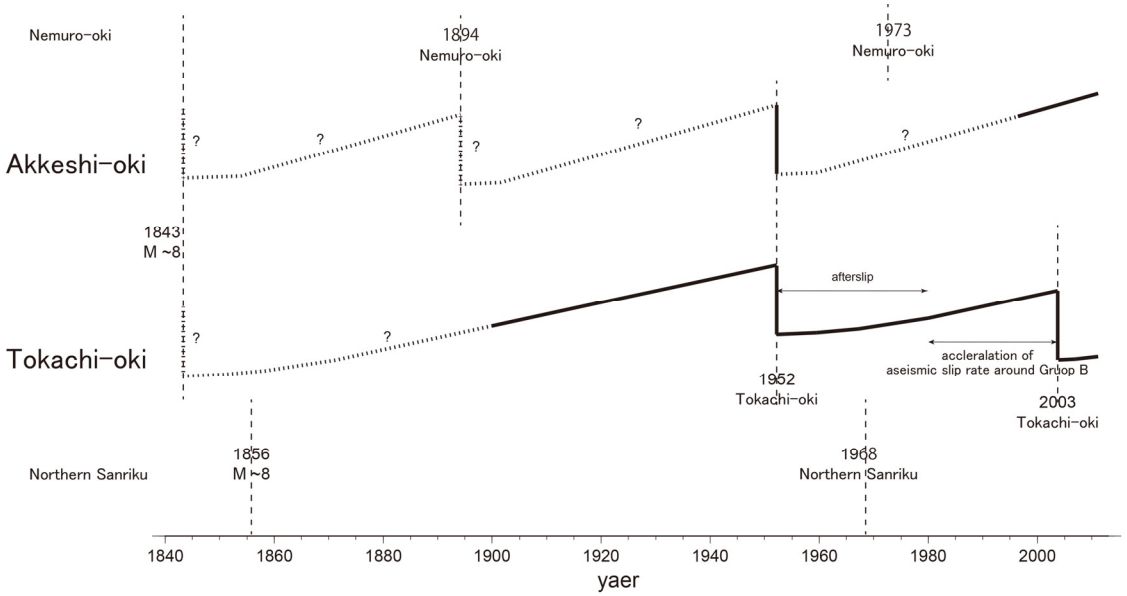

Figure 5-2. Schematic figure of slip history of each region. The history revealed by this study is shown in the black lines. The dotted lines are assumed based on historical earthquake data. The vertical broken lines indicate rupture area of the large earthquakes.

6. Conclusions

In this study, we investigated the interseismic, coseismic, and postseismic periods in the southernmost part of the Kuril subduction zone in the most recent 100 years to examine the *M*8 class earthquake cycle in this part.

To investigate the coseismic period, we performed the joint source inversions of the 1952 and 2003 earthquakes. We performed two inversions for the 2003 earthquake using the two datasets. One is the full dataset, while the other is a subset, whose amount is almost same as the dataset for the 1952 earthquake. The results revealed similar rupture processes, slip areas, and slip amounts for the two earthquakes in the Tokachi-oki region. However, the 1952 earthquakes differed from the 2003 earthquake in that the 1952 earthquake ruptured the Akkeshi-oki in addition to the Tokachi-oki region and was initiated by an M_w 6.1 earthquake.

To examine the interseismic and postseismic periods prior to and after the 2003 earthquake, we analyzed the recent GNSS data. We first investigated the crustal deformation rate prior to the 2003 earthquake and confirmed that there was no yearly scale transient event preceding the 2003 earthquake in the Tokachi-oki region. Then, we performed inversion analyses to obtain the yearly slip deficit/afterslip distribution between 25 September 2000 and 24 September 2010. The results revealed the following features: 1) the slip deficit rate in the Tokachi-oki region prior to the 2003 earthquake was stable; 2) the region with the large slip deficit rate corresponds to the main rupture area of the 1952 and 2003 earthquakes in the Tokachi-oki and Akkeshi-oki regions; and 3) the slip deficit rate in the Akkeshi-oki region was stable during the period from 25

September 2000–24 September 2010, except for the period just after the two M 7 earthquakes in the Akkeshi-oki region.

To examine the interseismic and postseismic periods which were not covered by the GNSS data, we investigated the crustal deformations and repeating earthquake in the most 100 years around Cape Erimo using the leveling survey data and analog seismograms. We also examined the effect of the crustal deformation due to medium (M $\geq$ 6.5) earthquakes to the data. The results suggested the following features in the Tokachi-oki region: 1) the afterslip of the 1952 earthquake continued until around 1980; 2) the state of plate interface prior to the 1952 earthquake is similar to that prior to the 2003 earthquake. Moreover, the acceleration of aseismic slip rate prior to the 2003 earthquake is indicated in the Urakawa-oki region.

Summarizing the above results, we examined the slip history in the southernmost part of the Kuril subduction zone since 1843. Because the Tokachi-oki region was covered by all the above analyses, we quantitatively examined the slip history during the earthquake cycles in the Tokachi-oki region. The results showed that the slip budget in the Tokachi-oki region is unbalanced not only in the single earthquake cycle but also in the multiple earthquake cycles since 1843. We suggested geophysical mechanisms of this unbalanced slip budget: stress transfer, temporal change of frictional properties, and changes of slip deficit rate. In the southern part of the Kuril subduction zone, historical *M*9 class earthquakes were suggested in the previous studies. Their supercycle can be another possible reason for the unbalanced slip budget. Because our analyses are based on seismological and geodetic data and we excluded the data after 2011 M_w 9.0 Tohoku earthquake, geological analyses and careful examination of the effect of the giant earthquake are necessary for further discussion of the earthquake cycle.

Appendix

Table A-1. Instrument constants for the seismographs at the teleseismic stations.

	Seismograph	Comp.	V	T_0	ε	V_m	T_1	T_g	Source
Florissant	Galitzin	UD				694	12	11.7	Alvarado and Beck [2006]
Tucson	Benioff	UD			h_1=0.8 h_g=1.0	3000	1	77	Microfilm V_m is from Alvarado and Beck [2006]
Tucson	Wood-Anderson	NS	466	8	77				Microfilm
Tucson	Wood-Anderson	EW	457	8	107				Microfilm
Pasadena	Benioff	UD				3000	1	90	Microfilm
Honolulu	Milne-Shaw	NS	124	12	20				Charlier and Van Gils [1953]
Honolulu	Milne-Shaw	EW	142	12	20				Charlier and Van Gils [1953]
Wellington	Milne-Shaw	NS	250	12	20				Scanned image
Riverview	Galitzin	UD				460	10.8	10.9	Station bulletin (04-06/1952)
Nizamia (Hyderabad)	Milne-Shaw	NS	249	12	20				Station bulletin (03/1952)
Nizamia (Hyderabad)	Milne-Shaw	EW	249	12	20				Station bulletin (03/1952)
Zurich	Mainka	NS	140	7	3				Charlier and Van Gils [1953]
Zurich	Mainka	EW	140	7	3				Charlier and Van Gils [1953]
Gottingen	Wiechert	UD	177	5.1	3.9				Estabrook et al. [1994]
Gottingen	Wiechert	NS	143	10.1	2.9				Station bulletin (unknown)
Gottingen	Wiechert	EW	140	13	4.1				Estabrook et al. [1994]
De Bilt	Galitzin	UD				740	12	12	Charlier and Van Gils [1953]
De Bilt	Galitzin	NS				310	25	25	Charlier and Van Gils [1953]
De Bilt	Galitzin	EW				310	25	25	Charlier and Van Gils [1953]
Toledo	Wiechert	NS	540	11	4.2				Station bulletin (02/1952)
Toledo	Wiechert	EW	530	11	4.1				Station bulletin (02/1952)
Lisbon	Wiechert	UD	205	4.9	2.67				Station bulletin (02/1952)

V: magnification. T_0: natural period. ε: damping ratio. V_m: peak magnification. T_1: natural period of pendulum. T_g: natural period of galvanometer. h_1: damping constant of pendulum. h_g: damping constant of galvanometer. We assumed $h_g = h_1 = 1.0$ except for the Benioff seismograph in Tucson.

Table A-2. Instrument constants for the seismographs of the near field stations.

	Seismograph	Comp.	V	T_0	ε	Source
Nemuro	JMA type 50	NS	1	6	8	Hamamatsu [1966]
	Wiechert	NS	80	5	6	Hamamatsu [1966]
Kushiro	JMA type 51	NS	1	6.2	13.5	Scanned image
	JMA type 51	EW	1	6.2	10.5	Scanned image
	JMA type 51	UD	1	6.0	5.4	Scanned image
	CMO portable	NS	40	4.0	7.7	CMO [1953]
	CMO portable	EW	40	4.1	6.7	CMO [1953]
Aomori	JMA type 50	UD	1	5.0	8.0	CMO [1953]
	Wiechert	UD	83	3.3	5.8	CMO [1953]
Hachinohe	JMA type 51	NS	1	6.0	8	CMO [1953]
	JMA type 51	EW	1	6.0	8	CMO [1953]
	Wiechert	NS	90	4.6	4.6	CMO [1953]
	Wiechert	EW	89	4.8	5.6	CMO [1953]
Miyako	JMA type 51	NS	1	6.0	8.0	CMO [1953]
	JMA type 51	EW	1	6.0	8.0	CMO [1953]
	Wiechert	NS	96	5.2	6.4	CMO [1953]
	Wiechert	EW	94	5.0	5.6	CMO [1953]

V: magnification. T_0: natural period. ε: damping ratio.

References

Akaike, H. (1980), Likelihood and the Bayes procedure, Trabajos de Estadistica y de Investigacion Operativa, 31, 143–166, doi:10.1007/BF02888350.

Aoi, S., R. Honda, N. Morikawa, H. Sekiguchi, H. Suzuki, Y. Hayakawa, T. Kunugi, and H. Fujiwara (2008), Three-dimensional finite difference simulation of long-period ground motions for the 2003 Tokachi-oki, Japan, earthquake, *J. Geophys. Res.*, 113, B07302, doi:10.1029/2007JB005452.

Alvarado, P., and S. Beck (2006), Source characterization of the San Juan (Argentina) crustal earthquakes of 15 January 1944 (Mw 7.0) and 11 June 1952 (Mw 6.8), *Earth. Planet. Sci. Lett.*, 243, 615-631, doi:10.1016/j.epsl.2006.01.015.

Baba, T., K. Hirata, T. Hori, and H. Sakaguchi (2006), Offshore geodetic data conducive to the estimation of the afterslip distribution following the 2003 Tokachi-oki earthquake, *Earth. Planet. Sci. Lett.*, 241, 281-292, doi:10.1016/j.epsl.2005.10.019.

Bullen, K. E. (1963), An introduction to the theory of seismology, 381 pp., Cambridge University Press, New York.

Bürgmann, R., M. G. Kogan, G. M. Steblov, G. Hilley, V. E. Levin, and E. Apel (2005), Interseismic coupling and asperity distribution along the Kamchatka subduction zone, *J. Geophys. Res.*, 110, B07405, doi:10.1029/2005JB003648.

Charlier, Ch., and J. M. Van Gils (1953), Liste des stations seismologiques mondiales, 500pp., Observatoire Royal de Belgique, Uccle.

Chlieh, M., J. P. Avouac, K. Sieh, D. H. Natawidjaja, and J. Galezka (2008), Heterogeneous coupling of the Sumatran megathrust constrained by geodetic and paleogeodetic measurements, *J. Geophys. Res.*, 113, B05305, doi:

10.1029/2007JB004981.

Chlieh, M., H. Perfettini, H. Tavera, J.‐P. Avouac, D. Remy, J.‐M. Nocquet, F. Rolandone, F. Bondoux, G. Gabalda, and S. Bonvalot (2011), Interseismic coupling and seismic potential along the Central Andes subduction zone, *J. Geophys. Res.*, 116, B12405, doi:10.1029/2010JB008166.

CMO (1953), A report of the Tokachi earthquake of March 4, 1952, *Quarterly Journal of Seismology*, 17, 1-130 (in Japanese).

Dambara, T. (1971), Synthetic vertical movements in Japan during the recent 70 years, *J. Geod. Soc. Japan.*, 17, 100-108 (in Japanese with English abstract).

Drewes, H. (2009), The actual plate kinematic and crustal deformation model APKIM2005 as basis for non-rotating ITRF, In: Drewes H. (eds) Geodetic Reference Frames. *International Association of Geodesy Symposia*, 134, 95-99, Springer, Berlin, Heidelberg, doi: 10.1007/978-3-642-00860-3_15.

Dziewonski, A. M., and D. L. Anderson (1981), Preliminary reference Earth model, *Phys. Earth Planet. Inter.*, 25, 297-356, doi:10.1016/0031-9201(81)90046-7.

Ekström, G., M. Nettles, and A. M. Dziewoński (2012), The global CMT project 2004–2010: Centroid-moment tensors for 13,017 earthquakes, *Phys. Earth Planet. Inter.*, 200-201, 1–9, doi:10.1016/j.pepi.2012.04.002.

El-Fiky, G. S., and T. Kato (1999), Interplate coupling in the Tohoku district, Japan, deduced from geodetic data inversion, *J. Geophys. Res.*, 104, 361-377, doi:10.1029/1999JB900202.

Estabrook, C. H., K. H. Jacob, and L. R. Sykes (1994), Body wave and surface wave analysis of large and great earthquakes along the Eastern Aleutian Arc, 1923–1993: Implications for future events, *J. Geophys. Res.*, 99, 11643–11662,

doi:10.1029/93JB03124.

Furumura, T. (2015), New source image of the Nankai Trough earthquakes, (available at http://www.gensai.nagoya-u.ac.jp/nankai-t/download/nu/9_nu_furumura.pdf ,last accessed on 20 November 2017, in Japanese).

Goldfinger, C., Y. Ikeda, R. S. Yeats, J. Ren (2013), Superquakes and Supercycles, *Seismol. Res. Lett.*, 84, 24–32. doi:10.1785/0220110135.

Hamada, N., and Y. Suzuki (2004), Re-examination of aftershocks of the 1952 Tokachi-oki earthquake and a comparison with those of the 2003 Tokachi-oki earthquake, *Earth Planets Space*, 56, 341–345, 10.1186/BF03353062.

Hamamatsu, O. (1966), Historical table of seismographs for routine observations in J.M.A Network, *Zisin*, 19, 286-305, doi:10.4294/zisin1948.19.4_286.

Hanks, T. C., and H. Kanamori (1979), A moment magnitude scale, *J. Geophys. Res.*, 84, 2348-2350, doi:10.1029/JB084iB05p02348.

Hashimoto, C., A. Noda, T. Sagiya, and M. Matsu'ura (2008), Interplate seismogenic zones along the Kuril–Japan trench inferred from GPS data inversion, *Nature Geoscience*, 2, 141-144, doi:10.1038/ngeo421.

Hashimoto, C., A. Noda, M. Matsu'ura (2012), The Mw 9.0 northeast Japan earthquake: total rupture of a basement asperity, *Geophys. J. Int.*, 189, 1-5, doi:10.1111/j.1365-246X.2011.05368.x.

Hatori, T. (1975), Tsunami magnitude and wave source regions of historical Sanriku tsunamis in northeast Japan, *Bull. Earthq. Res. Inst. Univ. Tokyo*, 50, 397-414 (in Japanese with English abstract).

Hayes, G. P., M. W. Herman, W. D. Barnhart, K. P. Furlong, S. Riquelme, H. M. Benz, E. Bergman, S. Barrientos, P. S. Earle, and S. Samsonov (2014),

Continuingmegathrust earthquake potential in Chile after the 2014 Iquique earthquake, *Nature*, 512, 295-298, doi:10.1038/nature13677.

Hertzell, S. H. and T. H. Heaton (1985), Teleseismic time functions for large, shallow subduction zone earthquakes, *Bull. Seismol. Soc. Am.*, 75, 965-1004.

Hikima, K. and K. Koketsu (2005), Rupture process of the 2004 Chuetsu (mid-Niigata prefecture) earthquake, Japan: a series of events in a complex fault system, *Geophys. Res. Lett.*, 32, L18303, doi:10.1029/2005GL023588.

Hikima, K., K. Koketsu, and Y. Tanioka (2005), Source process of the 2003 Tokachi-oki earthquake inferred from strong motions, geodetic data, far-field waveforms and tsunami data, *Chikyu Monthly special issue*, 49, 47-55 (in Japanese).

Hirata, K., E. Geist, K. Satake, T. Tanioka, and S. Yamaki (2003), Slip distribution of the 1952 Tokachi-Oki earthquake (M 8.1) along the Kuril Trench deduced from tsunami waveform inversion, *J. Geophys. Res.*, 108, 2196, doi:10.1029/2002JB001976, 2003.

Hirata, K., K. Satake, S. Yamaki, Y. Tanioka, Y. Yamanaka, and T. Nishimura (2007), Examination of the northeast edge of the 1952 Tokachi-oki earthquake tsunami source based on eyewitness accounts stated in previously published reports, *Zisin*, 60, 21-41, doi:10.4294/zisin.60.21, (in Japanese with English abstract).

Hirata, K., Y. Tanioka, K. Satake, S. Yamaki, and E. L. Geist (2004), The tsunami source area of the 2003 Tokachi-oki earthquake estimated from tsunami travel times and its relationship to the 1952 Tokachi-oki earthquake, *Earth Planets Space*, 56, 367-372, doi:10.1186/BF03353066.

Honda, R., N. Morikawa, H. Sekiguchi, T. Kunugi, and H. Fujiwara (2004), Ground motion and rupture process of the 2003 Tokachi-oki earthquake obtained from strong

motion data of K-NET and KiK-net, *Earth Planets Space*, 56, 317-322, doi:10.1186/BF03353058.

Horikawa, H. (2004), Fault geometry and slip distribution of the 2003 Tokachi-oki earthquake as deduced from teleseismic body waves, *Earth Planets Space*, 56, 1011-1017, doi:10.1186/BF03352543.

Ichikawa, S. (1971), Reanalyses of mechanism of earthquakes which occurred in and near Japan, and statistical studies on the nodal plane solutions obtained, 1926-1968, *Geophy. Mag.*, 35, 207-274.

Ito, T., and M. Hashimoto (2004), Spatiotemporal distribution of interplate coupling in southwest Japan from inversion of geodetic data, *J. Geophys. Res.*, 109, B02315, doi:10.1029/2002JB002358.

Itoh, Y., and T. Nishimura (2016), Characteristics of postseismic deformation following the 2003 Tokachi-oki earthquake and estimation of the viscoelastic structure in Hokkaido, northern Japan, *Earth Planets Space*, 68:156, doi:10.1186/s40623-016-0533-y.

Iwasaki, T., H. Sato, M. Shinohara, T. Ishiyama, and A. Hashima (2015), Fundamental structure model of island arcs and subducted plates in and around Japan, *American Geophysical Union Fall Meeting 2015*, San Francisco, U.S.A. Dec. 14-18, T31B-2878.

Iwata, T., and K. Asano (2011), Characterization of the heterogeneous source model of intraslab earthquakes toward strong ground motion prediction, *Pure Appl. Geophys.*, 168, 117-124, doi:0.1007/s00024-010-0128-7.

JMA (1957), Seismograms of strong earthquakes in Japan, 1923-1956, *Quarterly Journal of Seismology Supplementary Volume*, 22, 1-136.

Kasahara, M. (1975), A fault model of the Tokachi-oki earthquake of 1952, *Programme and abstracts, the Seismological Society of Japan.* (in Japanese).

Kanamori (1977), Seismic and aseismic slip along subduction zones and their tectonic implications, *in Island Arcs, Deep Sea Trenches and Back-Arc Basins*, edited by M. Talwani and W. C. Pitman, pp. 163‑174, AGU, Washington, D. C.

Kanamori, H., M. Miyazawa, and J. Mori (2006), Investigation of the earthquake sequence off Miyagi prefecture with historical seismograms, *Earth Planets Space*, 58, 1533–1541, doi:10.1186/BF03352657.

Kikuchi, M., and H. Kanamori (1991), Inversion of complex body waves—III, *B. Seismol. Soc. Am.*, 81, 2335-2350.

Kitada, M. (1931), A report of the earthquake on 17 February 1931 in Urakawa, Hokkaido, *Quarterly Journal of Seismology*, 6, 133-154.

Kogan, M. G., N. F. Vasilenko, D. I. Frolov, J. T. Freymueller, G. M. Steblov, B. W. Levin, and A. S. Prytkov (2011), The mechanism of postseismic deformation triggered by the 2006–2007 great Kuril earthquakes, *Geophys. Res. Lett.*, 38, L06304, doi:10.1029/2011GL046855.

Kogan, M. G., N. F. Vasilenko, D. I. Frolov, J. T. Freymueller, G. M. Steblov, A. S. Prytkov, and G. Ekström (2013), Rapid postseismic relaxation after the great 2006–2007 Kuril earthquakes from GPS observations in 2007–2011, *J. Geophys. Res. Solid Earth*, 118, 3691–3706, doi:10.1002/jgrb.50245.

Kohketsu, K. (1985), The extended reflectivity method for synthethic near-field seismograms, *J. Phys. Earth*, 33, 121-131, doi:10.4294/jpe1952.33.121.

Koketsu, K., K. Hikima, S. Miyazaki, and S. Ide (2004), Joint inversion of strong motion and geodetic data for the source process of the 2003 Tokachi-oki, Hokkaido,

earthquake, *Earth Planets Space*, 56, 329-334, doi:10.1186/BF03353060.

Koketsu, K., H. Miyake, H. Fujiwara, and T. Hashimoto (2008), Progress towards a Japan integrated velocity structure model and long-period ground motion hazard map, *Proc. 14th World Conf. Earthq. Eng.*, S10-038.

Koketsu, K., H. Miyake, and H. Suzuki (2012), Japan Integrated Velocity Structure Model Version 1, *Proc. 15th World Conf. Earthq. Eng.*, 1773.

Kumini, T., Y. Takano, M. Suzuki, T. Saitou, T. Narita, and S. Okamura (2001), Vertical crustal movements in Japan estimated from the leveling observations data for the past 100 years, *J. Geogr. Surv. Inst*., 96, 23-37 (in Japanese).

Larson, K. M., and S. Miyazaki (2008), Resolving static offsets from high-rate GPS data: the 2003 Tokachi-oki earthquake, *Earth Planets Space*, 60, 801-808, doi:10.1186/BF03352831.

Lindquist, K. G., K. Engle, D. Stahlke, and E. Price (2004), Global Topography and Bathymetry Grid Improves Research Efforts, *Eos Trans. AGU*, 85, 186-186, doi:10.1029/2004EO190003.

Loveless, J. P., and B. J. Meade (2010), Geodetic imaging of plate motions, slip rates, and partitioning of deformation in Japan, *J. Geophys. Res.*, 115, B02410, doi:10.1029/2008JB006248.

Matsuzawa, T., T. Igarashi, and A. Hasegawa (2002), Characteristic small‐earthquake sequence off Sanriku, northeastern Honshu, Japan, *Geophys. Res. Lett.*, 29, 1543, doi:10.1029/2001Gl014632.

Mavrommatis, A. P., P. Segall, and K. M. Johnson (2014), A decadal‐scale deformation transient prior to the 2011 Mw 9.0 Tohoku‐oki earthquake, *Geophys.*

Res. Lett., 41, 4486‑4494, doi:10.1002/2014GL060139.

Métois, M., A. Socquet, and C. Vigny (2012), Interseismic coupling, segmentation and mechanical behavior of the central Chile subduction zone, *J. Geophys. Res.*, 117, B03406, doi:10.1029/2011JB008736.

Miura, S, T. Suwa, A. Hasegawa, and T. Nishimura (2004), The 2003 M8.0 Tokachi-Oki earthquake – How much has the great event paid back slip debts?, *Geophys. Res. Lett.*, 31, L05613, doi:10.1029/2003GL019021.

Miyamura, J., and T. Sasatani (1986), Accurate determination of source depths and focal mechanisms of shallow earthquakes occurring at the junction between the Kurile and the Japan trenches, *Jour. Fac. Sci. Hokkaido Univ. Ser. VII (Geophysics)*, 8, 37-63.

Miyazaki, S. and K. M. Larson (2008), Coseismic and early postseismic slip for the 2003 Tokachi-oki earthquake sequence inferred from GPS data, *Geophys. Res. Lett.*, 35, L04302, doi:10.1029/2007GL032309.

Miyazaki, S., P. Segall, J. Fukuda, and T. Kato (2004a), Space time distribution of afterslip following the 2003 Tokachi-oki earthquake: Implications for variations in fault zone frictional properties, *Geophys. Res. Lett.*, 31, L06623, doi:10.1029/2003GL019410.

Miyazaki, S., K. M. Larson, K. Choi, K. Hikima, K. Koketsu, P. Bodin, J. Haase, G. Emore, and A. Yamagiwa (2004b), Modeling the rupture process of the 2003 September 25 Tokachi-Oki (Hokkaido) earthquake using 1-Hz GPS data, *Geophys. Res. Lett.*, 31, L21603, doi:10.1029/2004GL021457.

Moreno, M., M. Rosenau, O. Oncken (2010), 2010 Maule earthquake slip correlates with pre-seismic locking of Andean subduction zone, *Nature*, 467, 198-202, doi: 10.1038/nature09349.

Moriya, T. (1972), Aftershock activity of the Hidaka Mountains Earthquake of January 21, 1970, *Zisin*, 24, 287-297, doi:10.4294/zisin1948.24.4_287.

Moriya, T., H. Miyamachi, and S. Katoh (1983), Spatial distribution and mechanism solutions for foreshocks, mainshock and aftershocks of the Urakawa-oki earthquake of March 21, 1982, *Geophys. Bull. Hokkaido Univ.*, 42, 191-213, doi:10.14943/gbhu.42.191 (in Japanese with English abstrast).

Murakami, M., and S. Ozawa (2004), Mapped vertical deformation field of Japan derived from continuous GPS measurements and its tectonic implications, *Zisin*, 57, 209-231, doi:10.4294/zisin1948.57.2_209.

Murotani, S., H. Miyake, and K. Koketsu (2008), Scaling of characterized slip models for plate-boundary earthquakes, *Earth Planets Space*, 60, 987-991, doi:10.1186/BF03352855.

Nadeau, R. M., and L. R. Johnson (1998), Seismological studies at Parkfield VI: Moment release rates and estimates of source parameters for small repeating earthquakes, 88, 790-814.

Nadeau, R. M., and T. V. McEvilly (1999), Fault slip rates at depth from recurrence intervals of repeating microearthquakes, *Science*, 285, 718-721, doi:10.1126/science.285.5428.718.

Nagai, R., M. Kikuchi, and Y. Yamanaka (2001), Comparative study on the source processes of recurrent large earthquakes in Sanriku-oki region: the 1968 Tokachi-oki earthquake and the 1994 Sanriku-oki earthquake, *Zisin*, 54, 267-280, doi:10.4294/zisin1948.54.2_267 (in Japanese with English abstract).

Nakagawa, H., T. Toyofuku, K. Kotani, B. Miyahara, C. Iwashita, S. Kawamoto, Y. Hatanaka, H. Munekane, M. Ishimoto, T. Yustubo, N. Ishikura, and Y. Sugawara

(2009), Development and validation of GEONET new analysis strategy (version 4), *J. Geogr. Surv. Inst*., 118, 1–8 (in Japanese).

Nishimura, T. (2006), Fault model of the 1952 Tokachi-oki eartqhauke induced from geodetic data, *Chikyu Monthly*, 28, 441-447 (in Japanese).

Nishimura, T., T. Hirasawa, S. Miyazaki, T. Sagiya, T. Tada, S. Miura, and K. Tanaka (2004), Temporal change of interplate coupling in northeastern Japan during 1995–2002 estimated from continuous GPS observations, *Geophys. J. Int.*, 157, 901-916, doi:10.1111/j.1365-246X.2004.02159.x.

Nocquet, J. M., P. Jarrin, M. Vallée, P. A. Mothes, R. Grandin, F. Rolandone, B. Delouis, H. Yepes, Y. Font, D. Fuentes, M. Régnier, A. Laurendeau, D. Cisneros, S. Hernandez, A. Sladen, J.-C. Singaucho, H. Mora, J. Gomez, L. Montes, and P. Charvis (2017), Supercycle at the Ecuadorian subduction zone revealed after the 2016 Pedernales earthquake, *Nat. Geosci.*, 10, 145-149, doi:10.1038/ngeo2864.

Nozu, A., and K. Irikura (2008), Strong-motion generation areas of a great subduction-zone earthquake: Waveform inversion with empirical Green's functions for the 2003 Tokachi-oki earthquake, *Bull. Seismol. Soc. Am.*, 98, 180-197, doi:doi.org/10.1785/0120060183.

Okada, Y. (1992), Internal deformation due to shear and tensile faults in a half-space, *Bull. Seism. Soc. Am.*, 82, 1018-1040.

Ozawa, S., M. Kaidzu, M. Murakami, T. Imakiire, and Y. Hatanaka (2004), Coseismic and postseismic crustal deformation after the Mw 8 Tokachi-oki earthquake in Japan, *Earth Planets Space*, 56, 675-680, doi:10.1186/BF03352530.

Ozawa, S., T. Nishimura, H. Munekane, H. Suito, T. Kobayashi, M. Tobita, and T. Imakiire (2012), Preceding, coseismic, and postseismic slips of the 2011 Tohoku

earthquake, Japan, *J. Geophys. Res.*, 117, B07404, doi:10.1029/2011JB009120.

Philibosian, B., K. Sieh, J. ‐ P. Avouac, D. H. Natawidjaja, H. ‐ W. Chiang, C. ‐ C. Wu, H. Perfettini, C. ‐ C. Shen, M. R. Daryono, and B. W. Suwargadi (2014), Rupture and variable coupling behavior of the Mentawai segment of the Sunda megathrust during the supercycle culmination of 1797 to 1833, *J. Geophys. Res.*, 119, 7258–7287, doi: 10.1002/2014JB011200.

Robinson, D. P. and L. T. Cheung (2010), Source process of the M_w 8.3, 2003 Tokachi-Oki, Japan earthquake and its aftershocks, *Geophys. J. Int.*, 181, 334-342, doi:10.1111/j.1365-246X.2010.04513.x.

Romano, F., A. Piatanesi, S. Lorito, and K. Hirata (2010), Slip distribution of the 2003 Tokachi ‐ oki M_w 8.1 earthquake from joint inversion of tsunami waveforms and geodetic data, *J. Geophys. Res.*, 115, B11313, doi:10.1029/2009JB006665.

Sakoi, H., T. Matsuyama, T. Hirayama, I. Yamazaki, T. Yamamoto, M. Ichiyanagi, and H. Takahashi (2012), Moderate repeating earthquakes off Kushiro, eastern Hokkaido, Japan, *Zisin*, 65, 151-161, doi:10.4294/zisin.65.151.

Satake, K (2017), Great earthquakes in the 17th century along the Kuril and Japan Trenches, *Bull. Earthq. Res. Inst.* 92, 31-47 (in Japanese with English abstract).

Satake, K, K. Hirata, S. Yamaki, and Y. Tanioka (2006), Re-estimation of tsunami source of the 1952 Tokachi-oki earthquake, *Earth Planets Space*, 58, 535-542, doi:10.1186/BF03351951.

Sato, K., T. Baba, T. Hori, M. Hyodo, and Y. Kaneda (2010), Afterslip distribution following the 2003 Tokachioki earthquake: An estimation based on the Green's functions for an inhomogeneous elastic space with subsurface structure, *Earth*

Planets Space, 62:923, doi:10.5047/eps.2010.11.007.

Sasatani, T. (1985), A study of the strong ground motion of the western Hidaka, Hokkaido earthquake, *Geophys. Bull. Hokkaido Univ.*, 46, 69-83, doi:10.14943/gbhu.46.69 (in Japanese with English abstract).

Sapporo District Meteorological Observatory (1987), Report on the earthquake of the northern part of Hidaka mountains, January 14 1987, *Quarterly Journal of Seismology*, 51, 57-76 (in Japanese).

Savage, J. C. (1983), A dislocation model of strain accumulation and release at a subduction zone, *J. Geophys. Res.*, 88, 4984–4996, doi:10.1029/JB088iB06p04984

Sawai, Y., T. Kamataki, M. Shishikura, H. Nasu, Y. Okamura, K. Satake, K. H. Thomson, D. Matsumoto, Y. Fujii, J. Komatsubara, and Than Thin Aung (2009), (2009), Aperiodic recurrence of geologically recorded tsunamis during the past 5500 years in eastern Hokkaido, Japan, *J. Geophys. Res.*, 114, B01319, doi:10.1029/2007JB005503.

Scholz. C., and J. Campos (2012), The seismic coupling of subduction zones revisited, *J. Geophys. Res.*, 117, B05310, doi:10.1029/2011JB009003.

Seismology and Volcanology Research Departmant of Meteorological Research Insitutite, Seismology and Volcanology Department, Meteorological College, Sapporo Regional Headquarters, Sendai Regional Headquarters, Osaka Regional Headquarters, Fukuoka Regional Headquarters, and Okinawa Regional Headquarters (2014), Survey of moderate repeating earthquakes in Japan, *Tech. Rep. Meteor. Res. Inst.*, 72, 1-139, doi:10.11483/mritechrepo.72.

Shinohara, M., T. Yamada, T. Kanazawa, N. Hirata, Y. Kaneda, T. Takanami, H. Mikada, K. Suyehiro, S. Sakai, T. Watanabe, K. Uehira, Y. Murai, N. Takahashi, M. Nishino,

K. Mochizuki, T. Sato, E. Araki, R. Hino, K. Uhira, H. Shiobara, and H. Shimizu (2004), Aftershock observation of the 2003 Tokachi-oki earthquake by using dense ocean bottom seismometer network, *Earth Planets Space*, 56, 295-300, doi:10.1186/BF03353054.

Shimazaki, K., and T. Nakata (1980), Time-predictable recurrence model for large earthquakes, *Geophys. Res. Lett.*, 7: 279-282, doi:10.1029/GL007i004p00279.

Sieh, K., D. H. Natawidjaja, A. J. Meltzner, C. C. Chen, H. Cheng, K. S. Li, B. W. Suwargadi, J. Galetzka, B. Philibosian, and R. L. Edwards (2008), Earthquake supercycles inferred from sea-level changes recorded in the corals of west Sumatra, *Science*, 322, 1674-1678, doi:10.1126/science.1163589.

Somerville, P., K. Irikura, R. Graves, S. Sawada, D. Wald, N. Abrahamson, Y. Iwasaki, T. Kagawa, N. Smith, and A. Kowada (1999), Characterizing crustal earthquake slip models for the prediction of strong ground motion, *Seismol. Res. Lett.*, 70, 59-80, doi:10.1785/gssrl.70.1.59.

Suito, H., and J. T. Freymueller (2009), A viscoelastic and afterslip postseismic deformation model for the 1964 Alaska earthquake, *J. Geophys. Res.*, 114, B11404, doi:10.1029/2008JB005954.

Sun, T., and K. Wang (2015), Viscoelastic relaxation following subduction earthquakes and its effects on afterslip determination, *J. Geophys. Res.*, 120, 1329-1344, doi:10.1002/2014JB011707.

Suwa, Y., S. Miura, A. Hasegawa, T. Sato, and K. Tachibana (2006), Interplate coupling beneath NE Japan inferred from three-dimensional displacement field, *J. Geophys. Res.*, 111, B04402, doi:10.1029/2004JB003203.

Tada, A. (1987), Fault model of the 1982 Urawaka-oki earthquake and its tectonic

significance, *Zisin*, 40, 27-37, doi:10.4294/zisin1948.40.1_27.

Takeo, M., S. Ide, and Y. Yoshida (1993), The 1993 Kushiro-Oki, Japan, earthquake: A high stress-drop event in a subducting slab, *Geophys. Res. Lett.*, 20, 2607-2610, doi:10.1029/93GL02864.

Tanioka, Y., K. Hirata, R. Hino, and T. Kanazawa (2004a), Slip distribution of the 2003 Tokachi-oki earthquake estimated from tsunami waveform inversion, *Earth Planets Space*, 56, 373-376, doi:10.1186/BF03353067.

Tanioka, Y., Y. Nishimura, K. Hirakawa, F. Imamura, I. Abe, Y. Abe, K. Shindou, H. Matsutomi, T. Takahashi, K. Imai, K. Harada, Y. Namegawa, Y. Hasegawa, Y. Hayashi, F. Nanayama, T. Kamataki, Y. Kawata, Y. Fukasawa, S. Koshimura, Y. Hada, Y. Azumai, K. Hirata, A. Kamikawa, A. Yoshikawa, T. Shiga, M. Kobayashi, and S. Masaka (2004b), Tsunami run-up heights of the 2003 Tokachi-oki earthquake, *Earth Planets Space*, 56, 359-365, doi:10.1186/BF03353065.

Tanioka, Y., K. Satake, and K. Hirata (2007), Recurrence of recent large earthquakes along the southernmost Kurile-Kamchatka subduction zone, *Geophy. Monograph Series*, 172, 145–152, doi:10.1029/172GM13.

Uchida, N., and T. Matsuzawa (2013), Pre- and postseismic slow slip surrounding the 2011 Tohoku-oki earthquake rupture, *Earth. Planet. Sci. Lett.*, 374, 81-91, doi:10.1016/j.epsl.2013.05.021.

Uchida, N., T. Matsuzawa, T. Igarashi, and A. Hasegawa (2003), Interplate quasi-static slip off Sanriku, NE Japan, estimated from repeating earthquakes, *Geophys. Res. Lett.*, 30, 1801, doi:10.1029/2003GL017452.

Ueno, H., S. Hatakeyama, T. Aketagawa, J. Funasaki, and N. Hamada (2002), Improvement of hypocenter determination procedures in the Japan Meteorological

Agency, *Quarterly Journal of Seismology*, 65, 123-134 (in Japanese with English abstract).

Ustu, T. (1982), Catalog of large earthquakes in the region of Japan from 1885 through 1980, *Bull. Earthq. Res. Inst.*, 57, 401-463 (in Japanese with English abstract).

Wald, D. J., and P. G. Somerville (1995), Variable-slip rupture model of the great 1923 Kanto, Japan, earthquake: Geodetic and body-waveform analysis, *Bull. Seismol. Soc. Am.*, 85, 159-177.

Wallace, L. M., J. Beavan, R. McCaffrey, and D. Darby (2004), Subduction zone coupling and tectonic block rotations in the North Island, New Zealand, *J. Geophys. Res.*, 109, B12406, doi:10.1029/2004JB003241.

Wang, K., R. Wells, S. Mazzotti, R. D. Hyndmann, and T. Sagiya (2003), A revised dislocation model of interseismic deformation of the Cascadia subduction zone, *J. Geophys. Res.*, 108, 2026, doi: 10.1029/2001JB001227.

Wdowinski, S., Y. Bock, J. Zhang, P. Fang, and J. Genrich (1997), Southern California permanent GPS geodetic array: Spatial filtering of daily positions for estimating coseismic and postseismic displacements induced by the 1992 Landers earthquake, *J. Geophys. Res.*, 102(B8), 18057–18070, doi:10.1029/97JB01378.

Weatherall, P., K. M. Marks, M. Jakobsson, T. Schmitt, S. Tani, J. E. Arndt, M. Rovere, D. Chayes, V. Ferrini, and R. Wigley (2015), A new digital bathymetric model of the world's oceans, *Earth and Space Science*, 2, 331- 345, doi:10.1002/2015EA000107.

Wessel, P., and W. H. F. Smith (1998), New, improved version of the Generic Mapping Tools released, *Eos Trans. AGU*, 79, 579, doi:10.1029/98EO00426.

Wesson, R. L., D. Melnick, M. Cisternas, M. Moreno, and L. L. Ely (2015), Vertical deformation through a complete seismic cycle at Isla Santa María, Chile, *Nat. Geosci*,

8, 547-551, doi:10.1038/ngeo2468.

Yabuki, T., and M. Matsu'ura (1992), Geodetic data inversion using a Bayesian information criterion for spatial distribution of fault slip, *Geophys. J. Int.*, 109, 363-375, doi:10.1111/j.1365-246X.1992.tb00102.x.

Yagi, Y. (2004), Source rupture process of the 2003 Tokachi-oki earthquake determined by joint inversion of teleseismic body wave and strong ground motion data, *Earth Planets Space*, 56, 311-316, doi:10.1186/BF03353057.

Yamada, T., M. Shinohara, T. Kanazawa, N. Hirata, Y. Kaneda, T. Takanami, H. Mikada, K. Suyehiro, S. Sakai, T. Watanabe, K. Uehira, T. Murai, N. Takahashi, M. Nishino, K. Mochizuki, T. Sato, E. Araki, R. Hino, K. Uhira, H. Shiobara, and H. Shimizu (2005), Aftershock distribution of the 2003 Tokachi-oki earthquake derived from high-dense network of ocean bottom seismographs, *Zisin*, 57, 281-290, doi:10.4294/zisin1948.57.3_281 (in Japanese with English abstract).

Yamanaka, Y., and M. Kukuchi (2003), Source process of the recurrent Tokachi-oki earthquake on September 26, 2003, inferred from teleseismic body waves, *Earth Planets Space*, 55, e21-e24, doi:10.1186/BF03352479.

Yokota, Y. (2013), Seismo-geodesy to infer the physical process of the 2011 Tohoku earthquake, Ph-D thesis, The University of Tokyo.

Yokota, Y., T. Ishikawa, S. Watanabe, T. Tashiro, and A. Asada (2016), Seafloor geodetic constraints on interplate coupling of the Nankai Trough megathrust zone, *Nature*, 534, 374-377, doi:10.1038/nature17632.

Yokota, Y., and K. Koketsu (2015), A very long-term transient event preceding the 2011 Tohoku earthquake, *Nature Communications*, 6, 5934, doi:10.1038/ncomms6934.

Yoshida, S., K. Koketsu, B. Shibazaki, T. Sagiya, T. Kato, and Y. Yoshida (1996), Joint

inversion of near-and far-field waveforms and geodetic data for the rupture process of the 1995 Kobe earthquake, *J. Phys. Earth*, 44, 437–454, doi:10.4294/jpe1952.44.437.

Yoshioka, S., T. Mikumo, V. Kostoglodov, K. M. Larson, A. R. Lowry, and S. K. Singh (2004), Interplate coupling and a recent aseismic slow slip event in the Guerrero seismic gap of the Mexican subduction zone, as deduced from GPS data inversion using a Bayesian information criterion, *Phys. Earth Planet. Inter.*, 146, 513-530, doi:10.1016/j.pepi.2004.05.006.

Zhu, L., and L. A. Rivera (2002), A note on the dynamic and static displacements from a point source in multilayered media, *Geophys. J. Int.*, 148, 619–627, doi:10.1046-/j.1365-246X.2002.01610.x.

Acknowledgement

I would like to express my deepest appreciation to Professor Kazuki Koketsu for introducing me source inversions and his helpful advice and support. I am very grateful to Associate Professor Hiroe Miyake for her helpful discussion and encouragement. I would like to express my gratitude to my defense committee members: Profs. Kenji Satake, Ryosuke Ando, Hitoshi Kawakatsu, Takashi Furumura, Minoru Takeo, and Shingo Yoshida.

I would like to thank the National Research Institute for Earch Science and Disaster Resilience for providing the waveform data of the K-net, KiK-net, and F-net. I would like to thank the GSI for providing the F3 solutions. I would like to thank the Association for the Development of Earthquake Prediction and the Ministry of Education, Culture, Sports, Science, and Technology for providing the digital images of JMA seismograms.

Some station bulletins were obtained from the website of the SISMOS project. The plate models by Iwasaki et al. [2015] were constructed from topography and bathymetry data by GSI (250-m digital map), Japan Oceanographic Data Center (500m mesh bathymetry data, J-EGG500, http://www.jodc.go.jp/jodcweb/JDOSS/infoJEGG_j.html) and Geographic Information Network of Alaska, University of Alaska [Lindquist et al., 2004]. Figures were drawn using the General Mapping Tools [Wessel and Smith, 1998].

Last, but not the least. I would like to thank my family for their support and encouragement.